Ultra-Class Mining Shovel Track Roller Path Testing

by

Daley James Paterson

A thesis submitted in partial fulfillment of the requirements for the degree of

Master of Science

in
Mining Engineering

Department of Civil and Environmental Engineering
University of Alberta

Abstract

This thesis explores the development and preliminary operation of a new test method for roller and roller path arrangements on ultra-class mining shovels. The lack of existing lab-scale test methods discourage significant change, and restrict the development of the roller and roller path to minor adjustments to their geometry and material. Once in full operation the test method will allow for the optimization of existing, or the development of new, roller path technology for specific mining conditions. Preliminary testing has shown that with some improvements, the developed apparatus is capable of producing end-of-life roller path samples in four weeks of continuous operation. The impact of various damage models could then be characterized for sensitivity to provide further information on how to develop the optimal roller and roller path system. With further development, the test method developed here would allow for improving the roller and roller path technology at a more rapid pace. Improved rollers and roller paths would reduce the required maintenance time for a mining shovel, decreasing maintenance costs and increasing production.

Table of Contents

List of Tables

List of Figures

Chapter 1: Introduction

Mine profitability requires reliable equipment with resistance to harsh mine operating conditions. In terms of machinery that operates in a mine, there are fewer shovels (Figure 1) in the equipment fleet as they service multiple trucks. However, a shovel is a critical piece of equipment, as it operates directly in the exposure or extraction of the profitable commodity. Unexpected downtime for maintenance may cause a high opportunity cost or revenue loss as the resource remains in-situ. Ensuring high quality parts reduces unexpected breakdowns, but requires research and lab-scale tests prior to field-testing or deployment. Performing lab-scale tests reduces overall costs related to research and development as these tests produce results sooner, and have the potential to remove unsuitable candidates prior to field-testing.

Figure 1: 4100C Boss ultra-class mining shovel (After "4100CBoss-shovel," 2007).

The life of a set of shovel tracks is often determined by the life of the roller path. The roller path is built onto the inside of the tracks and allows the undercarriage to roll smoothly along the tracks. The undercarriage consists of the track shoes, front and rear idler pulleys, a rear drive wheel, and eight lower load rollers as seen in Figure 2. The lower load rollers support the weight of the shovel and move along the roller path. Due to high contact stresses, rolling contact fatigue, and debris contamination, the material loss on the roller path may cause the shoe to be disposed of pre-maturely (Boundary Equipment Co. Ltd., 2014). Specific damage mode mixtures are unique to each mine site, but the general characteristics for each mode can be identified.

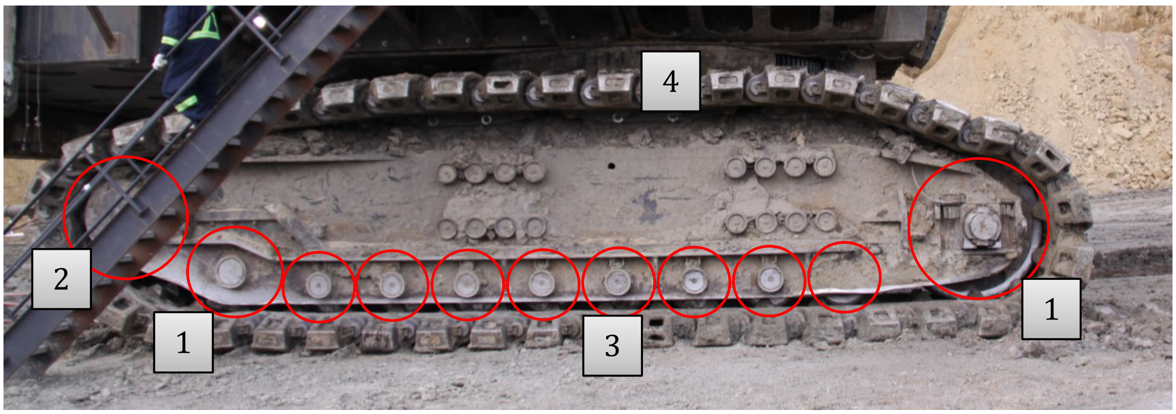

Figure 2: Shovel undercarriage, consisting of the idler pulley [1], drive wheel [2], lower load rollers [3], and track shoes [4]

Operating in an open pit mine subjects the roller path to debris contamination from two sources. First, sand-sized particles, and other ground material exposed to the atmosphere, may become airborne from wind erosion and be deposited on the roller path. Second, spillage from the digging face or track surroundings may introduce sand-sized or larger particles. Rock guards on the shovel prevent large boulder-sized materials from entering the roller path, but fail to prevent smaller sand or gravel-sized particles. Introducing particles or debris to the roller path leads to abrasion and gouging wear while the roller is in motion.

The shovel operation consists of both digging at the working face and walking (driving) between work locations. While digging, the shovel rolls on its roller path in reaction to digging and dumping motions, until it is stopped by track tension. Rolling under high loads introduced while working is expected to introduce multiple fatigue modes.

There is no current lab test for a track roller and track roller path (called the roller and roller path for the remainder of this document). As a result, design is reactionary and based on failures observed in previous models. This slows the development of newer, better, roller-path design. A lab test makes it possible to analyse new alloys or treatments, as well as shoe geometries, and test them in conditions equivalent to those seen in mines. Optimization of material for hard rock, soft, or abrasive mining conditions may increase the roller path service life, or reduce unexpected failure.

Current strategies consist of using two track steel alloys, A128 E1 and 4330. The A128 E1 alloy (also known as Hadfield or high manganese steel) is primarily used in hard rock mines and is generally the preferred alloy for track shoes due to its work-hardening abilities and resistances to abuse. The 4330 alloy (hardenable low alloy steel) is heat treated to a Brinell hardness of 340 (340 BHN) prior to service, and is primarily used in soft abrasive conditions such, as oil sands, as its hardening treatments increase its resistance to abrasion (Boundary Equipment Co. Ltd., 2014).

Chapter 2: Literature Review

2.1 Scaling Theory

2.1.1 Hoist Force and Suspended Load

When reproducing a set of equipment and conditions in a lab for testing, scaling offers a more manageable approach in terms of size and load. Conveniently, the general design of the shovel has changed very little in the past 60 years (Joseph, 2013). This persistent design allows for a direct scaling analysis using three shovel models including the P&H 4100, P&H 2300, and Dominion 500, with a dipper capacity of 44, 23, and 1.53 cubic meters respectively. The scale difference between the P&H4100 and the Dominion 500 can be seen graphically in Figure 3 with a total scale of 2.85 (Joseph & Shi, 2010).

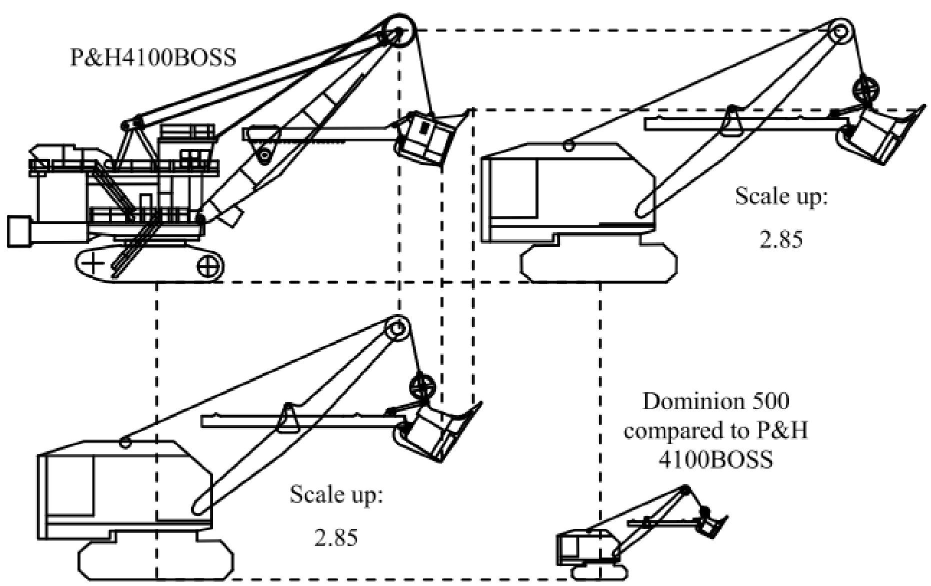

Figure 3: P&H 4100C Boss and Dominion 500 geometric comparison (After Joseph & Shi, 2010)

By using the ratio of hoist force and suspended load between the P&H 4100 and 2300 models, as seen in Table 1, the performance of each shovel can be compared for similarity. The two shovels were located in separate mine sites with the P&H 4100 in the oil sands at Fort McMurray and the P&H 2300 at a different mine site operating in hard rock (Joseph & Shi, 2010). While the digging conditions and equipment size varied, the ratio remained similar between the two shovels across the dig cycle suggesting that a lab model may be representative of multiple mining conditions with minor modifications such as the load magnitude or roller path material. The peak hoist force was determined using the ratios in Table 1. Table 2 shows the peak hoist force along with other specifications for the shovels.

Table 1: The hoist force (Fh) and suspended weight (G) ratio(s) (Adopted from Joseph & Shi, 2010)

Dipper Position	P&H 2300: F_h/G	P&H 4100: F_h/G
Tucked	0.85	0.83
Approaching face	0.85	0.83
Entering face	0.85	0.84
Digging	0.88	0.86
Exiting face	0.92	0.90

Table 2: Specifications for each shovel considered (After Joseph & Shi, 2010)

Parameter / Model	Dominion 500	P&H 2300	P&H 4100
Dipper capacity (m^3)	1.53 ($2yd^3$)	23 ($30yd^3$)	44 ($58yd^3$)
Dipper width (m)	1.2	2.9	3.6
Payload (kg)	2,600	39,000	75,000
Dipper handle (kg)	5,400	51,480	90,325
Suspended load (kg)	8,000	90,480	165,325
Peak hoist dig force (kg)	14000	125,280	285,560

Plotting the peak hoist force and suspended load against the dipper (bucket) capacity for the three shovels shows a linear relationship for the suspended load and a near linear relationship for the peak hoist force. This relationship is shown in

Figure 4: the dipper capacity for the three shovels studied is plotted against both the peak load and hoist force. Plotting a linear line for the peak hoist force indicates some discrepancy, with the P&H 2300 not in line with the P&H 4100 and the Dominion 500 (also in oil sand). As the peak hoist force represents the maximum force required throughout the dig cycle the discrepancy may be attributed to the digging conditions. The P&H 2300 operated in blasted and loose hard rock material while the P&H 4100 and Dominion 500 operated in in-situ material. While hard rock may result in a lower peak loading, the suspended load or total load remained the same with respect to the dipper capacity after the bucket had exited the face and was suspended in the air.

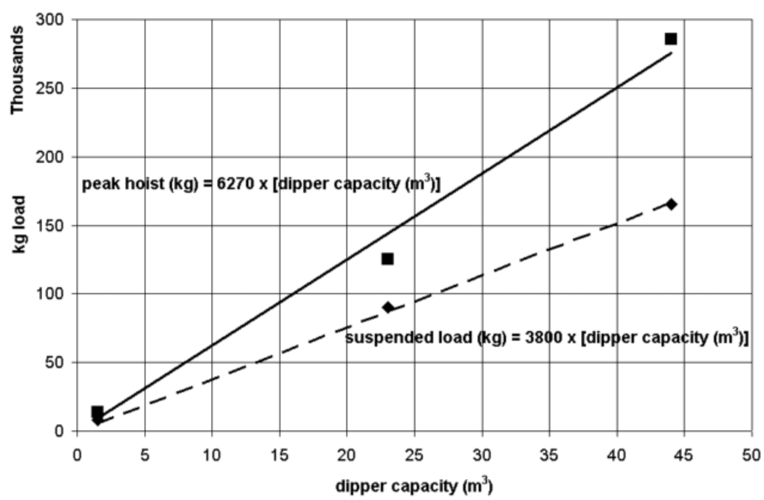

Figure 4: Dipper capacity comparison with the peak force and suspended load (After Joseph & Shi, 2010)

Due to the correlation between the peak hoist force and the size of the equipment, it was reasonable to expect a similar correlation for the loading on a roller and roller path arrangement between shovels of different sizes. This correlation suggests that it is possible to successfully recreate the roller and roller path arrangement in a laboratory using a single, programmable, roller.

2.1.2 Scaled Power Requirements

Different shovels have different power requirements. To determine the correspondence between the scale of the machine and its power requirements, a normalizing factor was developed (Joseph & Shi, 2010) for each shovel – shown in Table 3. The hoist forces were then normalized, by dividing the forces by their normalizing factor (Table 3), to create a unitless performance ratio that could be compared to determine commonality between the three shovels (see Figure 5). The defining features, such as peaks, plateaus, and cycles, were compared for an overall correlation between the small and ultra-class systems. The presence of a strong correlation suggest the power requirement and therefore the hoist forces were also scalable for lab testing (Joseph & Shi, 2010).

Table 3: Normalization factors for the three shovels (After Joseph & Shi, 2010)

Shovel performance data	Normalizing factor	Units
Dominion 500 hoist force	8000	kg
P&H 2300 hoist motor current	1300	A
P&H 4100 hoist motor current	1100	A

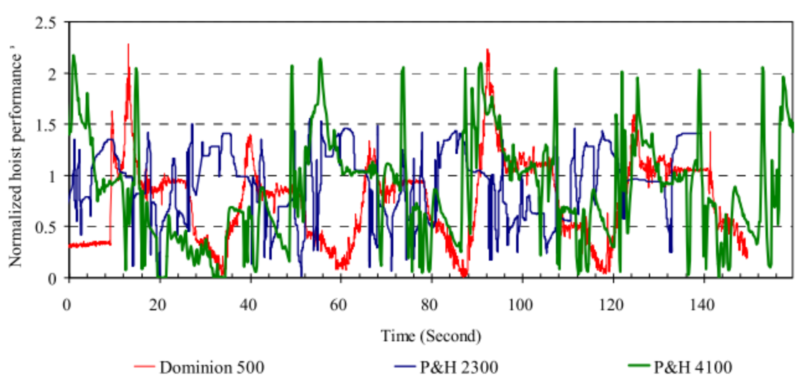

Figure 5: The normalized hoist performance for each shovel (After Joseph & Shi, 2010)

2.2 Railroad Comparison and Rolling Contact Fatigue

2.2.1 Rolling Contact Fatigue

In the absence of abrasives, rolling contact fatigue (RCF) was expected to be a driving damage mode to the roller and roller path system on an ultra-class mining shovel. RCF occurs as a roller passes over a material under high load causing sub-surface cracks and a progression to spalling. Spalling is defined as the surface material breaking into smaller pieces and occurs under high loads of both normal and shear stress. Under repeated loads or passes, the cracks grow and result in fractures and flaking.

The most direct correlation of RCF to the shovel roller path was found in the rail industry. Similar to a roller and roller path, a train uses hardened steel wheels to move along hardened steel tracks. RCF is a major cause for failure in track segments, and leads to their replacement (Patra, Bidhar, & Kumar, 2010). The rail industry in general has been increasing train loads, density, and speed in order to decrease operating costs (Patra et al., 2010). While these measures have succeeded in reducing operating costs, they have also increased maintenance costs, as it has become necessary to replace worn out rail segments and damaged axles or wheels. The wear was attributed to RCF, and could be divided into surface and subsurface cracking. While subsurface cracks have been initiated by defects in the rail, surface cracks are a more direct product of increased loads, traffic density, and speeds (Patra et al., 2010).

The stresses experienced by rails have routinely reached 1,500 MPa and exceeded 4,000 MPa with poorly fitted wheel and rail combinations (Patra et al., 2010). While a shovel's roller path ideally never reaches those stress levels under normal operating conditions (max 1,200, min 220 MPa), it experiences a much greater number of stress cycles per day. For example, the rail line located at Lisbon-Oporto in Portugal had been subject to 15 million tonnes per year, a load described as "considerable". The rail line has a planned lifespan of 20 years (Caetano & Teixeira, 2011). In contrast a typical 4100C Boss roller path has an expected life of 20,000 hours, equal to approximately 4 to 5 years of active service (Boundary Equipment Co. Ltd., 2014) and 40.6 million tonnes per year. Tables 4 and 5 show a summary of the usage of both the rail and the roller path.

Table 4: Summary of the Lisbon-Oporto Portugal rail line use

Peak Stress under Normal Operation	1,500 MPa
Stress Cycles per day*	1,825
Cars per day (4 rollers per car per rail)	456
Assumed average speed	80 km/h
Car length**	50m
Total active time per day	17 min

*(Caetano & Teixeira, 2011) **(CN Rail, 2013)

Table 5: Summary of P&H 4100 roller path use

Peak Stress under Normal Operation	1,200 MPa
Assumed availability	0.8
Assumed utilization	0.8
Rollers per track	8
Average cycle time*	45 sec
Total cycle count per day	9,800
Total active time per day	15.4 hr

*(Boundary Equipment Co. Ltd., 2014)

As seen in Figure 6, an un-deformed rail experiences both shear and pure compressive stress in the event of a moving, load-bearing wheel. If the wheel is applying frictional forces to the rail (e.g. braking or drive wheel) the shear stress amplifies and moves closer to the surface (Patra et al., 2010). While the 4100C Boss does not apply either loading or driving forces with the same rollers, the load bearing rollers would still induce shear stress at depth in the roller path and on the surface as a result of the combined resistive forces to the motion. These forces may include friction between the pin and bushing, but may also include rolling resistances between the rollers and roller path, or debris on the roller path.

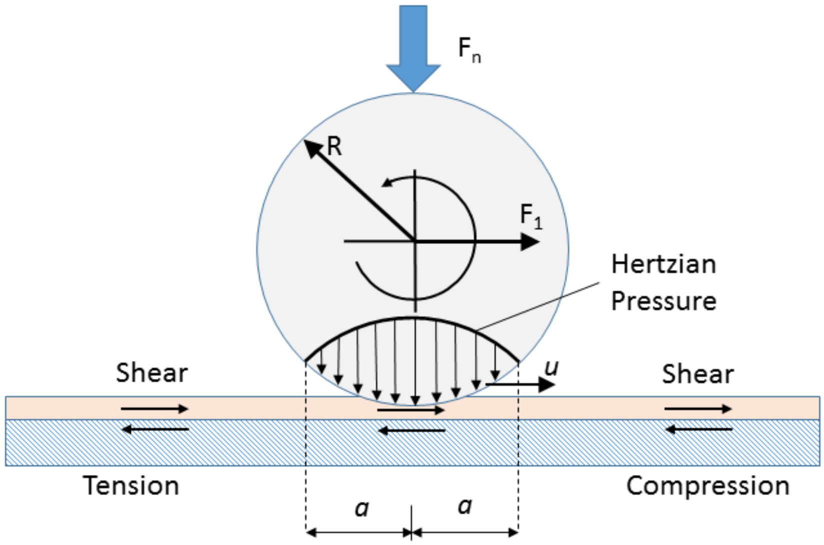

Figure 6: Stress variations near contact zone between wheel and rail (Adapted from Patra et al., 2010)

2.2.2 S-N Curve and P-F Intervals

The S-N curve is a common method of summarizing the effect that the cyclic forces have on a given material's life span (i.e. a material's fatigue behaviour). Figure 6 shows an S-N curve for a 300M grade steel sample. The stress ratio (R) is the ratio between the minimum and maximum stresses through each cycle – see equation [1]. For a stress ratio of R = -1, the minimum and maximum stresses would be equal and in opposite directions (e.g. max = 900 MPa in compression, min = 900 MPa in tension). An R = 0 ratio would result in the maximum stress being unchanged, but the minimum stress equalling 0 MPa, meaning the sample was in an unloaded state. As shown in Figure 7, the closer the stress ratio is to 1, the higher on the y-axis and the steeper the general slope of the curve. For any given stress ratio, a change in the maximum stress results in an exponential change in the required cycles to failure. In this example, a sample of 300M grade steel with a tensile strength of 1930 MPa was subject to 1,200 MPa stress cycles and failed in fewer than 10,000 cycles. A sample subjected to 700 MPa failed in fewer than 1,000,000 cycles.

$$R = \frac{\sigma_{min}}{\sigma_{max}} \qquad [1]$$

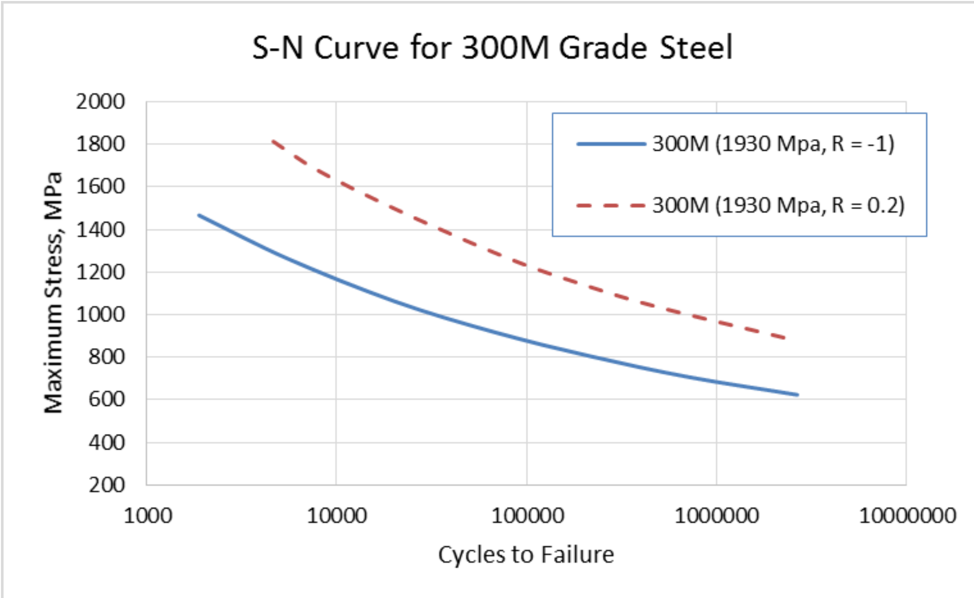

Figure 7: S-N curve for 300M grade steel heat treated to a tensile strength of 1930 MPa, R = -1 (Adapted from Boardman, 1990)

The potential to failure interval (P-F interval) is an expansion from the S-N curve, mapping the mean defect and mean fatigue life of the rail segments, or the interval between where defects first make an appearance and the end of life of the rail. An example of this interval can be seen in Figure 8. For an analysis of the rail S-N curve, the stress ratio was assumed to be 0 as the cycles were routinely between 1,500 and 0 MPa in compression while in use. Therefore, the variable was the maximum stress or the load on the rail cars. Following the S-N curve behavior a large stress cycle, or in this case a heavier rail car, would lead to defects and cause the rail to fail sooner, reducing its life. Similarly, a lower maximum stress would result in an extension of the rail life. The P-F interval was the difference between the manifestation of defects and the end of life of the rail. As the tonnage in Figure 8 was measured on a logarithmic scale, the effect of increasing the load on the rail exponentially reduced its total life.

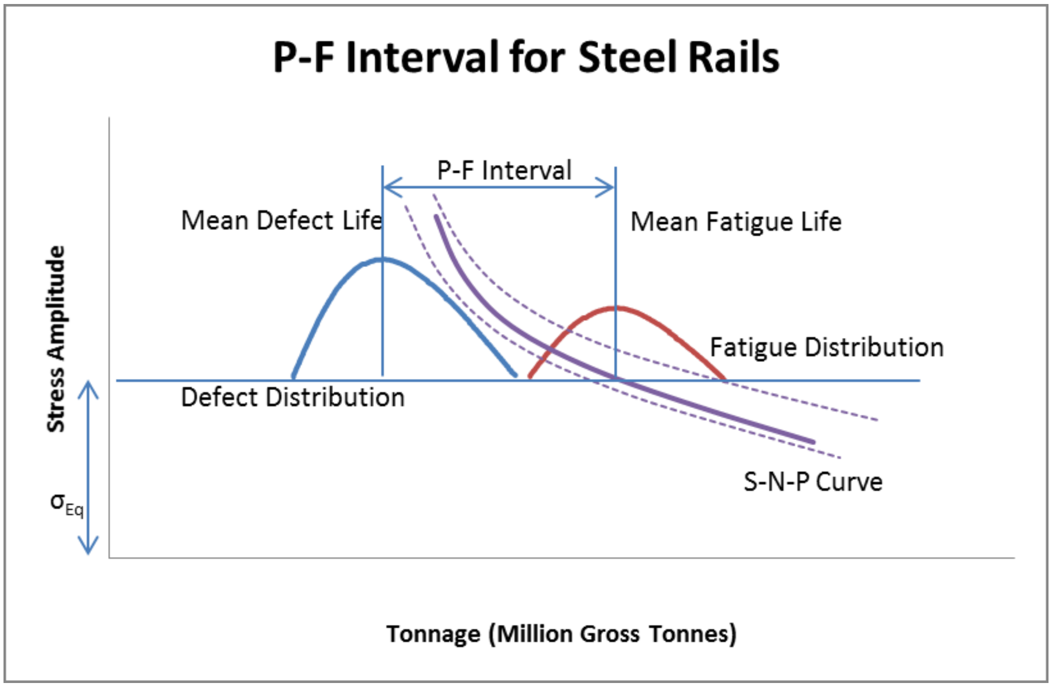

Figure 8: P-F interval – Adapted from (Patra et al., 2010)

Where:

- σ_{Eq} was the equivalent stress experienced across the life of the rail
- The S-N-P curve was the S-N curve for the rail material bounded by the data limits
- The defect distribution represented the range at which defects were first recorded during rail inspections
- The fatigue distribution was the range at which the rail failed due to fatigue and required replacement
- The P-F interval represented the difference between mean detection of defects and mean failure of the rail

The P-F interval in Figure 8 was targeted at the rail industry, and therefore measured rail life in units of tonnage. According to Patra et al. (2010) establishing a strong P-F interval is among the most important steps to create an effective preventative maintenance program. The P-F interval estimated the remaining rail life after the defects were observed, and allowed for scheduling the replacement or repair of the rail to reduce total down time (Patra et al., 2010). Unfortunately, due to the difference in workload, frequency, and conditions, the P-F interval must be determined independently for the mining industry and could not be approximated from Patra et al. Additionally, a true P-F interval could not be determined without testing the subject to failure. A shovel's roller path rarely reaches failure; having tracks fail in the field during active service is not ideal, as it can cause potential safety hazards and losses due to down time. Using the following steps, it is possible to estimate the point of failure by estimating the growth rate and initial size of the cracks (Patra et al., 2010):

1. Collect load data
2. Calculate max shear stress
3. Convert varying stress levels to an equivalent stress
4. Determine S-N curve and its mean from equivalent stress
5. Convert S-N curve cycles to million gross tonnes similar to Figure 8
6. Collect RCF data in million gross tonnes from field
7. Determine defect life and mean
8. Subtract means from steps 7 and 4, to obtain the P-F interval

2.3 Damage while Rolling

A known issue for rolling contact fatigue is high contact stress focused on a small contact area. Varying surface conditions react differently to the concentrated stress and result in multiple wear mechanisms (Stachowiak & Batchelor, 2005). Stachowaik and Batchelor (2005) outlined four operating conditions and their resulting wear. The operating conditions include a stiff roller operating on:

1. Unlubricated metals and non-oxide ceramics
2. Lubricated rolling
3. Oxide ceramics
4. Polymers

The most applicable occurrence was a stiff roller operating on “un-lubricated metals and non-oxide ceramics”, specifically the unlubricated metals, as shown in Figure 9. The surface of the material in direct contact with the atmosphere created an oxidized layer. As the roller moved over the oxidized layer, the high concentration of stress caused the layer to break or wear off (Stachowiak & Batchelor, 2005). The oxidation effect may not be as prominent on the roller path of a shovel due to the frequency of cycles, but spalling can still occur. Through cyclic loading, the wearing of the oxidized layer occurs repeatedly and causes the surface to wear or lose material over time. The material loss could be reduced by applying lubricants, but the wear from the cyclic stress loading would remain (Stachowiak & Batchelor, 2005).

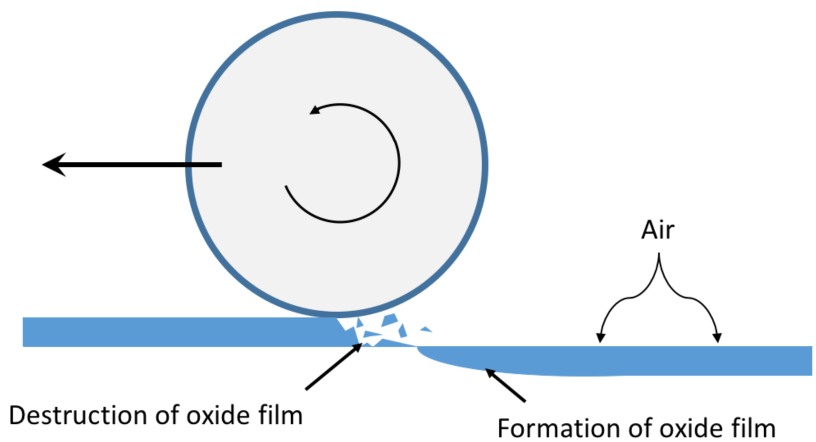

Figure 9: Unlubricated metals and non-oxide ceramics (Adapted from Stachowiak & Batchelor, 2005)

Stachowaik and Batchelor (2005) said that it is too difficult and not economical to achieve perfect lubrication where solid to solid contact was prevented. Contact can still be made directly through asperities or through debris suspended in the lubricant, as seen in Figure 10.

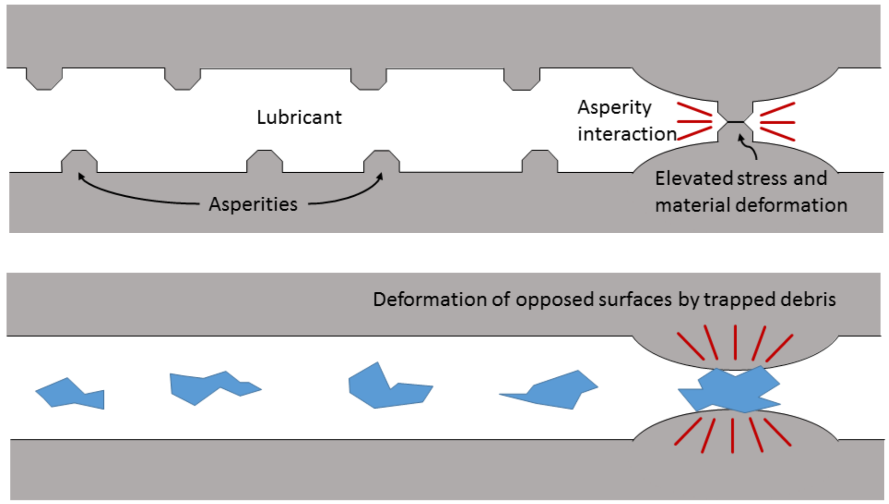

Figure 10: Contact between asperities and particles in lubrication (Adapted from Stachowiak & Batchelor, 2005)

With lubrication, solid to solid contact would still be common in mining conditions, because as a shovel operates outside, the roller path is exposed to ground material particles. Debris or other contaminants, like quartz crystals with a hardness of 1,200 Vickers, would adhere to the lubricant and persist on the roller path, causing abrasion and gouging. A constant flow of lubricant will prevent persistent contamination, but will also have negative effects, both economical and environmental due to the high volume required to maintain constant flow. According to Stachowaik and Batchelor (2005), "when the minimum dimension of the debris is greater than the minimum film thickness, damage to the contacting surface is inevitable." It is impractical to lubricate the roller path for ultra-class mining shovels, and will no longer be considered in this research.

Internal or cast-imbedded impurities form an initiation point for crack growth. Under cyclic loading, a subsurface crack can grow to form a surface flake. Flakes become debris particles that contribute to gouging and wearing while on the roller path. Pitting occurs on the surface material as flakes are removed, developing subsurface secondary cracks (see Figure 11) which contribute to further pitting or spalling. Spalling and pitting may form on the surface, but result in greater material loss when initiated on the subsurface (Stachowiak & Batchelor, 2005). The flake size in Figure 11 was exaggerated for demonstrative purposes.

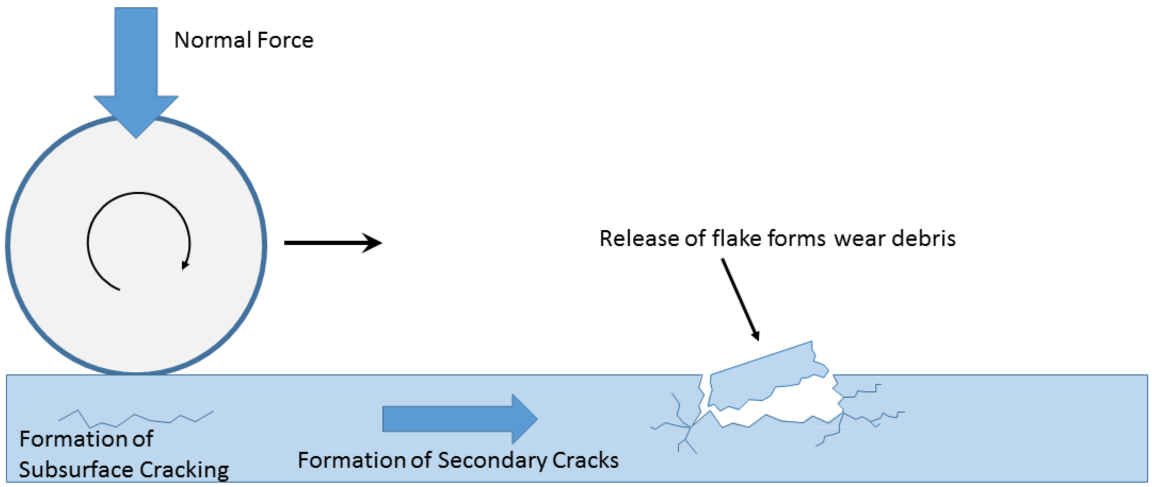

Figure 11: Flaking and formation of secondary cracks under cyclic roll loading (Adapted from Stachowiak & Batchelor, 2005)

2.4 Cyclic Fatigue Loading – 4340 Grade Steel

Determining the fatigue life of any grade of steel requires multiple factors such as stress concentrations, loading conditions, and temperature (Boardman, 1990). Figure 12 shows that increasing the tensile strength through heat treatment significantly increases the number of cycles required to fail the steel. Altering the temperature of the steel also affected the fatigue strength. A 300-degree Celsius change was required for a significant difference in the fatigue life (Boardman, 1990), but such a temperature change would not occur during regular shovel operations. Shovels work in open pit mines and are therefore affected by seasonal temperatures. The roller path temperature is also affected by regular use or load cycles. While it is something to be aware of, temperature change is not expected to be a major factor in the life of the 4330 roller path for the P&H 4100C Boss shovel.

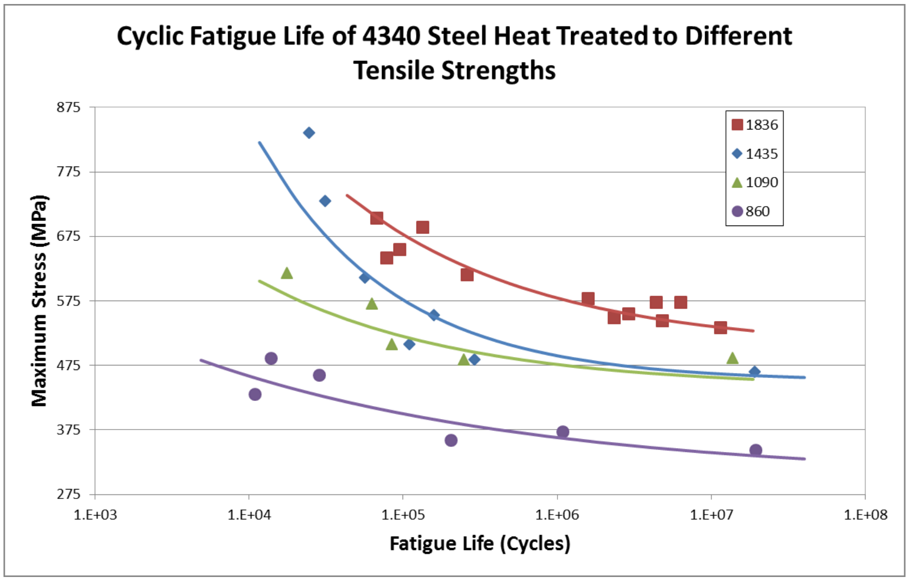

Figure 12: Fatigue life of 4340 steel, heat-treated to different tensile strengths (R = -1) (Adapted from Boardman, 1990)

According to Boardman (1990), the presence of defects, impurities, cracks, or notches had the greatest impact on fatigue life for steel alloys. Figure 13 shows the relationship for notches using a 4340 steel sample. In this example, adding a notch resulted in a difference of three orders of magnitude between the two points of similar stress cycles.

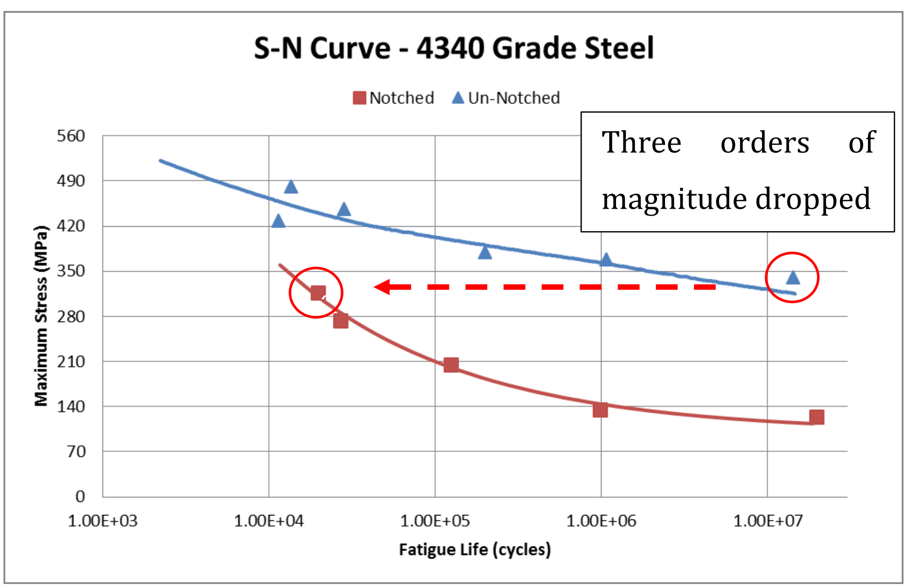

Figure 13: S-N Curve for Notched and Un-notched 4340 Steel. (Adapted from Boardman, 1990)

The range of the stress ratio tested by Boardman (1990) was 0.2 to -1. As the stress ratio was reduced, or moved closer to 1, the tolerable stress cycles were increased, as seen in Figure 14. For a given point on a shovel roller path, the stress ratio is assumed to be 0. The minimum load at a given point occurs as the roller path at that point is unloaded, and the maximum load occurs as the roller passes over it.

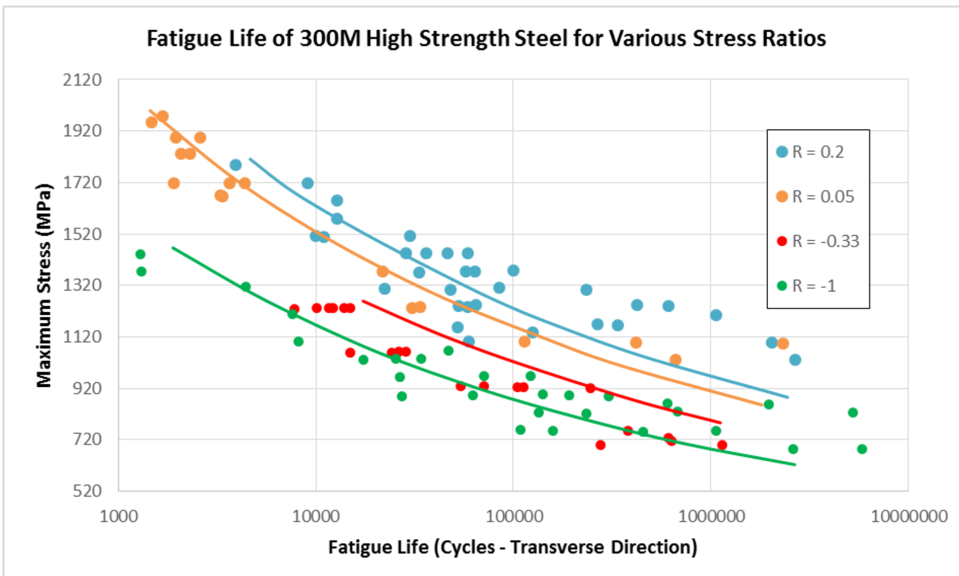

Figure 14: Fatigue life for 300M steel (a modified 4340 alloy) under cyclic loading, where R is the ratio between the minimum and maximum stress. (Adapted from Boardman, 1990)

Hadfield steel (a high manganese alloy) is known for its work-hardening abilities, or ability to rapidly increase in hardness as it is worked. As Hadfield steel is subjected to high stresses it produces a layer in the stressed region that is more resistant to fatigue or damage (Kang, Zhang, Long, & Lv, 2014). Hadfield steel is commonly used in the roller path of shoes in hard rock mining (Boundary Equipment Co. Ltd., 2014) and railway crossings (Kang et al., 2014).

Over the service life of a Hadfield steel roller path the hardness increases with the stress cycles. The fatigue strength of Hadfield steel increases with the stress ratio (Kang et al., 2014). As the loads on the roller path are equal to the ground reactive force, the stress ratio in the roller path increases proportionately to the hoist force. Because fatigue strength increases with the stress ratio, Hadfield steel is commonly used for the roller path in hard rock mines. Due to the high rate of work-hardening, it is unnecessary for the steel to undergo heat treatments and hardening prior to service. Therefore, while Hadfield steel initially has a poor resistance to wear, it will become highly resistant, but only after a certain level of wear has already occurred (Harzallah, Mouftiez, Felder, Hariri, & Maujean, 2010a). As seen in Figure 15, the initial 15,000 cycles produced the greatest rate of hardening followed by a lower rate thereafter. To reach a hardened state, the Hadfield steel must first deform. Harzalla et al. placed a Hadfield steel ball between two circular disks or tracks and rotated the lower track, causing the ball to spin. As the test progressed, the contact width between the ball and the plates increased, and as shown in Figure 15, the majority of deformation occurred in the same initial 15,000 cycles as the hardening. Hadfield steel shovel track shoes come new with the roller path fluted or grooved to allow space for the material to flow as they are worked (see Figure 16). Over the initial service life, the roller path flattens through shovel operation and can reach hardness levels in excess of 400 Brinell (BHN), increasing resistance to operational damaging (Boundary Equipment Co. Ltd., 2014).

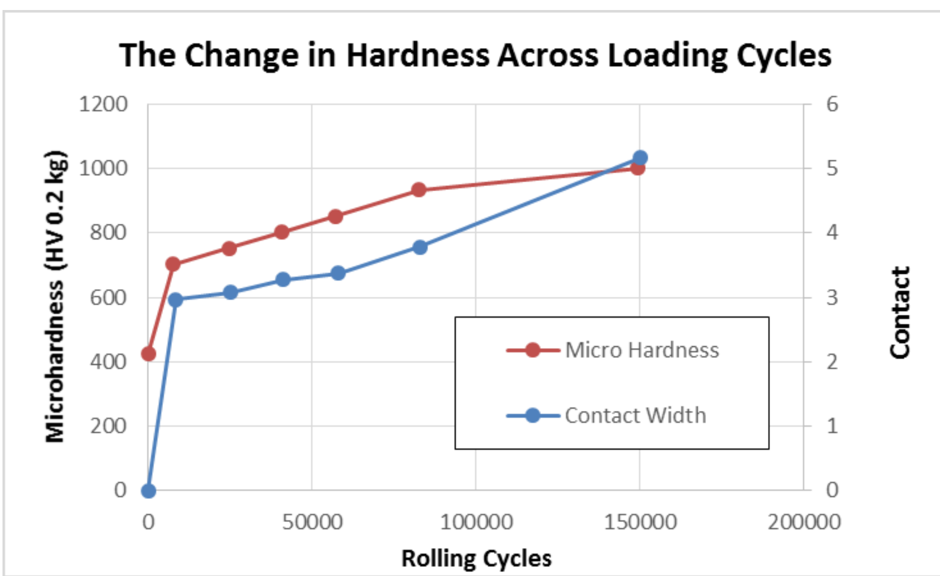

Figure 15: Vickers hardness change in relation to loading/rolling cycles. (Adapted from Harzallah, Mouftiez, Felder, Hariri, & Maujean, 2010b)

Figure 16: Roller path for high manganese shoes

2.5 Shear Crack Growth on Surface

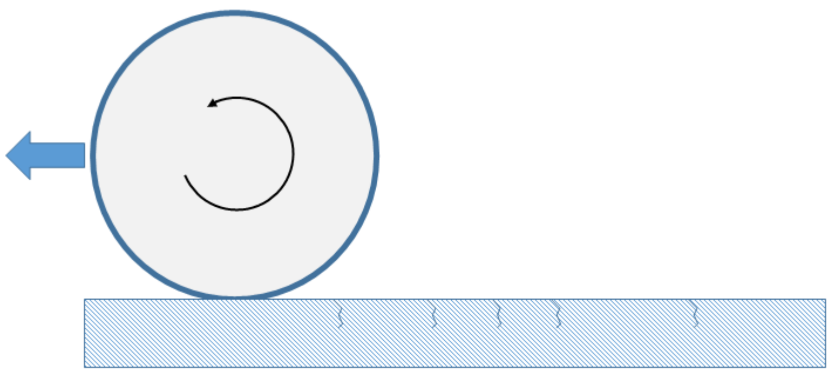

Figure 17: Surface cracks developed from wheel sliding or wheel induced tension

Surface cracks form as a result of the uni-directional flow of material from wheel friction and partial tangential forces. These cracks can cause an increase of 10x in shear strain when located on the surface and may lead to spalling or fracturing if permitted to grow (Ringsberg, 2005). According to Ringsberg (2005) shear-initiated cracks are driven by stresses associated with the wheel-rail interface. Material properties, lubrication, and loading determine if rolling contact fatigue or wear will drive rail damage.

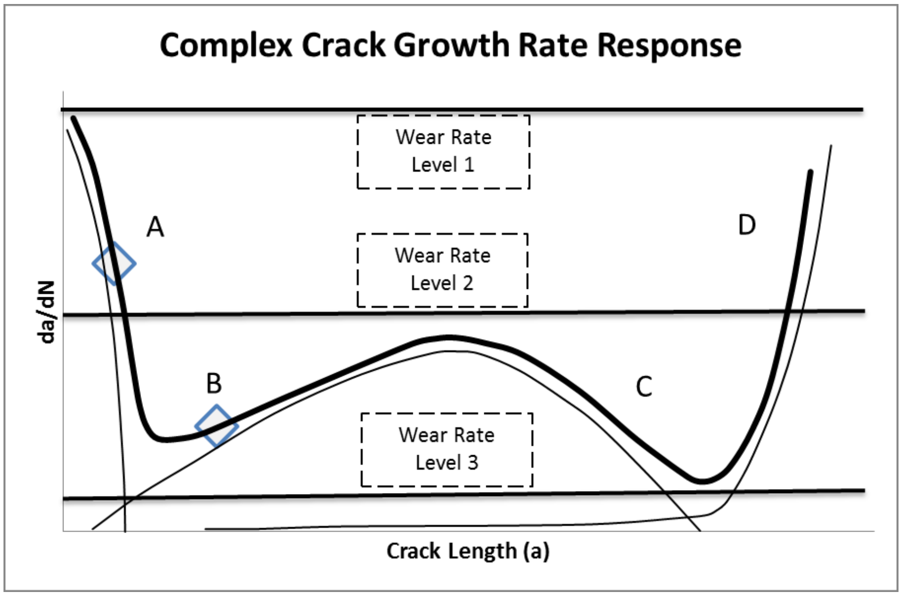

Figure 18: Life cycle of a crack in a rail scenario. (Adapted from Ringsberg, 2005)

Where:

a = the crack length.

N = the load cycle count.

da/dN = the change in crack length per cycle.

Figure 18 shows the life of a surface-shear crack and its relative growth rates. At initiation in Zone (A), the growth rate was high but rapidly decreased. Crack growth then became driven by low cycle fatigue. As it grew, the effective stress at the crack tip increased. Because of this increase in stress, the rate of growth also increased through Zone (B). The growth rate was stunted upon reaching the perimeter of the high stress zone, and as it was then subjected to lower stresses, the growth rate decreased as shown in Zone (C). Eventually the crack growth was dominated by bending and by tensile stresses and increased again to failure (Ringsberg, 2005).

While a rail is considered a rigid system subject to bending and flexing under the load of a train, the shovel track system is made of several shoes, pinned together, allowing for a degree of adjustment to ground and loading conditions. Flexibility would in effect protect the roller path from some of the bending forces, but it is not expected to protect the roller path from any tangential or shear forces.

Subsurface crack growth initially occurs within 20 degrees parallel to the surface. After exceeding a total crack length of 0.4mm, the direction changes and grows toward the surface and leads to spalling failure (Ringsberg, 2005). This directional change decreases the maximum shear strain range due to the geometry between the crack and the direction of the load. Ringsberg (2005) performed a finite element analysis of the crack growth but noted that it only accounted for one cycle, and therefore was an overestimation because it failed to account for work-hardening over a multi-cycle test. He observed that crack growth, even when truncated by wear, remained positive. The cracks continued to grow as material was worn off, showing that the crack growth rates were faster than the track wear rates. The roller path of a 4100C Boss shovel is subject to similar stress levels under normal operating conditions (see section 2.2) to those studied by Ringsberg (2005), suggesting that spalling is a contributing cause of material loss.

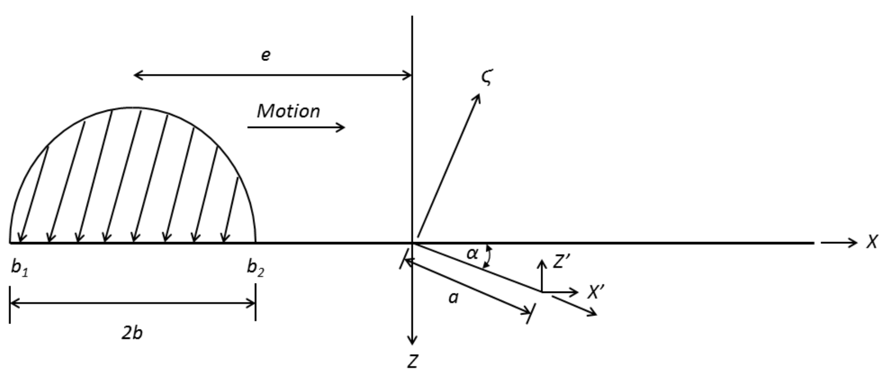

Figure 19: Finite element model used by Ringsberg to predict crack growth. (Adapted from Ringsberg, 2005)

2.6 Abrasive Wear

Abrasive wear is expected to be a major contributor to the damage seen on the roller path. Abrasion, while present at all mine sites, is particularly pronounced while mining oil sand or Bitumen. Bulldozer units, with hardened abrasion-resistant blades, operating at the Syncrude site in Fort McMurray required reskinning after 5000 hours of use due to excessive wear. Reskinning the blade required 20-40 man hours, with an additional 160 man hours for refurbishment of the damaged blade (Llewellyn & Tuite, 1995). Ground engaging tools (GET), such as bucket teeth on a 4100C Boss mining shovel, also experience high levels of abrasive damage. The volume of material loss to bucket teeth can be calculated using equations [2] and [2]. Using the example data from Chapter 4, and assuming an arrangement of nine chromium carbide teeth on the bucket, the volume of material lost per 12-hour shift was calculated to be 214 cm^3 for each tooth.

$$V = \frac{E_T}{Hv \times 10^9} \qquad [2]$$

$$E_T = \frac{((P_p - P_c\ ) \times t)}{2} \qquad [3]$$

Where:

V = the volume lost to abrasion (m^3).

E_T = the total energy absorbed by the bucket teeth (Joules).

Hv = Vickers hardness rating in GPa.

t = the time required to complete a dig (seconds).

P_p = the peak power level consumed by the hoist motor while digging (Watts).

P_c = the hoist motor power required to suspend the full bucket (Watts).

While ground engaging tools are pushed through or across abrasive material, a shovel's roller path is not, and requires spillage or other forms of deposition to occur. Additionally the deposited material is then compressed between the roller and the roller path. Therefore, while ground engaging tools experience low stress abrasion at near-total surface area coverage, the roller path experiences high stress abrasion at an unknown, but lower, coverage. Because of the dissimilar abrasive wear between the roller path and other surfaces, such as the bulldozer blade or bucket teeth, it is currently not feasible to predict the damage done to the roller path by abrasion. Development of a roller path specific test, would allow for the feasible analysis of abrasion damage, and provide a method to test new, abrasion-resistant, roller paths prior to field testing.

2.7 Summary

It is reasonable to move forward with the development of a roller path test. Research exists concerning spalling, crack growth, and rolling contact fatigue, the most similar of which is concerning the rail industry. While similar, the rail and roller path are subject to different loading patterns and environmental conditions. Increased frequency in stress cycles, a reduced oxidization period, and an increase in sand-sized particle contamination can all alter the life of the roller path. The impact each of these differences will have on the life of the roller path is unclear, particularly after stacking as it may, over- or underestimate the overall damage or material loss to the roller path. Abrasive wear, to be studied in the future, is expected to be a major contributor to roller path material loss followed by spalling and rolling contact fatigue. Scaling the roller and roller path arrangement for lab testing should provide an accurate basis to determine the effects of each mechanism for future roller and roller path design.

Chapter 3: Objectives

The purpose of this study is to construct an accurate scale model of the shovel roller and roller path arrangement that will make it possible to develop improvements to the system. Investigating an unproven roller path may increase service life and a reduce maintenance costs. New materials and geometries for either the track shoes or rollers could be tested. Adding site-specific intrusive material to the roller path would make it possible to more closely represent the mining conditions. The lab apparatus was to be both programmable and customizable to apply a range of scenarios. Initially the lab arrangement would be set to reproduce current damage as seen on the shovel. After accuracy is shown, new materials or geometries may be tested. The indicator for roller path life used by industry is depth of material lost, and was the target for reproduction in the lab. For vertical loading the cube root scaling method was used to produce equivalent contact stress on the roller path. Because the contact stresses in the lab are set to be the same as those in the field, it's not necessary to scale the horizontal motion of the roller on the roller path. Maintaining one to one horizontal motion is positive in that it yields a larger sample for analysis and is less likely to over- or underestimate the effect of abrasion and gouging. For more information on the dig cycle and the process that causes the suspected wear, see Section 4.2.

The design objectives were set as:

1. Collect and analyse hoist data to determine roller and roller path loads.
2. Design a test apparatus that mimics the field conditions at a lab scale including:
    a. The loads experienced the roller(s).
    b. The movement of the roller on the roller path.
    c. The contamination of the roller path with mine specific debris.
3. Reduce the required time to fail the lab scale roller path to a manageable level

The experimental objectives were set as:

1. Operate apparatus under constant supervision and monitor for design flaws.
2. Confirm the re-creation of roller path damage as seen in the field including:
    a. Abrasive wear
    b. Gouging wear
    c. Indentation
    d. Rolling contact fatigue
    e. Toe-nailing or the flow of material along the roller path (See section 6.2.5 for description)
3. Evaluate wear rates and confirm the validity of the cube root scaling method in determining loads used in the lab.
4. Evaluate the coupon wear behavior using microscopy.

Chapter 4: Field Data and Behavior

To accurately recreate the field stresses and conditions in the laboratory environment, testing included the use of a true load-bearing roller from a smaller shovel, coupons made with similar material and heat treatments as the roller path, and a system of hydraulics to mimic the motions that occur during the dig cycle.

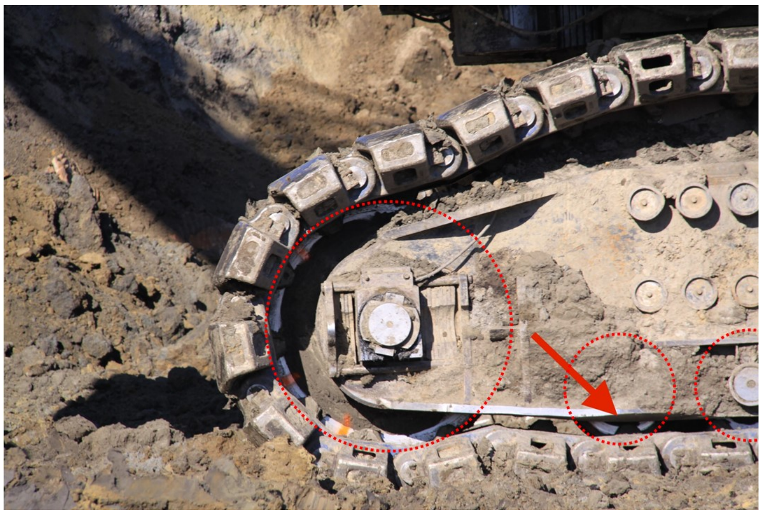

Figure 20: Lower load bearing roller to recreate on a 4100 XPC

4.1 Pre-Testing Data Collection and Analysis

To determine the forces on the lower load rollers, the following steps were used:

1. Hoist data was collected from field scale shovel operations (volts, amps, time, speed).
2. Conversion of hoist power requirements to hoist force (MN).
3. Forces on shovel body were reduced to body force and hoist force (downwards), and ground reactive force (upwards) – see Figure 21.
4. The location of the ground reactive force was determined through a summation of moments using the free body diagram seen in Figure 21.
5. The ground reactive force was expanded across the length of the track system
6. The expanded reactive force was reduced to points on rollers.

7. For negative forces on rollers, the force was reset to zero and steps 5 & 6 were repeated with the track system shortened to exclude the now zeroed roller.
8. The dig cycle key phases were isolated to produce an average load for each roller in each phase.

Step 7 was necessary as it is impossible to have negative loading on the roller path. Such loading would indicate a tensile load between the unattached roller and roller path. Tension is not possible as the roller would be suspended above the roller path with a total load of 0 MN. Resetting the force to zero for the suspended roller allowed the ground reactive force to be spread across the rollers still in contact with the ground. Removing the free hanging rollers from the equation decreased the magnitude or the load on the rollers to the expected real world value, as they were no longer over compensating for negative loading on the system. Further details on each step will be illustrated below. See Appendix H for code used to run steps 4 – 7 for each data point.

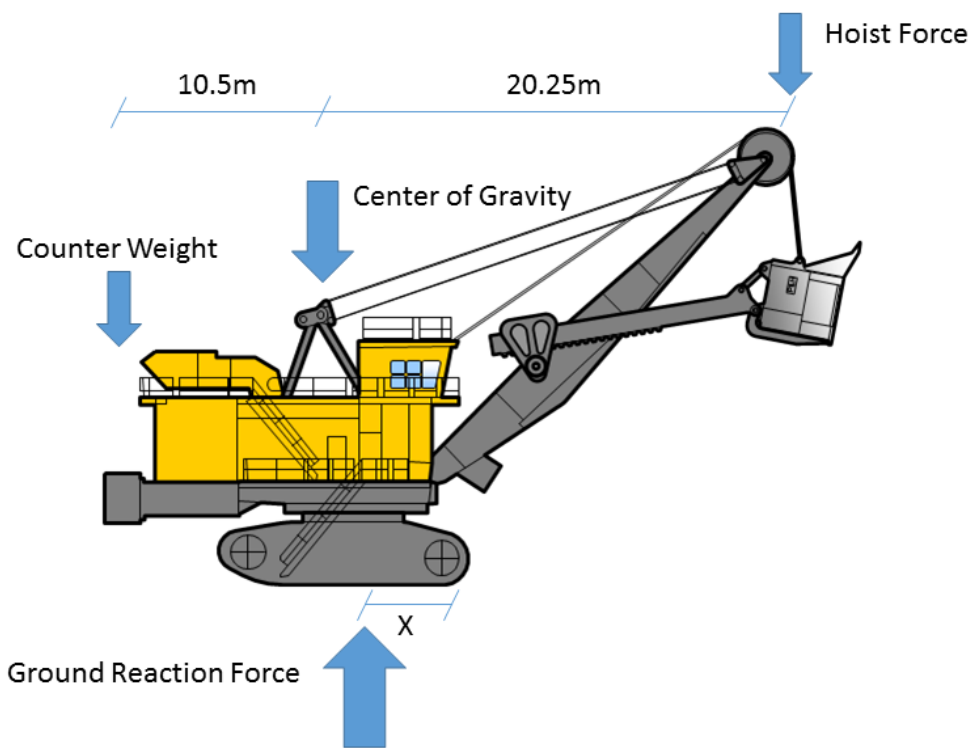

Figure 21: Free Body Diagram of Shovel and Forces (Adapted from Marek, 2006)

Step 1 – Collecting the data. Hoist force data was already in the database at the University of Alberta for the 4100C Boss shovel digging in the oil sands. Additional hoist data was collected from a 4100 XPC (Sunhills Mining, 2015). The report included time, voltage, amperage, field amperage, and rope position.

Step 2 – Equation [4] was used to convert from volts and amps into Newtons of force.

$$F = \frac{(V_1+V_2)*A}{v} * \eta \qquad [4]$$

Where:

F = Force in Newtons

V_1 = Voltage of hoist motor 1

V_2 = Voltage of hoist motor 2

A = Current in Amps

v = Velocity of hoist rope in m/s

η = Hoist motor efficiency rating *

* Note: While the standard hoist motor efficiency rating is 86% (Joseph & Shi, 2012), an efficiency of 100% was used for this analysis (see section 6.2.2 for further details).

The velocity was calculated between readings, using the difference between the rope positions. Each data point was 0.1s. Velocity was calculated with equation [5]:

$$v = \frac{(d_1-d_2)}{0.1} \qquad [5]$$

The resulting force was then graphed and is shown in Figure 22.

Step 3 – The 4100C Boss tare weight was 1,410,184 kg (Joy Global, 2012) or 13.83 MN and balanced over the pivot point while the bucket was suspended and empty. Using the hoist force data the tare hoist force was determined to be 0.64 MN, which was then subtracted from the total weight of the machine to determine a resultant vehicle weight of 13.19 MN. The center of gravity of the shovel was located 20.25m from the hoist rope according to a summation of moments about the hoist rope, similar to equation [7] and can be seen in Figure 21.

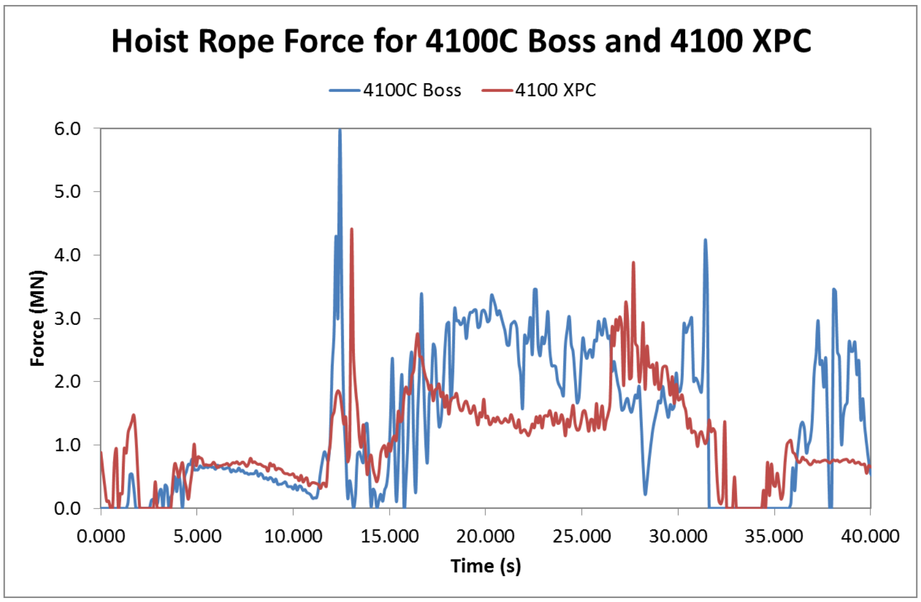

Figure 22: Hoist rope forces of the 4100C Boss and 4100 XPC shovels

Step 4 – The magnitude of the ground reactive force for each point in the data set was calculated by summing up the hoist force for that data point calculated in Step 2. The location by was calculated summing moments about the 4100C Boss center of gravity using equation [6]

$$F_R = F_{CW} + F_H + F_M \qquad [6]$$

$$L_R = \frac{F_{CW} * L_{CW} + F_H * L_H}{F_R} \qquad [7]$$

Where all locations were taken with respect to the 4100C Boss center of gravity (See Figure 21) and:

L_R = Location of the reactive force
F_R = Magnitude of the reactive force
F_{CW} = Counter weight
L_{CW} = Location of counter weight
F_H = Hoist force
L_H = Location of hoist force
F_M = Machine tare weight

Step 5 – To distribute the reactive force across the load rollers, it was first necessary to convert the reactive force into a distributed load. Equations [8] and [9] were rearranged for w_1 and w_2.

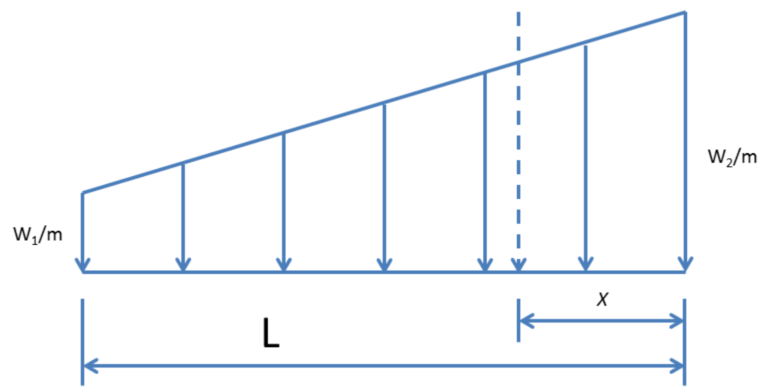

Figure 23: Relationship between a point and distributed load

The original equations were:

$$W = (w_1 + w_2)\frac{L}{2} \quad [8]$$

$$X = \left(\frac{2w_1+w_2}{w_1+w_2}\right)\frac{L}{3} \quad [9]$$

Equations [8] and [9] were re-arranged as:

$$w_1 = \frac{3X}{2W} - \frac{2W}{L} \quad [10]$$

$$w_2 = \frac{4W}{L} - \frac{3X}{2W} \quad [11]$$

Where:

- W = The ground reactive force.
- L = The supported length of track (6.4 meters in this case).
- x = The location of the reactive force corresponding to Figure 21.
- w_1 = The total load on the heel end of the track system.
- w_2 = The total load on the toe end of the track system.

Note: The toe end of the track system is the front end, or the end closest to the working face. The heel end is the rear most end, located under the counterweight of the shovel.

Step 6 – Due to the true geometry of the undercarriage, the reactive force is not a distributed load but instead a collection of several point loads, one point on each roller. To determine the magnitude of these point loads the length of the chassis was divided into equal portions centered on the rollers and the distributed load in each portion was summed onto the roller as shown in Figure 24.

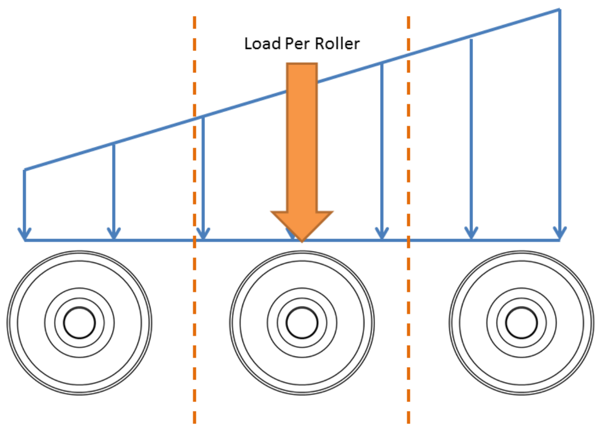

Figure 24: Concentrating the distributed load onto the lower rollers

Note: The load per roller was the summation of the distributed load, within the rollers area of influence marked by the dashed lines.

Step 7 – In the event of negative loading on any of the rollers, the outermost (toe or heel) negatively loaded roller was reset to a zero force value and the chassis length

(L) was shortened by the supported portion of that roller (0.8 meters). Steps 5, 6, and 7 were repeated until no negative force values remained.

Step 8 – The key dig cycle steps are as follows:

1. The bucket is empty and suspended in the air (after dumping into truck)
2. The shovel is in the empty tucked position
3. The shovel is in mid dig (digging forces are highest)
4. The bucket is full and suspended in the air

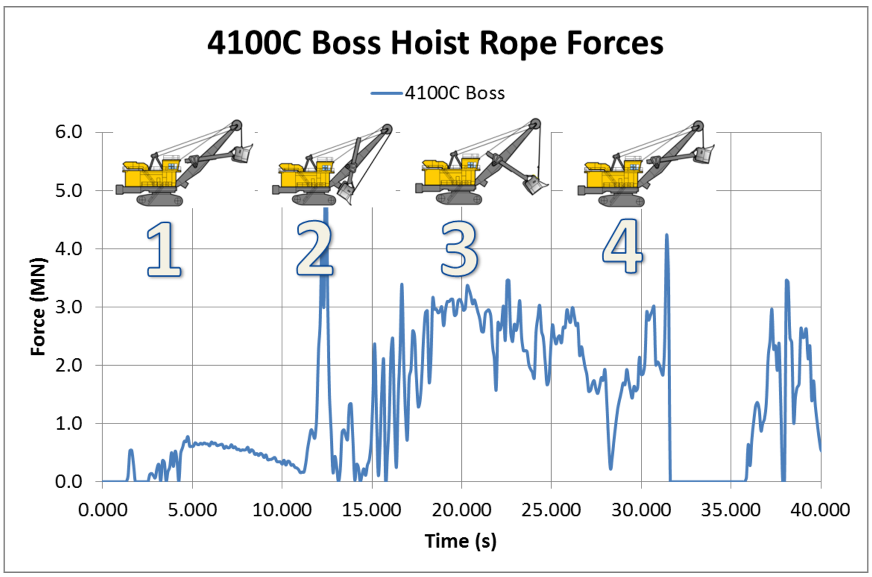

Figure 25: Key steps for one dig cycle on a P&H 4100 XPC (Adapted from Marek, 2006)

Unfortunately, isolating these key steps in a dig cycle required some human judgment, and therefore introduced error to the process. The bounds of each phase were identified, and events such as the large spike in Phase 2 were excluded. This large spike in force represents the initial contact between the bucket and the ground. To include it would overestimate the loading on the lower rollers when the shovel is sitting empty and tucked.

Following these steps produced the loading profile shown in Figure 26. The curvature in both the max digging and full suspended steps were a result of reducing the data points to an average. Individual data points result in linear loading across the load bearing rollers. Figure 27 shows the calculation of the distribution of average loads Figure 27. The mean was then taken to obtain an expected value of the load on each roller per cycle. See Appendix C.1 for all phases.

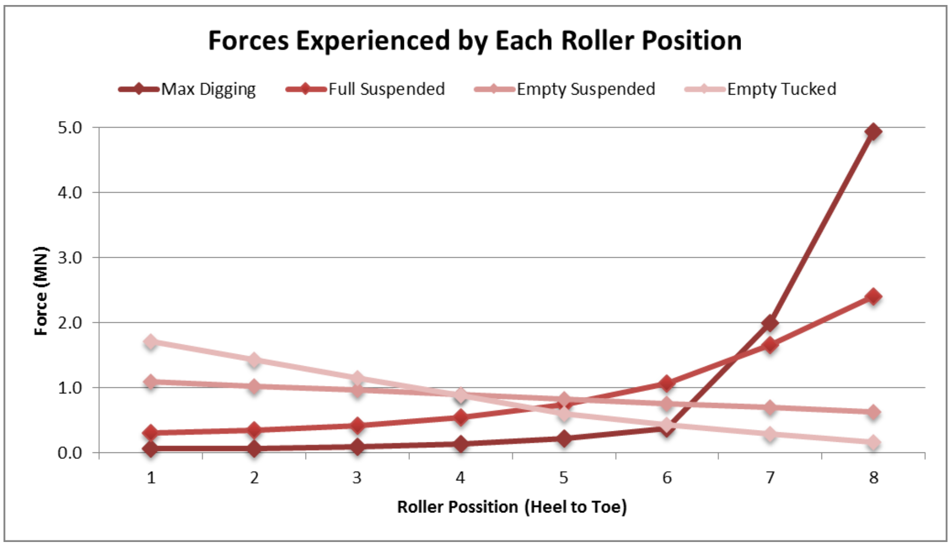

Figure 26: Load levels for the rollers in each key dig cycle phase. Position 1 under the counterweight and Position 8 at the face.

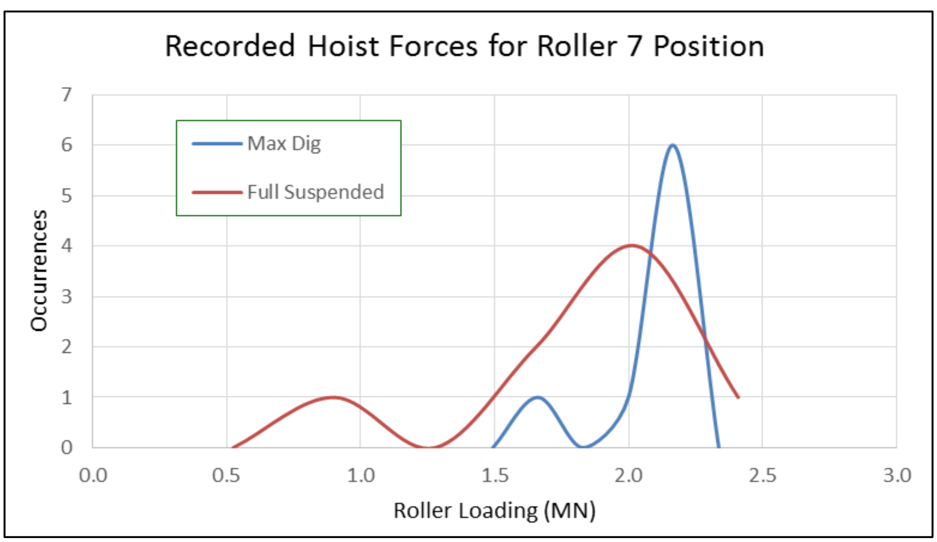

Figure 27: Distribution of roller loads at Position 7 for both the max digging and full suspended phases

The large spikes in the hoist force created problems in analysis. While equations [10] and [11] assume that the system is stable, the hoist forces at the large spikes were high enough to tip a shovel over. Due to the brief, impact like nature of the loads, tipping did not occur and it was assumed that the shovel remained stable. The roller loads calculated at the spikes ranged from -2×10^6 MN to 6×10^6 MN, which was incorrect and large enough to obscure the correct results calculated elsewhere. The calculated roller forces and the sum of the machine weight with the hoist force were compared and revealed that the two forces were equal until the ground reactive force was directly under roller position 8 (the most forward position), the position at which the discrepancy occurred. To eliminate this issue of shovel imbalance, a maximum hoist force was selected at 3 MN which placed the ground reactive force slightly behind roller position 8. A hoist force of 3.13 MN placed the ground reactive force directly under position 8 but was not used, as a discrepancy was observed between roller loads and ground reaction forces. All hoist forces were capped at 3 MN with the excess added to the force at the next data point to maintain the total force observed. The process was repeated for the entirety of the data set as shown in Figure 28.

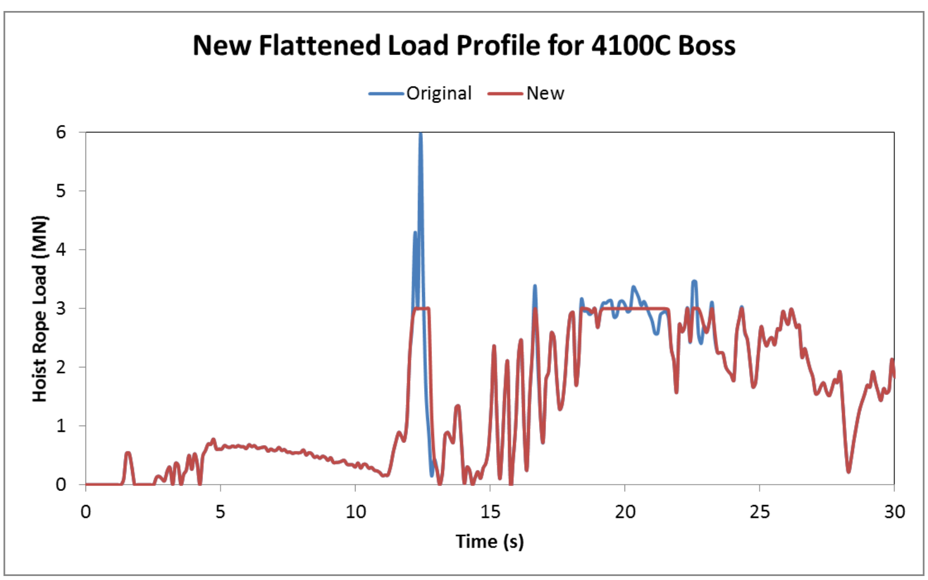

Figure 28: Hoist rope forces after flattening at 3 MN

After calculating the loads for each roller position on the shovel, the cube root scaling method was then used to determine the lab scaled loading for each roller position. The scale factor used in this scaling law was 2.61, the scale difference between the diameter of the shovel's roller (30") and the test roller (11.5"). See section 5.2 for more details on the test roller.

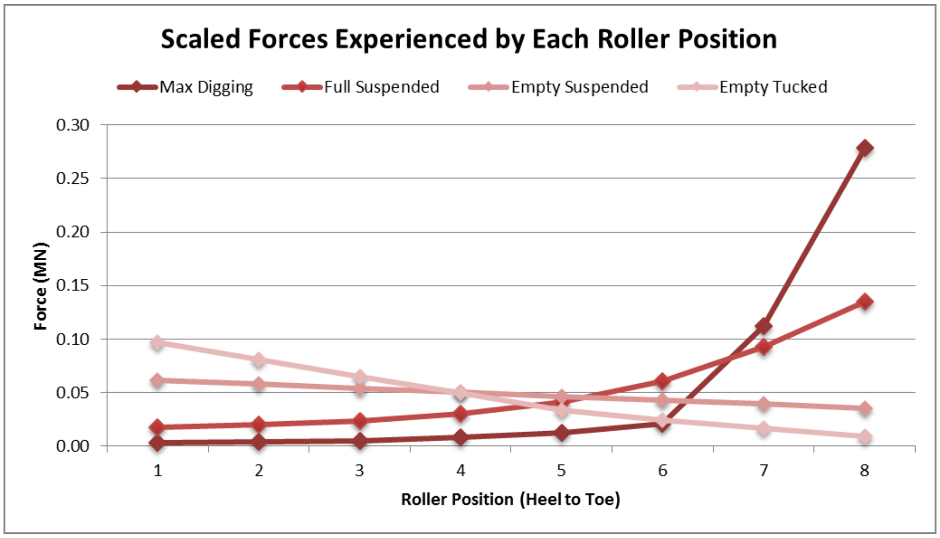

Figure 29: Load levels for each roller position after cube root scaling was applied

4.2 Field Behaviour to Reproduce

The observation of a 4100 XPC shovel in operation (Sunhills Mining, 2015) revealed that the movement of the roller on the roller path was as follows:

1. The shovel started in the tucked position.
2. Immediately upon bucket contact with the face, the roller rolled backwards approximately three inches on its tracks, depending on track tension.
3. The shovel completed a dig.
4. Upon rotating to dump its load, the shovel rolled forwards to its starting point on the tracks.
5. The shovel dumped, rotated back to the working face, and returned to the tucked position.

The roller path loading was assumed to remain constant through the roller movement. This assumption holds in Step 2 of the dig cycle but fails in Step 4 if evaluating an individual cycle, and only holds if evaluating multiple cycles. At the initial stage of Step 4, the shovel was in line with its tracks with the bucket filled. The ground reactive forces were focused under the front rollers at this stage (see Figure 26). Upon rotation, the loaded bucket passed directly over the toe end of one track as it moved to its final position over the truck approximately 90 degrees from its original position. While passing over the toe, the forces were focused in the front most rollers of that track and are reduced in the rollers of the opposing track - see section 6.2.4 for an alternate load profile simulating this behavior. Truck loading is performed on both sides of the shovel however, and considering a combination of multiple load cycles the assumption of steady load is expected to hold for the trial test and proof of concept.

Figure 30 shows roller path damage rates that were collected from the field. As the sample roller paths were made from the A128 E1 alloy, the surface deformation was initially high but later reduced to a seemingly linear rate. Because the data resolution was poor, it was not known how quickly the initial deformation happened in stage 1 of Figure 30, and how much roller path material was lost from damage. However, material loss rates observed at later stages could be identified to be 0.118 mm/hr for stage 2 and 0.093 mm/hr for stage 3.

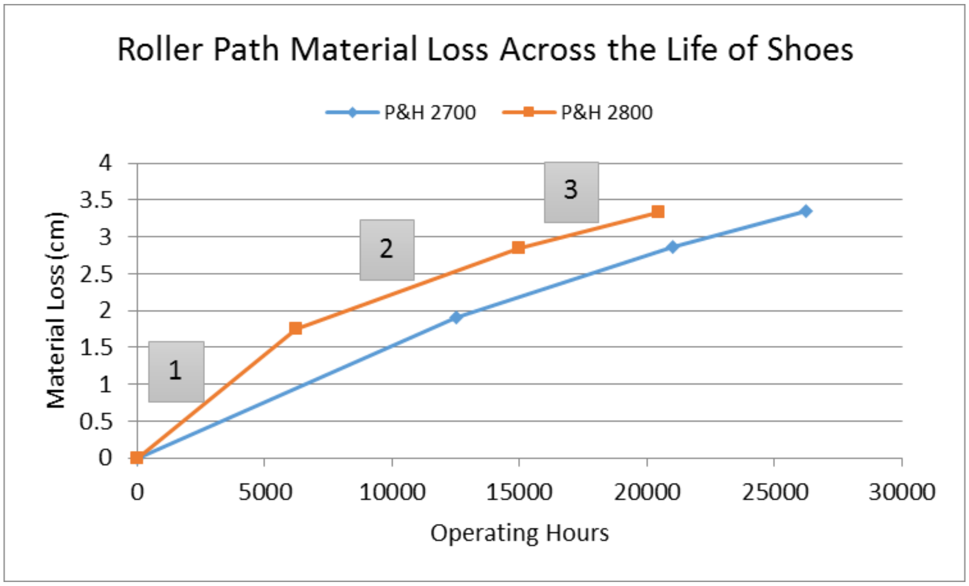

Figure 30: Reported material loss for A128 E1 roller paths (Adapted from Engineering, 2014)

Chapter 5: Apparatus Design, Build, and Assembly

The test apparatus, or the mechanical components of the test method, was designed to be programmable with a safety factor of two at its weakest point, to allow for differing load profiles at a higher magnitude. If the strength of the apparatus is required to be increased, the components to first address are the lower shuttle plate rollers (safety factor of 2.15, see Section 5.3) and the shuttle plate (safety factor of 6.25). See Appendix D for apparatus construction drawings, Appendix E for the material specification sheets for the coupons and shuttle plate, and Appendix F for the specification sheets for each electrical or hydraulic component.

5.1 Coupons

The two primary materials used for the track shoes of the ultra-class shovels are an A128E1 high manganese steel alloy, and a 4330 grade steel alloy heat treated to between 331 to 388 BHN (Boundary Equipment Co. Ltd., 2014). The A128E1 alloy is favored in hard rock mines due to the work-hardening features of the material, the 4330 alloy is used primarily in highly abrasive conditions as it is heat treated and resistive to abrasion. For the purposes of field verification 4340 and A128 E1 grade steels were used and are seen in Figure 31. The 4340 coupon was used due to availability and heat treated to 360 BHN to match the hardness of the 4330 roller path used in the field, performance was expected to be similar.

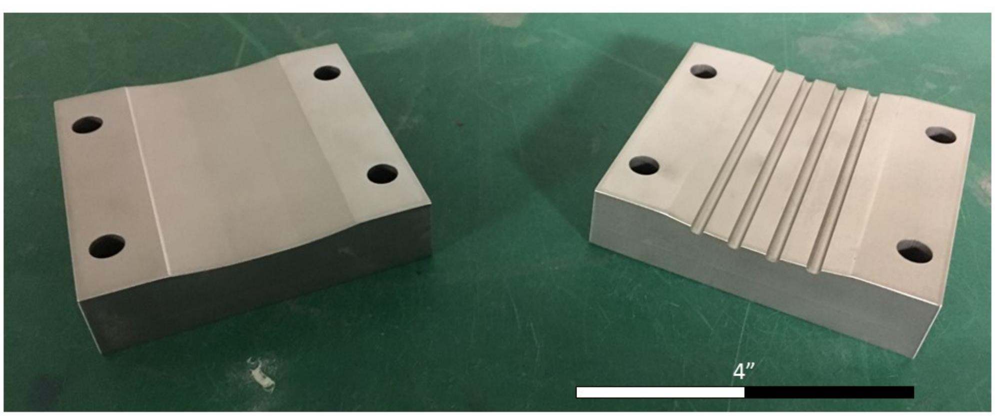

Figure 31: Test coupons, 4340 (left) and A128 E1 (right) – see Appendix D for dimensions

The flutes in the A128 E1 coupon allow the material room to flow from wear for the purposes of work-hardening similar to the true roller path. A128 E1 is not generally heat treated as extensively prior to active service and instead is worked to achieve the hardening process.

5.2 Main Load Roller

The scale of the test model was driven by the size of the roller. Due to availability constraints, an 11.5-inch diameter lower load roller from a 1963 Bucyrus Erie 22-B shovel was selected. The 22-B roller differs from the P&H 4100C boss roller as the 4100 roller is made of 4340 grade steel and heat treated to 400 BHN (Boundary Equipment Co. Ltd., 2014), where the 22-B roller is made of a manganese-steel (Bucyrus Erie, 1963). Between heat treatments and past field use, the 22-B roller had an estimated hardness of 450 BHN. A 2.5” round shaft 9” in length was fabricated to be used as the main roller pin or axle.

Figure 32: Main load roller; mounted onto the loading frame (left), and isolated (right)

5.3 Lower Apparatus

The base apparatus was constructed with eight lower shuttle rollers and two brass guides to restrict the motion of the shuttle plate to a single direction as seen in Figure 33 and Figure 34.

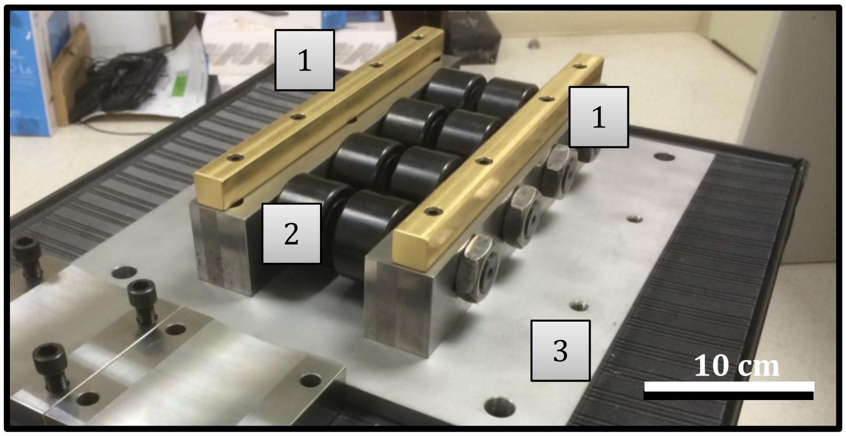

Figure 33: Base apparatus with shuttle removed showing: brass guides [1], lower shuttle rollers [2], and base plate [3]

Four shuttle rollers and one brass guide were mounted to each of the roller mounts (see Appendix D). The roller mounts were then attached to the base plate (Figure 33) which was then mounted to a Material Testing System Series 793 (MTS) loading frame base plate as seen in Figure 34. The apparatus was oriented for the shuttle to travel perpendicular to the viewing angle for ease of use and safety (see Appendix F.8 for risk assessment). The orientation placed the hydraulic ram on the opposing end of the frame from the operator in the event of a failure. The shuttle and coupon were then installed on the base apparatus and the primary roller attached to the loading cylinder for the MTS frame in line with the shuttle.

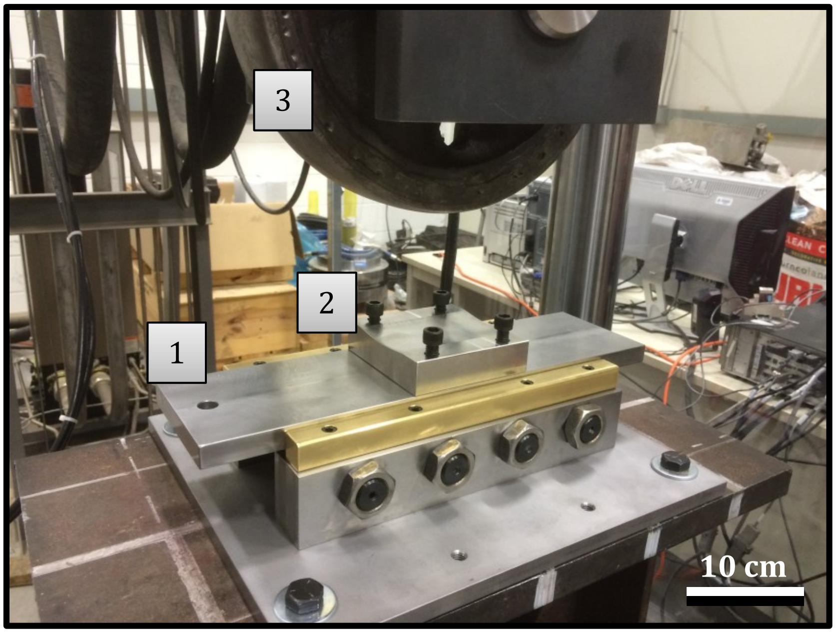

Figure 34: Base apparatus with shuttle [1] and coupon [2], installed below the main load roller [3]

5.4 Hydraulic System for Horizontal Movement

For the purposes of matching hardware, imperial units will be used for this section. The strength requirements for the system are seen in Table 6.

Table 6: Strength requirements for hydraulics

Max Main Roller Load	12,650 lbs
Friction Coefficient*	0.15
Required Horizontal Force	1,900 lbs

*Estimated from bushing rating (0.05 – 0.15)

Selecting a safety factor of 1.5 and a maximum pressure rating of 3,000 psi (standard rating for hydraulic rams) the calculated required bore (internal diameter) was 1.1 inches. To provide the required force a hydraulic cylinder with a 1.5” diameter and 9” stroke was selected. The roll speed in the field was measured via camera time stamp to be approximately 0.7 in/s, with a total roll distance of 2.5±0.5 inches. To match this speed, the required volume of hydraulic fluid per 3” stroke was calculated to be 5.41 cubic inches based on the 1.5” cylindrical chamber.

The required 5.41 cubic inch volume with a 4 second roll time produced a required 0.7 GMP of hydraulic oil.

A 1 HP Hydro-Tek power unit was selected with a maximum rating of 3,000 psi and 0.7 GPM of continuous flow to match the hydraulic ram. A flow rate valve was placed on the solenoid valves' main input line to reduce speed as needed, and a secondary flow rate valve was placed on the line leading to the rod end of the ram for the purposes of matching retraction speed to extension speed. Retraction required a speed reduction as the presence of the rod reduced the available volume in the hydraulic chamber and resulted in an increase in retraction speed. Both flow rate valves were mounted directly to the solenoid valve on their respective lines and the ram placed in line with the coupon/shuttle path (see Figure 35). The active running pressures for the hydraulics in this test were read at 500 psi during cylinder extension and 2,400 psi during retraction. The increased psi while retracting was as a result of the restricted flow rate valve placed to match the speed of travel.

As seen in Figure 35, two u-rods were used to extend the support structure beyond the main base plate for use by the hydraulic ram system. At the end of the u-rods a cross bar was placed, connecting the two rods, and provided a mounting base for the ram. The solenoid valve was also placed at the end of the u-rods for convenience reasons. The rod end of the ram was then pinned to the shuttle in the half-inch mounting hole as seen in Figure 35.

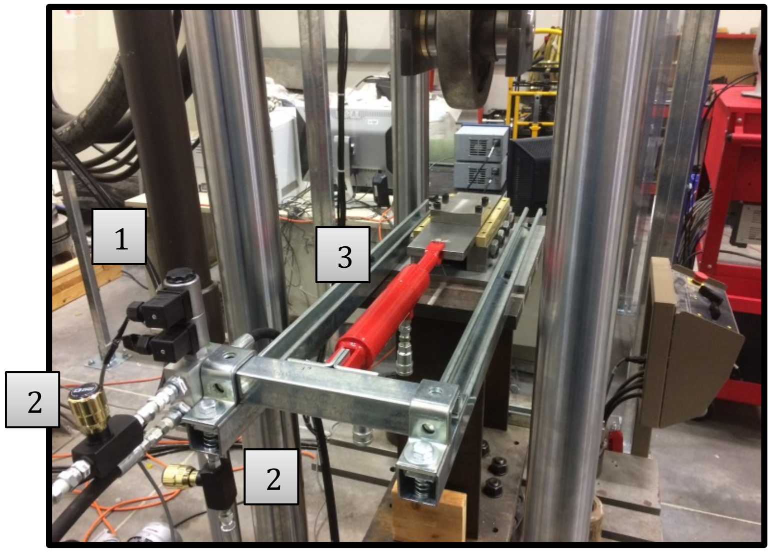

Figure 35: Hydraulic ram system: Solenoid valve (1), flow restrictor valves (2), hydraulic ram (3), and power unit shown in Figure 36

Figure 36 provides a better view of the power unit used for the horizontal ram (lower left corner of Figure 35).

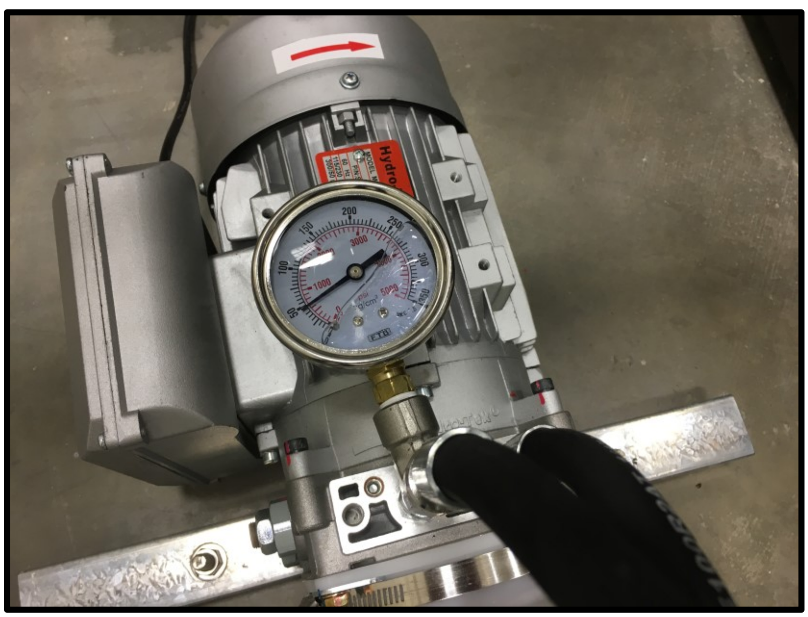

Figure 36: 1 HP Hydro-Tek power unit (pump)

5.5 Electronics

An electronic system was used to control the horizontal ram from the MTS system and included the following (for specification sheets see Appendix F):

- Hydac Solenoid Valve (WK10G-1)
- E-Switch Limit Switch (LS-085-15-06-F045-C1-A)
- OMRON Relay (G2R-1--SD12S)
- MTS Flex Test control unit

The wiring for the electrical system can be seen in Appendix F.6 and F.7. Appendix F.6 represents the sensory system and includes the limit switches that are mounted on each end of the shuttle plate listed as LS1 and LS2. LS1 was mounted on the ram end of the shuttle and LS2 on the free end. At each end a stopper was placed mounted magnetically to the loading frames base plate. As the shuttle moved in either direction the limit switch would press into the stopper and be triggered. Full details on the program used to control this motion will be listed later in this section.

Appendix F.7 represents the ram control system and includes two power supplies, two power relays, and a 3-position solenoid valve. The solenoid valve was powered by the 24 volt power supply. While unpowered the valve remained in the neutral position, feeding the hydraulic oil directly back to the pump, bypassing the ram. The two relays are used to power the solenoid valve in either the S1 or S2 coils. Powering the S1 coil directed oil to the rod end of the ram and caused it to retract. Powering the S2 coil directed oil to the base end and caused the ram to extend. The relays were controlled using the 12 volt system and the flex test control unit. In the MTS program, turning the digital output 1 to “high” would trigger the relay controlling S1 and retract the ram. Digital output 2 extended the ram.

5.6 Bracing and Stability

The main platform of the MTS loading frame required stabilization. While able to support high loads, it was adjustable with little effort. Unfortunately, because of the cycling horizontal loading the platform would slowly adjust in tilt and rotation. To prevent adjustment it was secured to the foundations T-slots using threaded rods and bolts (Figure 37). The threaded rods also allowed for minor adjustments to be made to the tilt of the platform to align the coupon with the roller. Alignment was done by tightening one side of rods or the other.

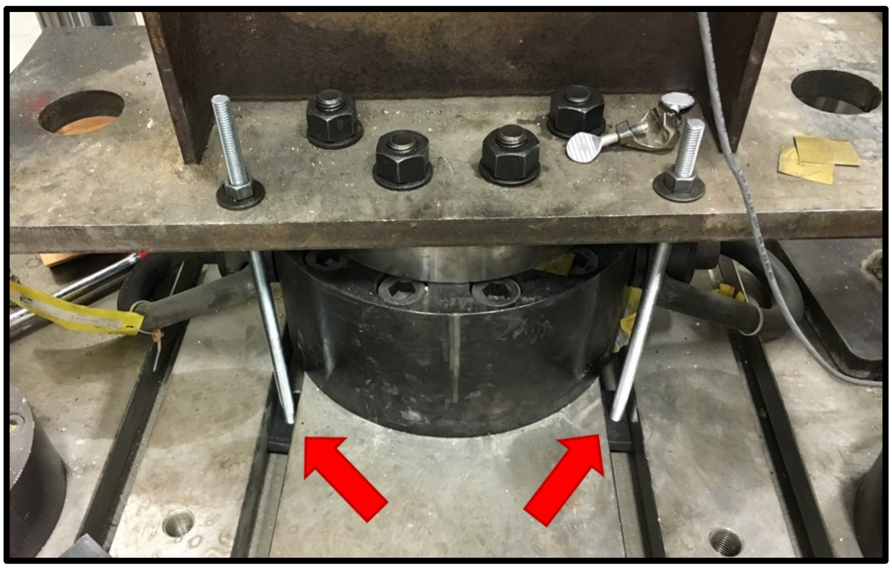

Figure 37: T-Slot stabilizers for leveling and fixing the platform

While trial testing, it was observed that the horizontal movement of the coupon caused a horizontal flexing of the main load cylinder. Additionally over several load cycles the MTS load cylinder would rotate, causing the main roller to rotate out of alignment with the path of the coupon. A brace was added to prevent both issues, bracing the roller and the load cylinder to which it was mounted against the main supports of the MTS frame and can be seen in Figure 38. The brace added to one side only to counter the flexing of the load cylinder under high load. Should the test load be changed in the future to a high load in both directions of shuttle movement, bracing should be added to both sides. This brace also prevented the main cylinder from rotating in its load cell by bracing both supporting walls of the main roller frame as seen in Figure 38.

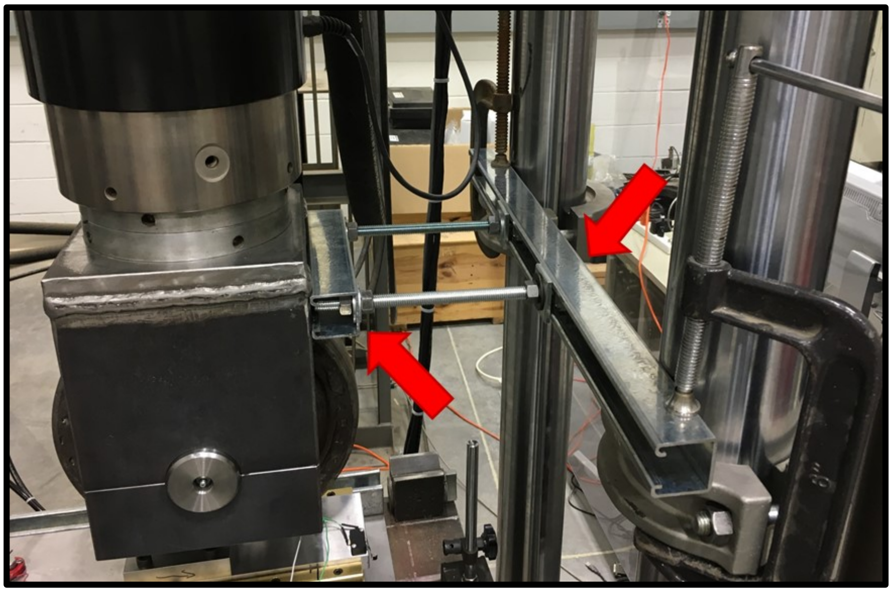

Figure 38: Horizontal brace to prevent horizontal movement and cylindrical rotation of the primary roller

5.7 MTS Program

The MTS program was setup to begin by resetting the coupon to a starting position prior to proceeding with the test. The data limit detector in step one was put in place as a precautionary measure should the limit stops on the shuttle fail and the coupon be pushed out from under the roller. The data limit detector was set to trigger should the roller move 5 mm below the original coupon surface elevation with the intent on increasing this limit if required due to roller path material loss. The program was setup as follows and can be seen in Figure 39.

1. Data Limit Detector – A safety module set to trigger at 5mm below the original roller path surface to stop the MTS frame should the roller fall off the end of the coupon
2. Home Start – initiated the retraction of the horizontal ram
3. Home Switch – watched for the shuttle to reach the starting position (trigger of limit switch 1)

4. Home Stop – stopped the retraction of the ram upon the trigger of the home switch in step 3
5. Ramp Base – ramped the load up to the base value (17 kN)
6. Loop – The remainder of the test occurred within this loop
    1. Ramp Peak – ramped the load up to the peak value (112.6 kN)
    2. Ramp High – ramped the load down to the high value (96.2 kN)
    3. Extend Start – began the extension of the horizontal ram
    4. End Switch – watched for the shuttle to reach the end position (trigger of limit switch 2)
    5. Extend Stop – stopped the extension of the ram upon the trigger of End Switch in step 4
    6. Ramp to Low – ramped the load down to the base value (17kN)
    7. Retract Start – began the retraction of the horizontal ram
    8. Home Switch – watches for the shuttle to reach the starting or home position (trigger of limit switch 1)
    9. Retract Stop – stopped the retraction of the ram upon the trigger of the home switch in step 8
7. Return to zero – upon completion of 2880 cycles (8 hours of testing) the loop ended and the roller was lifted 1cm off the coupon

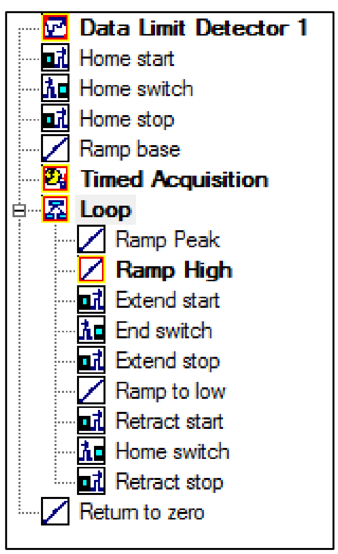

Figure 39: Screenshot of the program used for running the MTS frame

5.8 Operation of Test Apparatus

As mentioned in Section 4.2, the shovel rollers did not move on the roller path while digging or dumping of its bucket. The rolling occurred prior to digging and dumping while the load was relatively constant. To mimic this observed rolling behavior, the loading frame was programmed to wait for the coupon to be completed before the load is ramped up or down as seen in Section 5.7. The target profile is represented in Figure 40, and is described as:

- Under a load of 17kN, the coupon is moved under the roller a total of 2.5 inches – corresponding to initial roll while the shovel is empty and tucked.
- The coupon is held stationary while the load ramps up to a peak of 112.6kN and back down to 93kN – corresponding to the active dig of the shovel.
- The load is held constant at 93kN while the coupon is moved back to its starting position – corresponding to the roller movement during the rotation of the shovel.
- The coupon is held constant while the load is reduced to its original low of 17kN – corresponding to the shovel dumping its load into the truck.

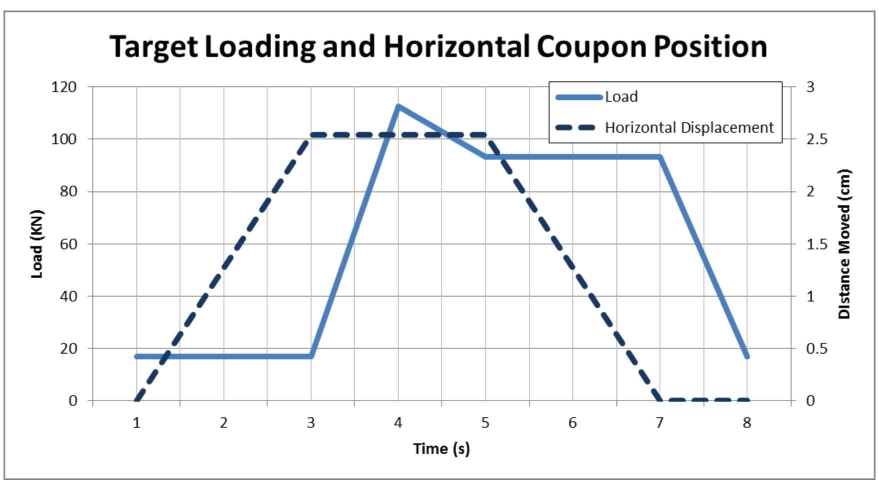

Figure 40: Desired load profile and coupon positioning for the test

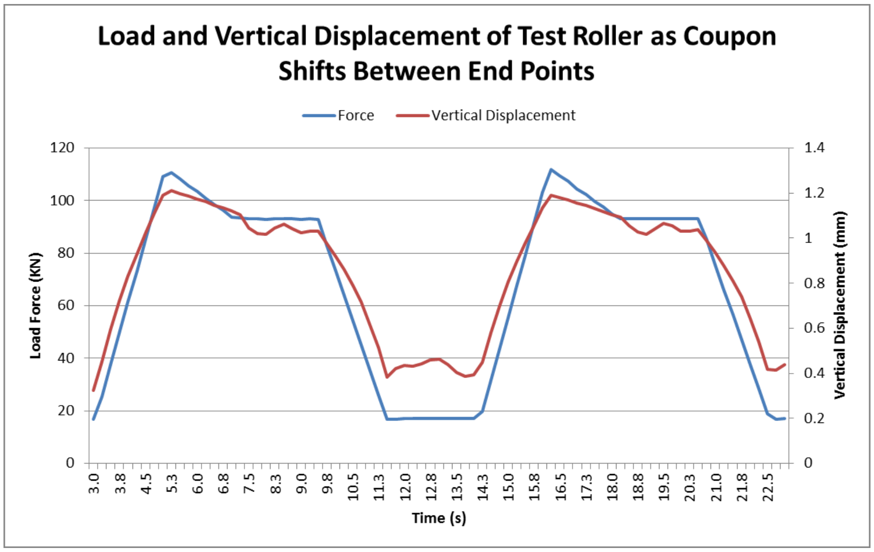

Figure 41: Actual load cycle and vertical displacement of loading ram with a sample rate of 4 per second.

It can be seen in Figure 41 that while the force is held constant the vertical displacement does not. The main load roller was not perfectly round and was expected to be the primary cause of the roughness of the vertical displacement. Variability was introduced in the system by rotating the roller to a new position every testing session. Should complete automation be required the MTS frame could be programed to rotate the main roller through a series of ram extensions while lifting the main roller off the coupon for the ram retraction. The rotation module could be added prior to or after the loop as set in Section 5.7.

The variability in the vertical displacement in Figure 41 was not directly seen as problematic, it does however verify the un-rounded shape of the roller. The un-uniform roller profile reduced the contact area and increased contact stress between the roller and the roller path. See Section 6.2.3 for further details.

Chapter 6: Results and Discussion

6.1 Results

6.1.1 Apparatus Performance

The overall performance of the apparatus was as expected and without issue. The load did not exceed the apparatus strength, and the chosen hydraulic system moved the coupon close to the desired velocities. Table 7 shows the required hydraulic pressure. The resulting speed of the coupon, measured using loading frame wait times, was 0.038 m/s, falling short of the target 0.045 m/s by 17%. The total horizontal coefficient of friction for the system, calculated from the hydraulic pressures, was 0.07.

Table 7: Required hydraulic pressure for horizontal movement of coupon.

Push (frame load = 93kN)	500 psi
Pull (frame load = 17 kN	2,400 psi*

* A flow restrictor was placed on the hydraulic line to reduce the speed of retraction resulting in a higher pressure

The paint or coating of the lower black shuttle rollers was removed throughout the test, leaving a polished surface. No further damage was seen and the rollers never exceeded 39% of their maximum rated load. The load was not perfectly distributed however, as one side of the roller set had a small zone of unpolished surface, as shown in Figure 42, and is likely due to roller misalignment. Similarly, the bottom of the shuttle plate sustained little visible damage. The area in contact with the lower rollers darkened in color – likely from the roller paint – with the side corresponding to the unpolished roller zone taking on less discoloration. The brass guides were worn faster than expected with each more than 50 grams of material over the course of the test duration (see Table 8). The brass shavings required regular cleaning, as they would contaminate the roller faces, creating an uneven contact surface and higher stress zones between the shuttle and the shuttle rollers. See Section 6.2.1 for further discussion on design changes to address the concerns surrounding the brass guides.

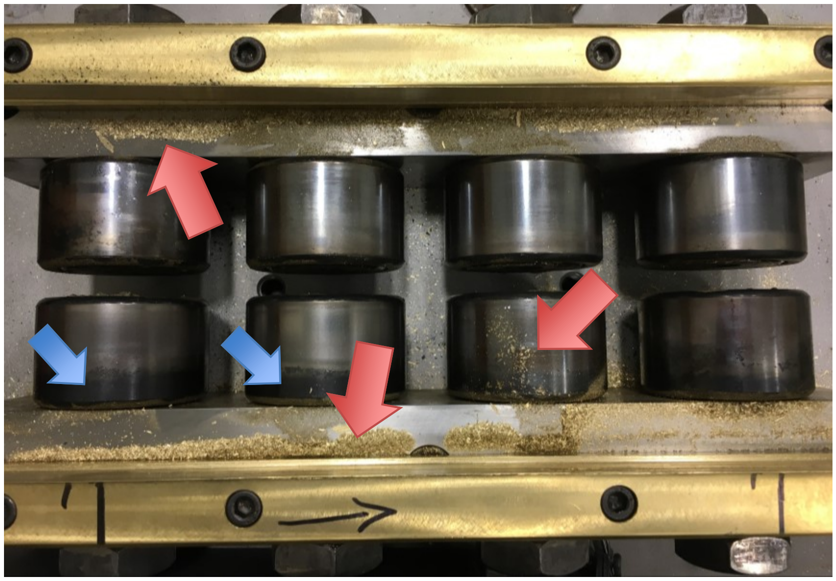

Figure 42: Brass shavings after one day of testing (large red arrows) and the shuttle roller unpolished zone (small blue arrows).

Table 8: Mass of brass guide material before and after testing.

Guide Number	Starting Mass (g)*	Finishing Mass (g)	Mass Loss (g)
Brass Guide 1	820.83	770.46	50.37
Brass Guide 2	820.83	764.32	56.51

* As the guide wear wasn't foreseen to be an issue, the original guides were not weighed prior to testing. A replacement set was made to identical specifications with masses of 820.98 and 820.68. The reported starting mass is an estimate based on the average of the two replacement guides.

6.1.2 Wear Rate

The duration of the test was 76122 load cycles. Each load cycle consisted of one loop outlined in Section 5.7 and represented one dig cycle of the shovel in the field. Table 9 compares the duration of the lab and field tests.

Table 9: Test Duration.

Cycles	76,122
Lab Hours	213
Equivalent Field Hours	1,189.4
Field Roller Path Life	25,000
Progress to Failure Point*	4.8%

*By completed field hours

The material lost through the course of the test did not reach the expected values. The loss rate will be discussed further in “6.2.2 Testing Accuracy.” See Table 10 below for a complete breakdown of expected and achieved material lost.

Table 10: Test and Field Comparison.

Test Mass Lost	1.67	g
Test Volume Lost	0.21	cm^3
Test Volume Lost (scaled to field level)	3.78	cm^3
Field Volume Lost	34.58	cm^3
Damage Rate Achieved in Lab*	10.9%	

*When compared to rates observed on the shovel

Where the field volume lost is the volume of material lost pro-rated to the test cycle count.

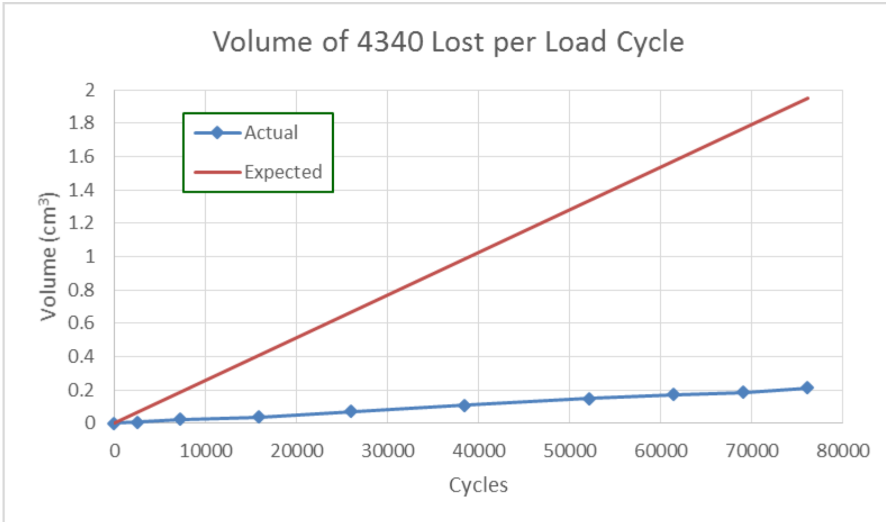

Figure 43: Actual and expected lab volume lost volume lost comparison for the first 76,000 cycles; the expected rate was taken from stage [1] of Figure 30, and assumed a linear loss of material.

The roller and roller path contact stresses initially peaked at 808 and 740 MPa while respectively stationary and rolling, but reduced to 570 and 522 MPa as the contact area between the roller and roller path increased through the test (see section 6.2.3).

6.1.3 Dry Rolling Wear

Abrasive debris were not added to this iteration of the test apparatus to first allow for discovery of design flaws; therefore, all damage and material loss to the roller path was due to the dry roller on roller path interaction. Figure 44 shows the wear across the roller path. Because of the mismatch in the roller and roller path profiles (see section 6.2.1 and 6.2.3 for details), the center of the roller path indicates the initial stages of damage, and the outer zones represent a more developed stage of roller path damage.

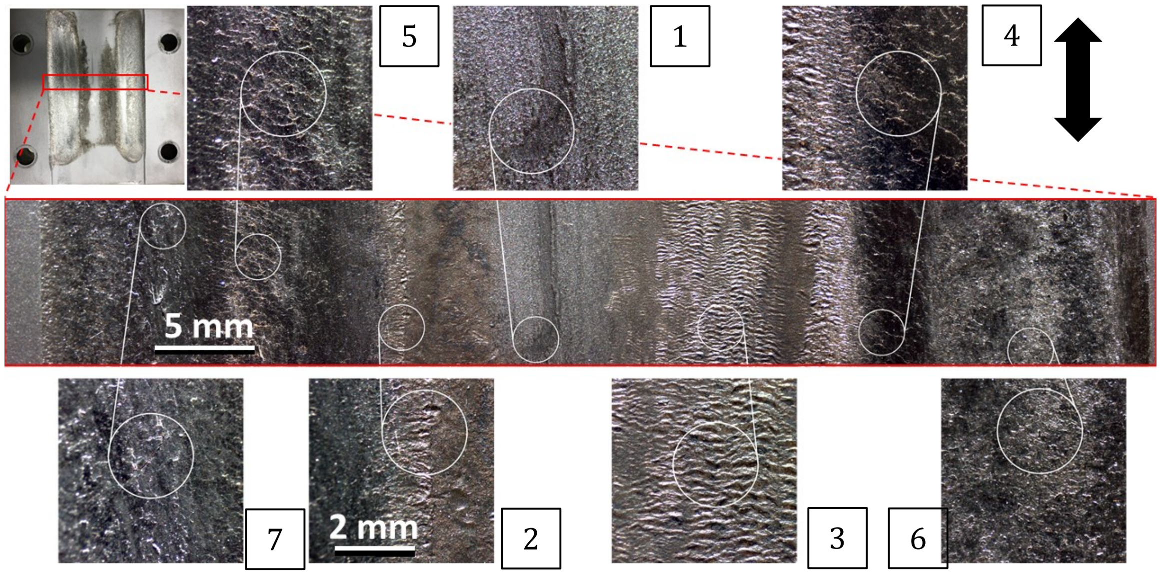

Figure 44: Complete roller path section, at 8x and 16x magnification, arrow indicates direction of roll (Nychka, 2016).

Where each zone in Figure 44 indicates a stage in the development of roller path damage (Nychka, 2016):

1. An undamaged zone with a single abrasive or ploughing scar, likely from debris generated in Stage 6.
2. Denting develops, likely from contamination of particles between roller and roller path.
3. Berms develop from plastic deformation around the dents, indicated from the wavy pattern in this region.
4. The berms flatten in line with the roller path; they become very thin flakes and may overlap resembling a fish-scale texture, see also Figures 45 and 46.
5. More flattened berms.
6. Deformation of berms (now flakes) reach failure limit and break off through shear or fracture, adding debris to the roller path and leaving a pit behind, starting the process over.
7. Ploughing scratches formed as the roller compresses the debris created in Stage 6. A crack is also seen, likely due to surface shear crack growth as described in Section 2.5.

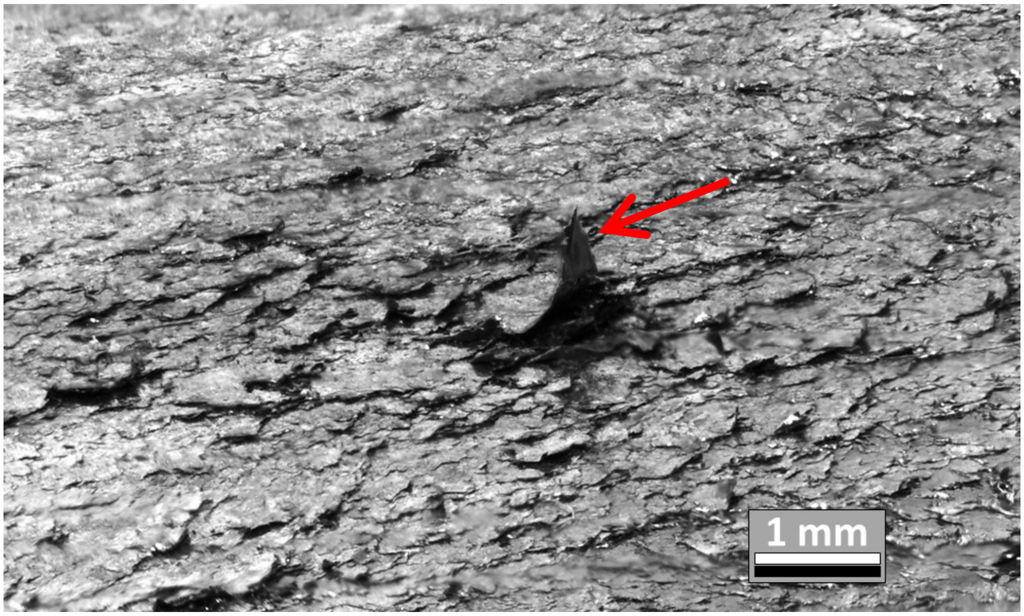

Figure 45: Composite image (16x magnification) of the flattened berm zone on the roller path showcasing a thin flake peeling off the surface.

Figure 45 shows the flattened berm zone on the roller path with a large flake curling upwards about to fracture loose. The flattened berms overlap each other, many are beginning to curl upwards, preparing to fracture or spall off the surface. A clearer image of the large flake and immediate surrounding area can be seen in Figure 46.

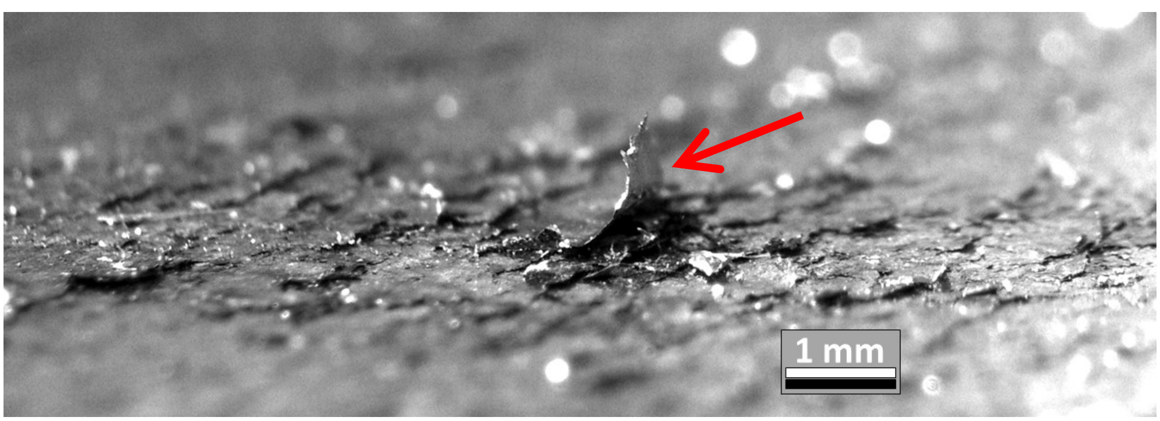

Figure 46: Single image of the flattened berm zone featuring the large flake at 16x magnification.

6.2 Discussion

6.2.1 Observed Problems and Proposed Solutions of the Apparatus

An early goal was to achieve unsupervised testing to allow for testing over nights and weekends, but this was not realized with the current iteration of the test apparatus. The following recommendations would address the known issues preventing unsupervised operation.

1. Replace the brass guides with a three-quarter inch track roller, similar to the lower shuttle rollers.
2. Add a data detection module to the MTS program, watching for major and repeated deviations from the target load and terminate the program when triggered.
3. Add a signal out module to the MTS program, sending the stop command to the horizontal ram when the previous module is triggered.
4. Add a data limit module to the MTS program to trigger the stop signal if it took more than 10 seconds for the ram to complete the extension or retraction.
5. Add a webcam to watch the test and take photos of the coupon, and a remote desktop client to the MTS control computer for remote monitoring.
6. Add a remote emergency stop function.
7. Instruct the operator to conduct remote periodic checks on the test while away.
8. Machine the roller to give uniform profile and to match the coupon's roller path radius.

Many of the known operational concerns were produced from the material loss to the brass guides and the loading frame being out of calibration. Prior to calibration, the MTS frame would occasionally and rapidly oscillate the load, continually over correcting itself until the load dropped to below approximately 40 kN. Calibrating the frame solved the issue, but adding a data-limit detector is recommended should the frame fall out of calibration. The brass guides wore down more than was expected and resulted in brass shavings that got under the shuttle and into the rollers, as seen in Figure 42. The chosen rollers were sealed to prevent contaminating their bearing systems, but the brass got in between the rollers and the shuttle, introducing an uneven contact surface and high stress zones. Due to the contamination, the brass and rollers were cleaned once per day or seven hours of testing time. If testing is conducted full time (24 hours per day, seven days a week) it is required to reduced or eliminated the need for such cleaning.

Another symptom of the brass wear was the widening of the allowable path for the shuttle. Widening the path permitted the coupon to deviate from the intended position and resulted in the roller exiting the roller path, increasing contact stress on one side but reducing it on the other. Additionally, the shuttle was no longer in line with the ram, resulting in heightened friction between the shuttle and guide, and an acceleration of the wear on the brass guides. Increasing the friction between the guide and shuttle resulted in a skipping motion and uneven material loss. Removing the brass guides and introducing a three-quarter-inch roller would solve both issues. Placing one roller in each mounting hole for the brass guides would be sufficient. Some modification and rethreading to the holes may be required. An example of a suitable roller can be found in Appendix A.

The remaining steps to improve the apparatus are to increase loading frame's ability to recognize and react properly to unforeseen issues. For example, Recommendation 2 at the beginning of this section was based on personal observation. It was seen that most problems, such as excessive wear on the brass guides, were accompanied by an oscillation in the load as the frame reacted to the changing condition. Some deviation must be allowed: it was common for the load feedback to read a single point well outside the target load, and may occur several times a day. The reason for the load deviations was unknown, but were assumed to be sensory and were not addressed. The deviations occurred across a single data point and often failed to register on the output screen. Therefore, the test did not need to be shut down, but may warrant a further check.

6.2.2 Testing Accuracy

As mentioned previously the test produced 10.9% the required wear rates to match those seen in the field. Because of the reduced wear rate, the test lasted for 4.8% of the cycles required to reach failure but only removed 0.52% of the required volume. The wear rate was likely due to the following reasons, ranked in order of probable severity:

1. The debris or material that would normally be found in the field were not included in the first iteration (e.g. bitumen).
2. The load levels were too low.
3. The coupon became unstable as mentioned in 6.2.1.
4. The test used 4340 steel instead of 4330 steel.

As part of the test, it was assumed that material loss rates of 4330 and 4340 were comparable. To prove the accuracy of the test apparatus, it was necessary to reproduce known wear rates as seen on the shovel roller path. Data was obtained for a P&H 2700 XPB and 2800 XPA. Both shovels use the same 72” shoe made from A128 E1 Hadfield Steel (Boundary Equipment Co. Ltd., 2014). Due to supplier restrictions on 4330 grade steel, coupons of 4340 grade steel were used; this steel has similar traits and was more readily accessible. Inaccuracies may be introduced with this change such as a change in fatigue or abrasion resistance, and therefore further investigation for a source of 4330 material should be conducted.

The damage rate recorded in the lab was 10.9% the rate observed in the field data (Section 4.2) assuming linear wear rates. The trial test was 4.8% in length and resulted in 0.5% volume lost when compared to a shovel. A specific correction could not be determined with confidence; additional testing is required. Considering the volume lost however, it was assumed that the lab scale test performed more slowly than required to match the field. The current test iteration lacked the input of debris, which is likely the driving cause of the reduced damage rate as shown in Figure 43. Adding debris such as sand or bitumen would increase the rate of material loss to the roller path, but at an unknown level. Using a sensitivity analysis to include debris on the roller path would provide insight about the effect of contamination on roller path life. Determining the sensitivity of the roller path to debris could provide information about specific concentrations of roller path contamination for estimating the damage effects at a specific mine site.

Along with adding debris to the roller path to achieve a 1:1 cycle representation from lab to field, it may be necessary to increase the loads. As the test run only reached 0.5% volume loss on the roller path to reach failure, it was unreasonable to predict load increase with confidence. The stress analysis shown in 6.2.3 can assist in predicting required load level changes. It should also be noted that for the test run, the load profile of roller position 7 was used, as seen in Figure 47. Roller position 1, which resides at the back of the shovel, experienced a similar load profile with a high rolling load of 96.8 kN compared to 93.2 kN at position 7. The points at which rolling occurred on the roller path were when the bucket made initial contact with the ground, and while rotating with the bucket suspended and full of material. It should be noted however that the forces indicated in Figure 47 are skewed towards roller position 8, as a the shovel's hoist motor was assumed to have a 100% efficiency, where in actuality it is at 86%. The true efficiency was determined late in the course of this research and the resulting roller forces can be seen in Figure 48, but were not used in the development and initial operation of the test method. Table 11 compares the roller forces between the two efficiency ratings.

Table 11: Sample load comparison between efficiencies

Efficiency	100%	86%
Roller 7 Full Suspended (kN)	93.2	82.1
Roller 6 Full Suspended (kN)	60.5	61.7

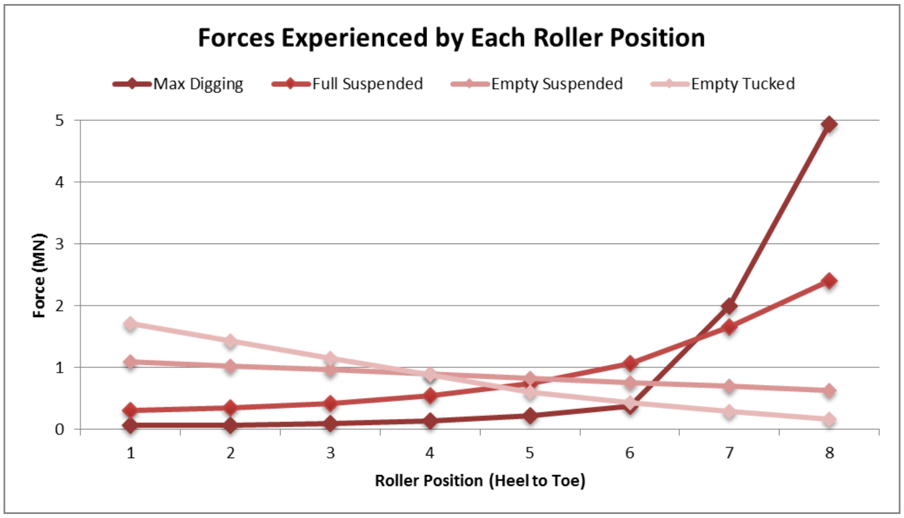

Figure 47: Loads at each roller position for key phases of the dig cycle

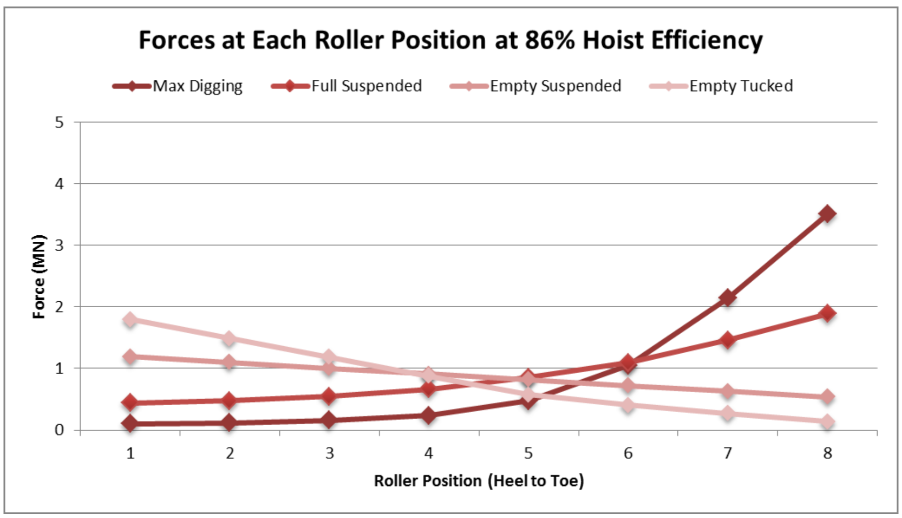

Figure 48: Loads at each roller position with a hoist motor efficiency of 86%

The most noticeable difference in changing the hoist motor efficiency to 86% is the reduction in the extreme loads on the front rollers at positions 7 & 8. The roller positions 1 – 6 remain similar between both efficiencies. The implications this efficiency change would have on the test which, focused on roller position 7, is a peak load value increase of 7% to 120.6 kN, a high load decrease of 11.9% to 82.1 kN, and a base load decrease of 10.3% to 15.2 kN. The damage done to the rolling zone would be decreased, but there would be an increase in fatigue damage where the roller path experiences the peak load.

6.2.3 Stress Analysis

Stress analysis was performed to learn about the damage caused directly by the loading of the roller on the roller path. Equations [12] and [13] (Bamberg, 2006) were used to determine contact area and peak contact stresses.

$$\rho_{max} = \frac{2F}{\pi b L} \qquad [12]$$

$$b = \sqrt{\frac{4F\left[\frac{1-\upsilon_1^2}{E_1}+\frac{1-\upsilon_2^2}{E_2}\right]}{\pi L\left(\frac{1}{R_1}+\frac{1}{R_2}\right)}} \qquad [13]$$

Where:

- ρ = Contact stress
- F = Contact force
- L = Contact length
- b = Contact half-width
- E = Modulus of elasticity
- v = Poisson’s ratio
- R = Radius of cylinder

R_2 was set to infinity to represent a flat roller path surface as opposed to a cylinder. The contact length (L) changed dynamically throughout the test. Initial coupon design matched the curvature to a measured profile on the roller. The roller surface curvature was not consistent and did not match the coupon initially, requiring a break in the phase. A break in phase may also be required in the field, but would vary in length between individual track systems. Machining the roller into a continuous profile is recommended for future tests to increase its consistency, repeatability, and to make it more representative of multiple roller and roller path arrangements. In Figure 49 the progression in roller and roller path contact area is shown. The correlated progression of contact stress is shown in Figure 50.

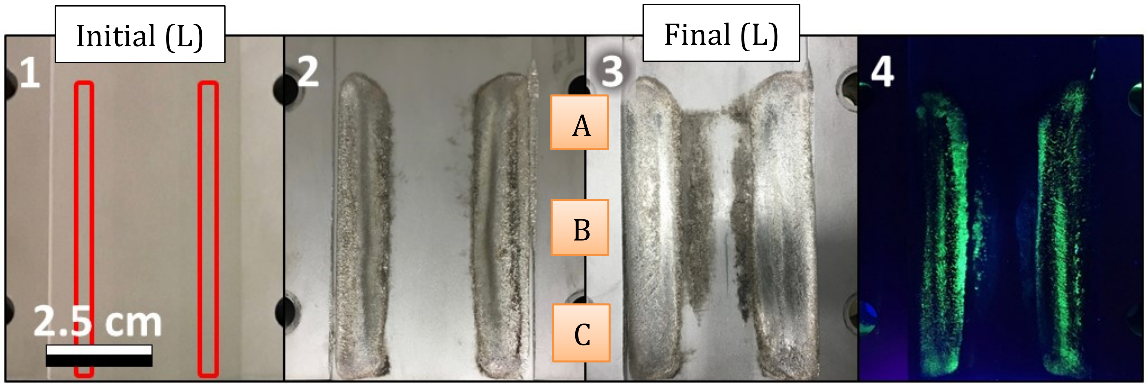

Figure 49: Coupon roller-path contact area through test. 1) Unworn coupon with initial contact outlined 2) Partially worn coupon 3) Coupon after 76,000 cycles, approaching full roller path contact 4) Green highlights denote cracks, folds, and damage

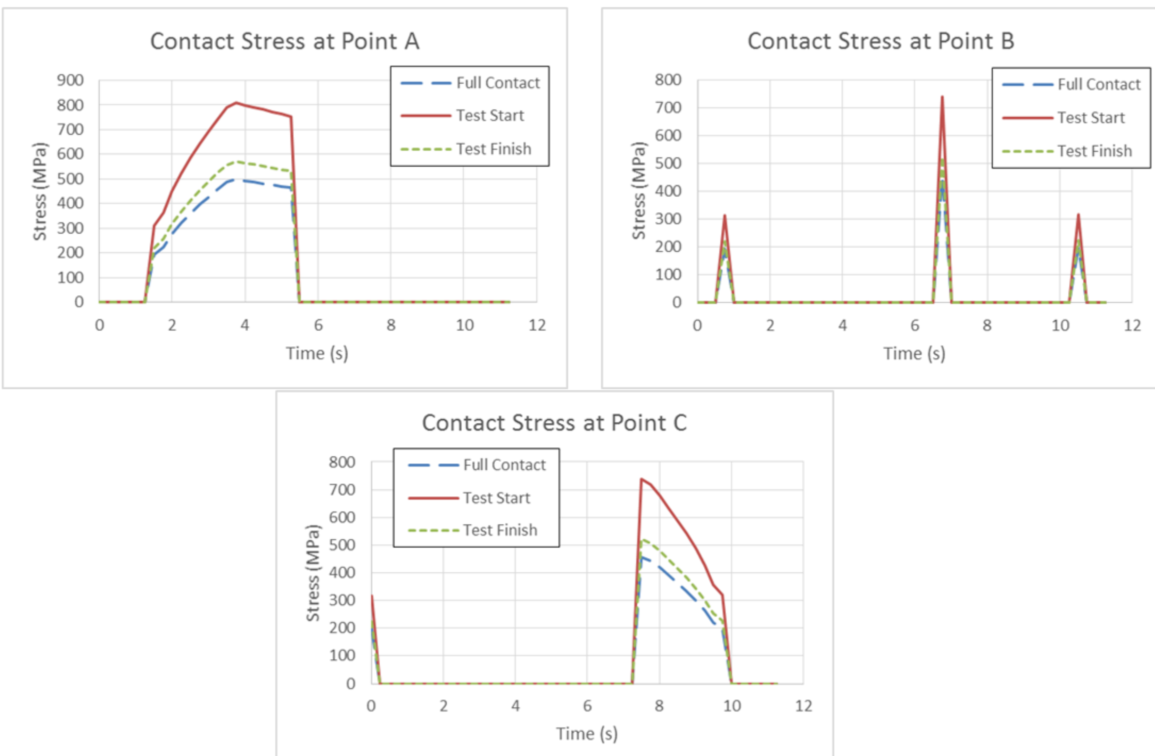

Figure 50: Stress levels experienced at each point labeled in Figure 49

Calculated contact stress levels between the roller and roller path are shown in Table 12.

Table 12: Roller and roller path contact stresses (MPa)

Initial Stationary	808

Initial Rolling	740
Final Stationary	570
Final Rolling	522
Full Contact Stationary	500
Full Contact	457
4340 Yield Strength	≥ 760*
4340 Endurance Limit	500**

*(Boundary Equipment Co. Ltd., 2014) ** (eFatigue, 2016)

While initial contact stresses far exceeded the endurance limit of the roller path, stresses assuming full roller path contact reduced to below the endurance limit while moving, and matched it while stationary. Equations [12] and [13] (Bamberg, 2006) were used to evaluate contact stresses for a P&H 4100C Boss at roller position 7 and resulted in 802 MPa while stationary and 730 MPa while moving. The inequality between contact stresses may be attributed to the calculation method. Equations [12] and [13] assume pure elastic deformation. While the roller path achieved a yield strength of 760 MPa or greater (Boundary Equipment Co. Ltd., 2014) through heat treatment, some plastic deformation was required in the formation and flattening of the berms seen in Figure 44. Further investigation into the direct contact stress is recommended to determine the continued use of the cube root scaling method, or an adoption of a different method, for future work. Assuming a pure elastic deformation, a load increase of 2.7x may be required to match the lab and field stresses. As mentioned in Chapter 5, the apparatus's part with the lowest factor of safety was the lower shuttle rollers at 2.15. Should a load increase be required it may be necessary to replace the lower shuttle rollers. A suitable replacement can be found in Appendix A.

6.2.4 Alternate Load Profiles

The load profile assumed for the test run of the apparatus held the load constant while moving the coupon. In the field, after the shovel completed the dig cycle, it rotated its body to dump the load in a truck that was typically parked alongside the shovel. Through the rotation, the distribution of loads changed on the rollers as seen in Figure 51. Passing the loaded bucket over a corner of the tracks increased the rollers' load in that corner. The shovel counterweight at the same time passed over the opposite corner of the tracks, resulting in a similar effect. The loads experienced by rollers elsewhere in the track system were reduced. For simplification, it was assumed in the test run that because the shovel rotated in both directions equally, the loads would balance and could be held continuous. A more detailed load profile, which may be required, is shown in Figure 52. No modifications to the apparatus would be required for a dynamically changing load profile.

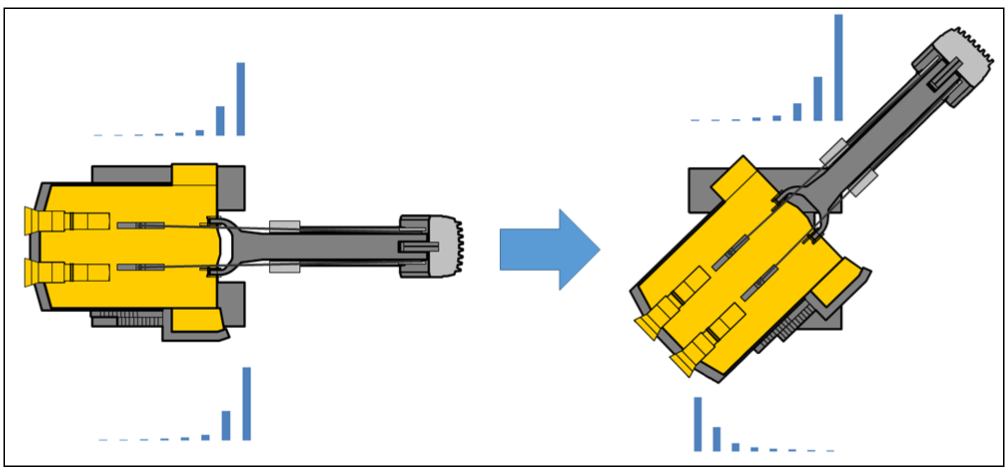

Figure 51: Effect of shovel rotation on track roller load (Adapted from Marek, 2006)

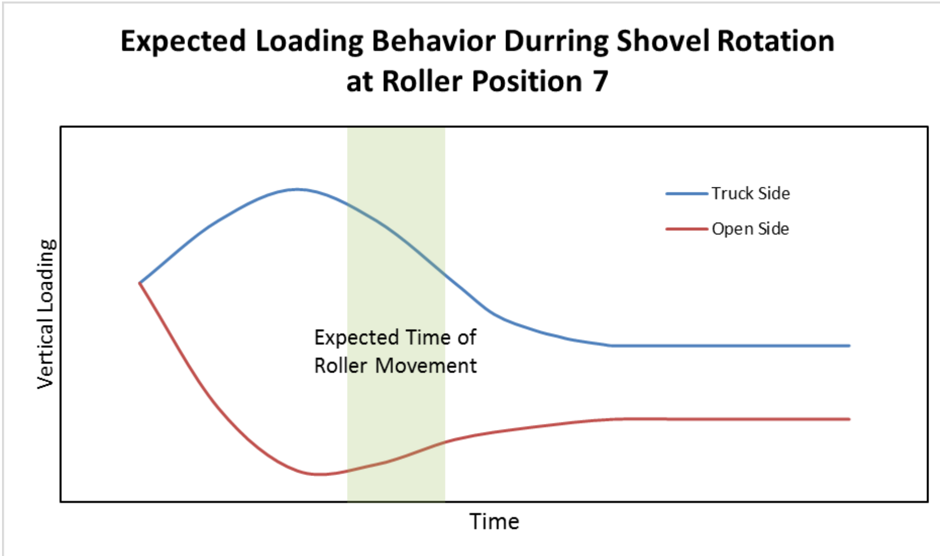

Figure 52: Load profiles of the two rollers at positions 7 and 8 during shovel rotation

6.2.5 Toenailing and Material Flow

To allow for track flexibility, gaps are placed between the roller paths of each shoe in the field. As the roller moves off the shoe and crosses the gap, the stress concentration increases at the roller path ends, and results in material flowing towards and extending beyond the end of the roller path. The effect, called toenailing, causes the paths of adjacent shoes to collide as the track flexes from use, and increases the stress and damage throughout the system. During the set-up of the test apparatus, while the MTS program was being developed, the coupon was moved out from under the roller. While leaving the roller path was unintentional, the instance showed a possibility of the toenailing effect (see Figures 53 and 54). It may be possible to recreate toenailing using a modified coupon design, possibly with a notch cut out of the middle of the roller path.

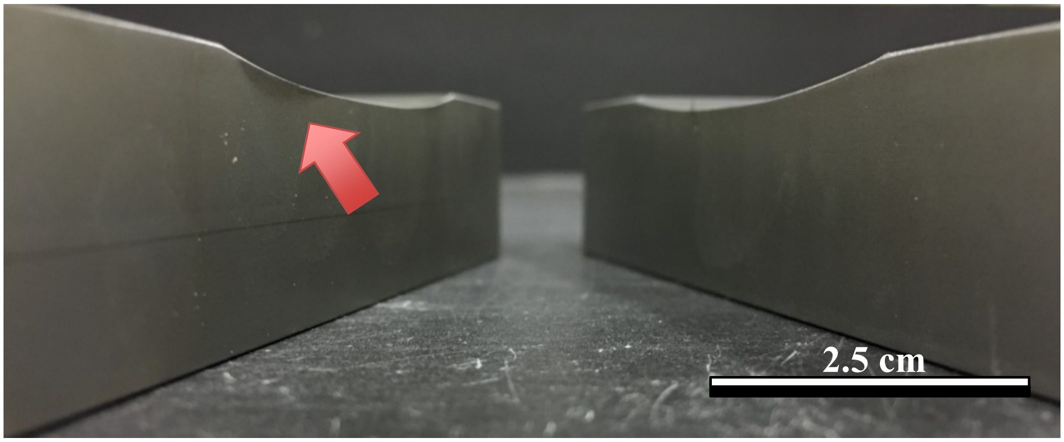

Figure 53: Possible toenailing re-creation (left) compared to unworn coupon (right)

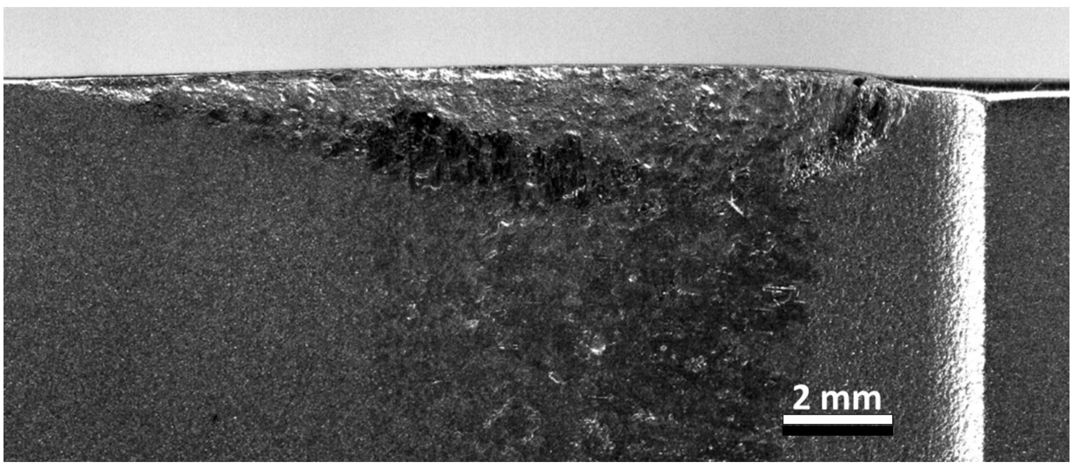

Figure 54: Possible toenailing re-creation, top view at 8x magnification

Possible re-creation of the toe-nailing effect was further supported in Figure 55. From the lighting, it can be seen that the worn zone is built up higher in elevation than the original surface. Because the roller stopped before reaching the edge of the coupon, the roller path material did not flow off the edge, but build up at the end point of the wear zone. This flow was because of the creation of berms, and folding them over in line with the rollers movement. The folding and flattening of the berms is indicated by the fish-scale like pattern, in the worn zone of Figure 55. This particular zone is exaggerated from the addition of the material from the wear scare located at the top of the figure. The scar formed in the initial setup, prior to bracing the loading frame, and its material was pushed down into the roller path, where it flowed outwards, to the edge of the roller path, through the toenailing effect as described earlier.

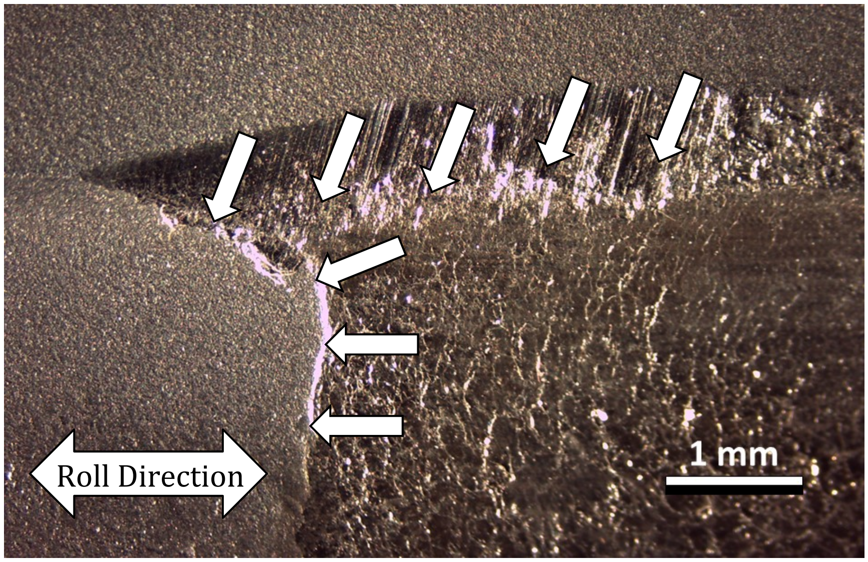

Figure 55: Edge of roller path wear zone at 16x magnification. The arrows indicate the flow path of material, and the light source is located to the left of the sample.

6.2.6 Test Length

It was impractical to run a test with a duration equivalent to the average roller path life as observed on a shovel. The test length had to be reduced while still producing damage similar to that seen on a shovel roller path. To satisfy this requirement the following were not modeled into the test method:

1. Operator lunch and coffee breaks or crew changes.
2. Expected or planned downtime for maintenance.
3. Unexpected downtime for maintenance.
4. Idle time while waiting for trucks.

The cycle time for each dig could also be truncated or reduced. It was expected that the leading cause of damage was the roller moving under a high load across the roller path. All non-essential moments were removed or reduced from the dig cycle, as seen in Figure 56. Truncating the dig cycle reduced the total time of one cycle from 45 to 10 seconds. The combination of ignoring shovel down time and unessential cycle time reduced the overall roller path life from 25,000 hours as seen in the field to a lab life of 670.

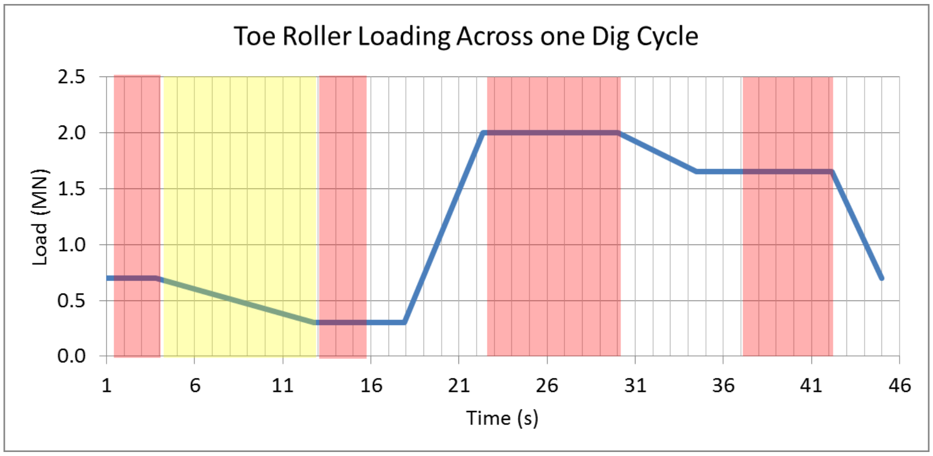

Figure 56: Truncation of dig cycle, red = removed, yellow = reduced

As mentioned in Section 6.1, the trial test spanned eight weeks and resulted in 76,122 completed cycles over a space of 213 hours. The rate of material loss to the coupon roller path in the lab was recorded to be 10.9% of the rate seen on the shovel roller path in the field ($0.28cm^3$ vs $2.6cm^3$ respectively per 100,000 cycles), assuming linear wear rates. Using the following steps, the rates recorded in the lab may be increased to match the observed rates seen in the field. These steps were mentioned previously, but are reiterated here for emphasis.

1. Testing 24 hours a day, seven days a week unsupervised would increase the test rate by 4.8x. For this study, testing was done a maximum of seven hours per day.
2. Debris, dirt, or sand should be added to introduce abrasive and gouging wear.
3. The load profile should be adjusted to match the field damage 1:1.

If followed these aforementioned methods are expected to match the roller path material lost rates in the lab to the rates in the field, and reduce the total time to fail a coupon from 168 weeks to 4 weeks. It is recommended that load adjustments be made only after the addition of debris, as it is expected for debris will make up the majority of the difference between observed field and lab damage rates. Regardless of steps taken to reduce test lengths and increase automation, general maintenance of the apparatus will be required periodically. Maintenance and operation will be discussed further in Section 8.3.2. Test length may be subject to change based on the shovel type and digging conditions.

Chapter 7: Conclusions and Future Work

7.1 Conclusion

While basic function of the test method has been established, some improvements and calibration are required before active testing can occur. Resolving problems that manifested during the initial testing run and preparing for potential future unseen issues are key, as these steps will make it possible to conduct both supervised and unsupervised tests. The following steps are recommendations based on the first test run:

1. Replace brass guides with three-quarter-inch rollers.
2. Add modules to the MTS program to watch for various issues as mentioned in 6.2.1, and shutdown not only the MTS but the horizontal ram as well.
3. Add a webcam and remote emergency stop for remote checkup.

While the three steps outlined would eliminate the known issues, general checkups should be required for periodic maintenance, such as rotating the main and lower shuttle rollers for re-lubricating the bushing and bearings, weighing the sample, and taking other readings as desired for test purposes. A checkup would also include inspecting for unknown problems. Following these steps would allow testing to be completed in a maximum of four weeks without the expense of producing a full track system.

All objectives listed in chapter 3 were met with the exception of those involving roller path contamination, abrasive damage, and gouging damage. It is expected adding debris to the roller path will accelerate the damage done considerably, though the exact amount remains to be discovered. The damage done by the debris is expected to progress faster than the wear seen in the Dry Rolling section (6.1.3) and therefore reduce the amount of berms and flakes seen on the surface. Another objective that may require further work is validating the use of the cube root scaling method and determining the exact loads to use in the test. While the rolling contact stress remains below the yield strength of the roller path, some plastic deformation is occurring; therefore, investigation into the direct contact stress assuming elastic-plastic deformation may be needed. While the calculated stress reduced throughout the test as the contact area increased (as seen in section 6.2.3), the wear rate of the roller path did not, but remained relatively constant (see Figure 43). It is therefore recommended that priority is given to 24 hour operation and the addition of debris contamination, and continuing the analysis of stress and wear rates afterwards.

7.2 Future Work

Future work recommendations are, first, to improve the test apparatus as outlined in sections 7.1 and 6.2.1; and, second, to further develop the method of breaking down hoist data into roller loads.

The current iteration of the apparatus design tests the roller path for rolling contact fatigue and cyclic fatigue. Future work priorities should focus on:

1. Adding debris (sand sized particles, bitumen, or mine-specific ground material) to the roller path and developing a sensitivity analysis.
2. Improving the apparatus to allow unsupervised testing.
3. Adjusting the load profiles, if required, to match field damage rates.
4. Comparison of microscopic damage between a worn field shoe and lab coupon to assist in adjustments to load profile and debris contamination.

Modifications could be made to permit testing the entire track system. Adding a tray on the shuttle in place of the coupon would allow rocks and dirt to be placed underneath a set of linked shoes. Such a set-up would allow the shoes to flex as seen in the field. Periodic disturbance of the ground material would be required to avoid ruts or settlement.

Developing the data analysis method used in this research could allow mine operations to regularly monitor live loading on roller paths. The periodic monitoring of loads could then be used to predict the remaining life of the roller path. Should extending the life of the roller path in this manner prove to be impractical, an analysis such as the one conducted for this study could at minimum, provide a predictable end-of-life date for budgeting purposes.

Works Cited

4100CBoss-shovel. (2007). Retrieved March 14, 2016, from http://i74.photobucket.com/albums/i260/mitchtim/Shovels/4100CBoss-shovel.jpg

Bamberg, E. (2006). Contact Stresses and Deformations. In *Mechanical Engineering 7960* (pp. 1–10). University of Utah.

Boardman, B. (1990). Fatigue Resistance of Steels. *ASM Handbook*, *1*, 673–688. Retrieved from http://hdl.handle.net/2060/19930083139

Boundary Equipment Co. Ltd. (2014, April). Personal Comunication. Edmonton.

Bucyrus Erie. (1963). 22-B Series Two Crawler Machine Section A - Lower Works.

Caetano, L. F., & Teixeira, P. F. (2011). Availability Approach to Optimizing Railway Track Renewal Operations. *Journal of …*, (May), 548–556. http://doi.org/10.1061/(ASCE)TE.1943-5436

CN Rail. (2013). Equipment. Retrieved February 11, 2016, from https://www.cn.ca/en/our-business/transportation-services/rail/equipment

eFatigue. (2016). Fatigue Calculator. Retrieved February 20, 2016, from https://www.efatigue.com/fatiguecalc.html

Harzallah, R., Mouftiez, a., Felder, E., Hariri, S., & Maujean, J. P. (2010a). Rolling contact fatigue of Hadfield steel X120Mn12. *Wear*, *269*(9-10), 647–654. http://doi.org/10.1016/j.wear.2010.07.001

Harzallah, R., Mouftiez, a., Felder, E., Hariri, S., & Maujean, J. P. (2010b). Rolling contact fatigue of Hadfield steel X120Mn12. *Wear*, *269*(9-10), 647–654. http://doi.org/10.1016/j.wear.2010.07.001

Joseph, T. G. (2013). Personal Conversation.

Joseph, T. G., & Shi, N. (2010). Scaling To Full Size Dipper Design Via Geometric and Performance Field Data. *Proceedings of the World Congress on Engineering*, *II*, 1–7.

Joseph, T. G., & Shi, N. (2012). A revised dipper - ground equilibrium derivation for shovels operating in oil sand and soft ground. *Cim Journal*, *3*(1), 47–53.

Joy Global. (2012). 4100C Boss Electric Mining Shovel - AC Drive Product Overview.

Retrieved June 1, 2014, from http://www.joyglobal.com/docs/default-source/product-documents/surface/electric-rope-shovels/xs-5491-1_4100c_boss_ac_bro.pdf?sfvrsn=24

Kang, J., Zhang, F. C., Long, X. Y., & Lv, B. (2014). Cyclic deformation and fatigue behaviors of Hadfield manganese steel. *Materials Science and Engineering A*, *591*, 59–68. http://doi.org/10.1016/j.msea.2013.10.072

Llewellyn, R., & Tuite, C. (1995). Hardfacing Fights Wear in Oil Sands Operation. *Welding Journal*.

Marek. (2006). P&H 4100. Edmonton: JPi Canada. Retrieved from http://www.jpicanada.com/home_pa.htm

Nychka, J. (2016, March 11). Personal Conversation.

Patra, A. P., Bidhar, S., & Kumar, U. (2010). Failure Prediction of Rail Considering Rolling Contact Fatigue. *International Journal of Reliability, Quality and Safety Engineering*, *17*(03), 167–177. http://doi.org/10.1142/S0218539310003731

Ringsberg, J. W. (2005). Shear mode growth of short surface-breaking RCF cracks. *Wear*, *258*(7-8), 955–963. http://doi.org/10.1016/j.wear.2004.03.043

Stachowiak, G. W., & Batchelor, A. W. (2005). Fatigue Wear. In *Engineering Tribology (3rd Edition)*. Elsevier. Retrieved from https://app.knovel.com/web/view/swf/show.v/rcid:kpETE00012/cid:kt00CASJD1/viewerType:pdf/root_slug:engineering-tribology?cid=kt00CASJD1&page=3&q=fatigue wear&b-q=fatigue wear&sort_on=default&b-subscription=TRUE&b-group-by=true&b-search-type=tech-reference

Sunhills Mining. (2015, March 9). Site Visit.

Appendices

Appendix A: Part Recommendation for Design Improvements

1. To replace the brass guides a set of ¾ inch diameter rollers are recommended. The roller found on this web page would be a suitable candidate: http://www.mcmaster.com/#cam-followers/=10n003k
   It is capable of sustaining a load of 1,600 Lbs at maximum rotation and 2,000 or 4,100 Lbs at no rotation depending on the model used. These specifications exceed the required strength of approximately 400 Lbs while moving.

2. A suitable lower shuttle roller replacement candidate is the High-load variant of the currently used roller found at McMaster-Carr: http://www.mcmaster.com/#cam-followers/=117kku7
   The roller is capable of 16,000 lbs (vs the currently used rollers at 8,000) and of the same diameter (2.5”). The roller support may require re-threading.

Appendix B: Apparatus Progression

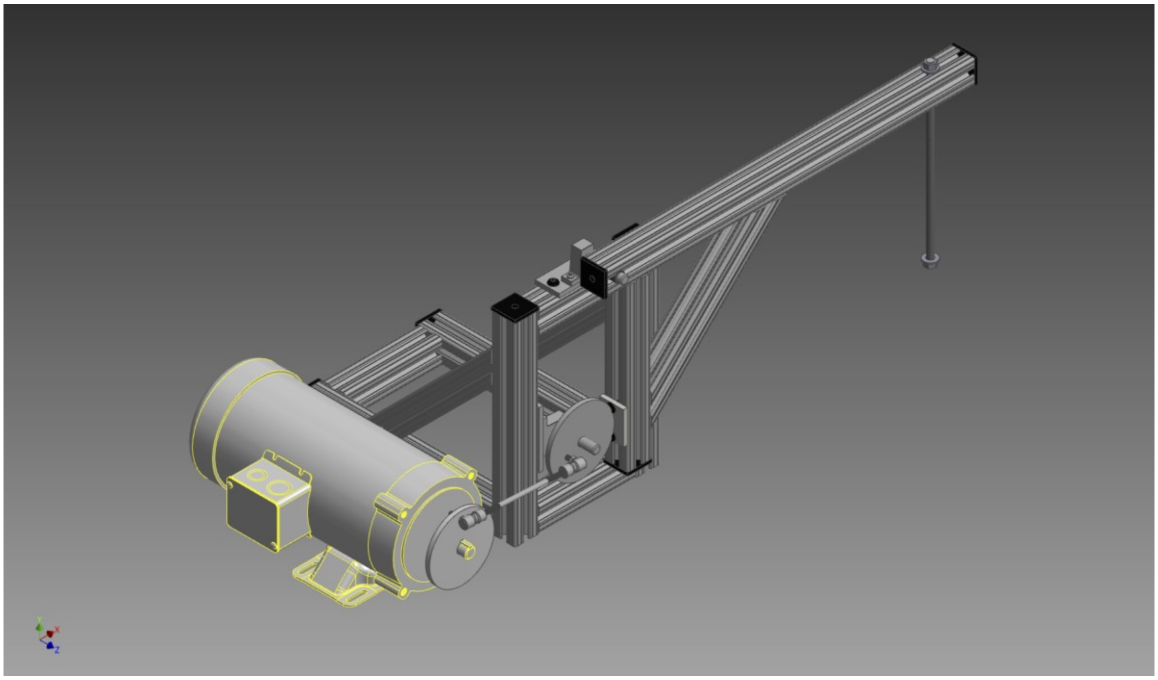

Figure 57: Apparatus Version 1

Initial plans were to use a small 4 inch roller attached to an electronic motor as shown in Figure 57. This setup would allow for easy switching of the coupon and rollers to test different hardness'. There were two major flaws with this design however, the first being the fixed coupon position and the second being the extreme scale. While the static coupon was fixable using a small rail system, the scale was the critical reason for stopping the test design as any errors would be compounded. It was decided to go bigger in order to increase the testing confidence.

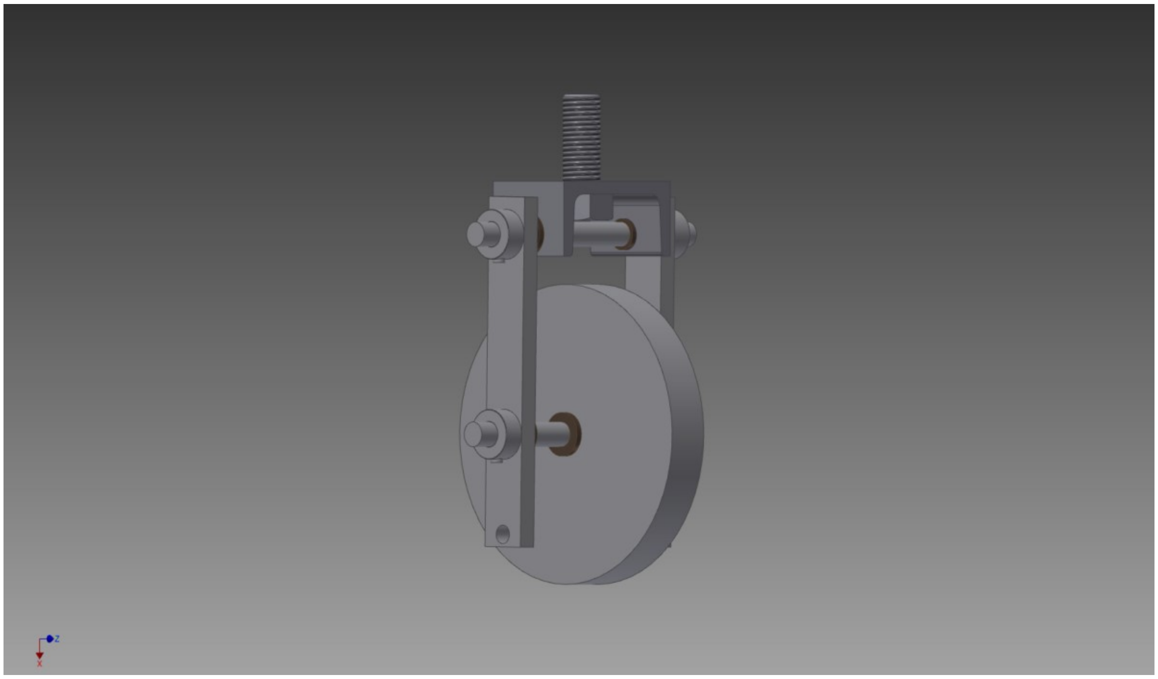

Figure 58: Apparatus Version 2

The second version design for the system was to have a fixed coupon mounted on the baseplate of the MTS loading frame, a double axel roller (as shown in Figure 58) would be mounted in the loading ram. The roller was designed to be 8 inches in diameter and was to be pushed back and forth using the same electric motor that was to be used in version 1 of the design. This design failed in that the motor was not capable of pushing the roller back to the center position once it left. Additionally a roller from a drill rig by was made available. While this drill rig roller was ultimately not used (in favor of the Bucyrus 22-B roller), the possibility of using a true roller of similar properties as the shovel lower load roller directly influenced the decision to move beyond apparatus version 2.

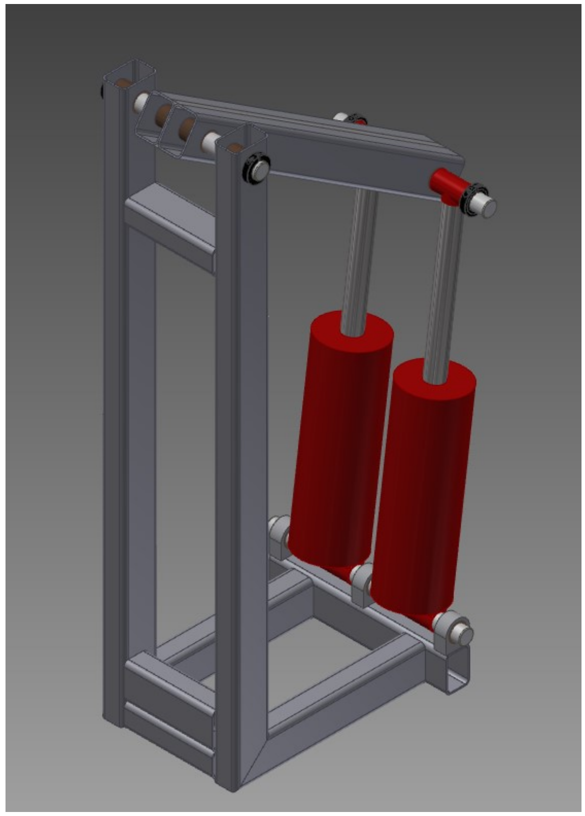

Figure 59: apparatus Version 3

In an attempt to cut the costs of the project, version 3 utilized two hydraulic pistons as springs once combined with a hydraulic accumulator. This design mounted the track coupon above the cylinders on the angled beam. As the loading frame pushed down the beam would rotate causing the point of contact on the coupon to move. It was discovered geometrically that due to the non-zero radius of the roller, the required length of roll was not practicably achievable.

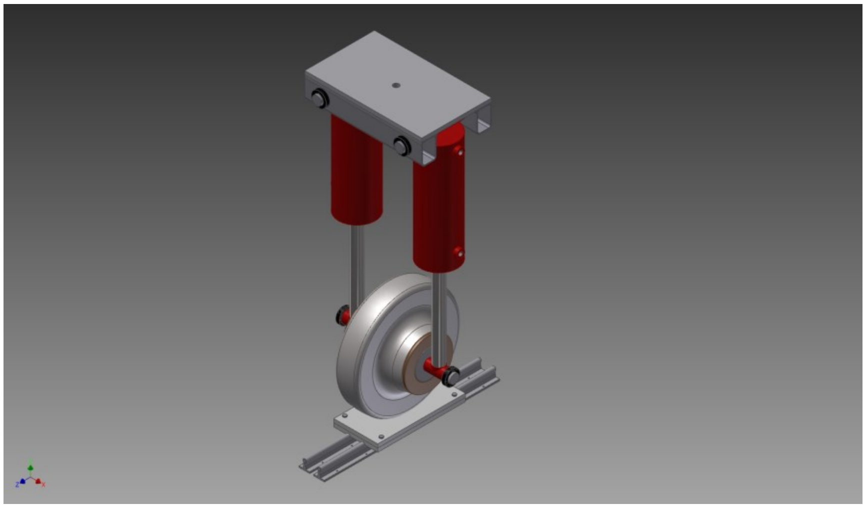

Figure 60: Apparatus Version 4A

Apparatus version 4A was a minor concept design, drawn to test the idea of having the MTS loading frame directly move the coupon instead of having a separate system.

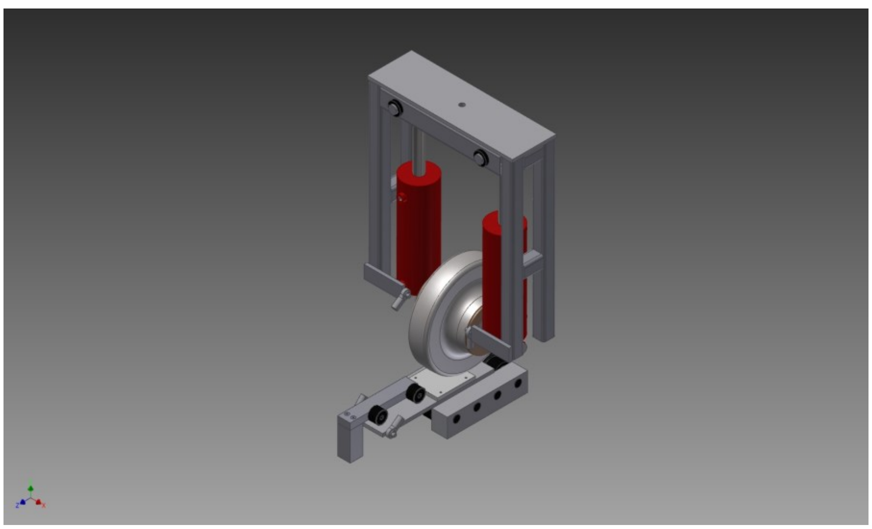

Figure 61: Apparatus Version 4B

Version 4B was considered to be the final design. It utilized the piston/accumulator spring setup as version 3 did to create a vertical movement with the changing loads. The frame surrounding the pistons would be linked to the shuttle, causing the shuttle to move exactly with the changing loads in the frame. As the pistons were compressed the frame would lower pushing on the links which would move the shuttle/coupon out. Similar for the reverse scenario. After a site visit (Sunhills Mining, 2015), it was determined that this test was not representative of the real world scenario due to the motion and the loading being so directly tied together.

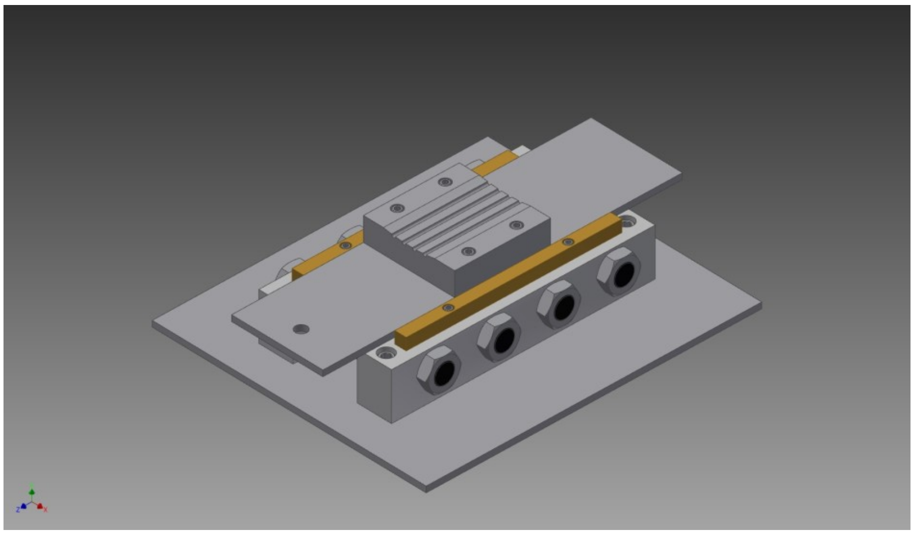

Figure 62: Apparatus Version 5 – Concept

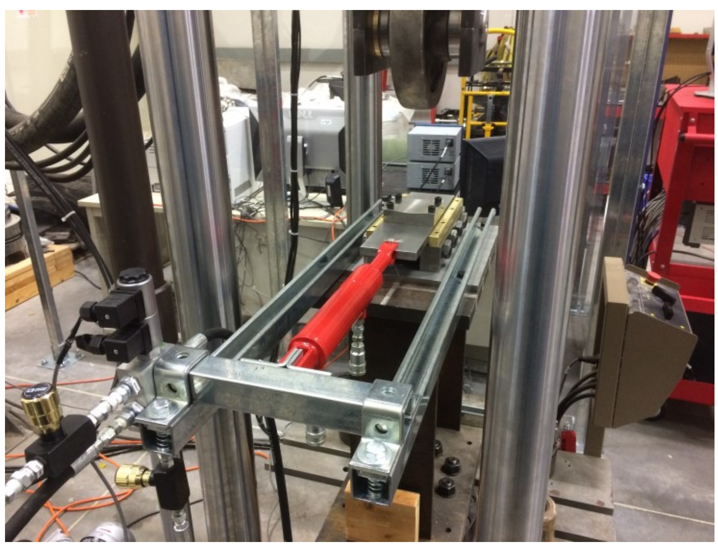

Figure 63: Apparatus Version 5 – Working Prototype

The final design removed the need of having the frame directly control everything and returned to using a separate system for coupon movement. Using a hydraulic ram attached to the shuttle in Figure 62, the coupon would be pushed back and forth under the frame mounted roller. The MTS software, using trigger points in the load cycles to initiate the movement of the coupon, controlled the ram. Using this system the motion of the coupon could be programed, allowing for the coupon to be pushed or held in place independent of the actual motion or loading from the MTS frame. The decision for independent control of load and coupon movement came as a field study at Sunhills Mining revealed the rocking action on the track occurred when the load was constant, and was held rigid while the shovel was actively digging or dumping its load it.

Appendix C: Additional Notes

C.1 Lower Roller Field Loading Profiles

Below are shown the load levels experienced by each roller position for each phase of the dig cycle. Data for eight dig cycles were represented with the error bars representing the minimum and maximum average load. Roller position 1 was to the heel (rear) of the shovel under the counterweight, and roller position 8 was at the toe (front) of the shovel. The phase with the widest range of roller loading was the "Full Suspended Phase" as each load was unique in the data. Lower suspended loads represented a partially loaded bucket, while higher suspended loads represented a fully loaded bucket. The phase with the narrowest range was the empty suspended phase because the bucket would always weigh the same while empty. The only variation from the empty bucket weight would be in the event of carry back material. The distribution on the max digging phase was likely due to the required hoist force on each dig, varying with material density, ground penetration, or dig speed. The distribution on the empty tucked phase was likely due to how far into the tucked position the bucket was taken before beginning the next dig cycle. Other factors not considered here may also contribute (e.g. presence of large rocks).

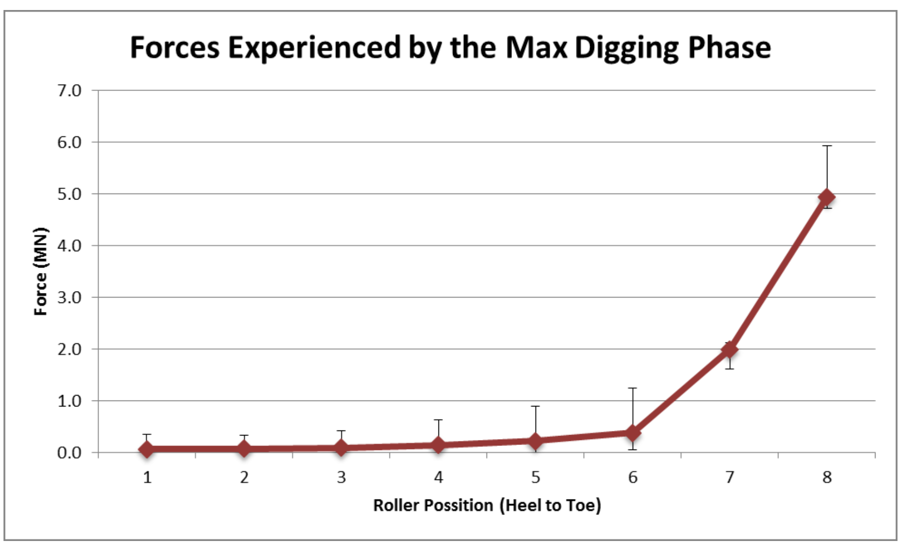

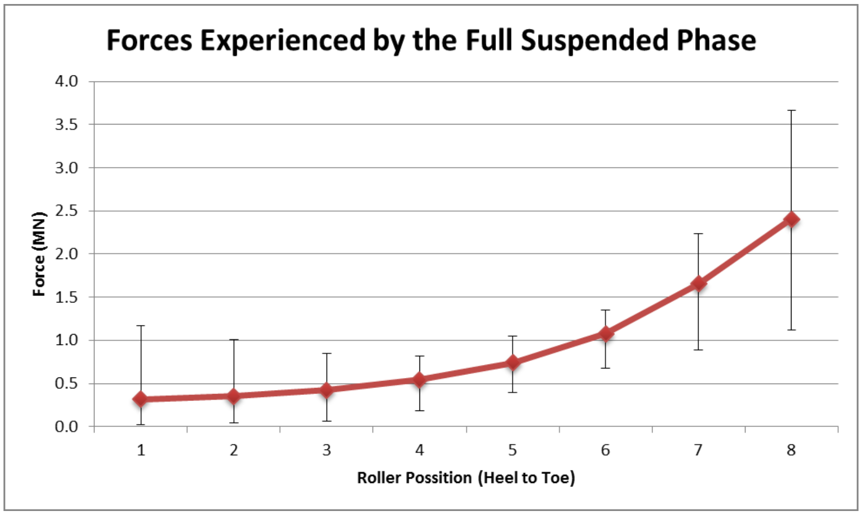
Forces Experienced by the Full Suspended Phase
Force (MN)
4.0
3.5
3.0
2.5
2.0
1.5
1.0
0.5
0.0
1
2
3
4
5
6
7
8
Roller Possition (Heel to Toe)

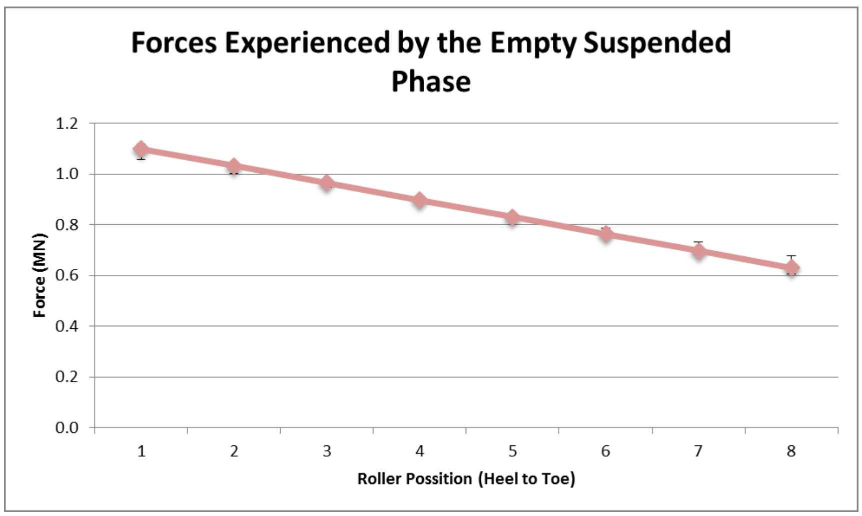
Forces Experienced by the Empty Suspended Phase
Force (MN)
1.2
1.0
0.8
0.6
0.4
0.2
0.0
1
2
3
4
5
6
7
8
Roller Possition (Heel to Toe)

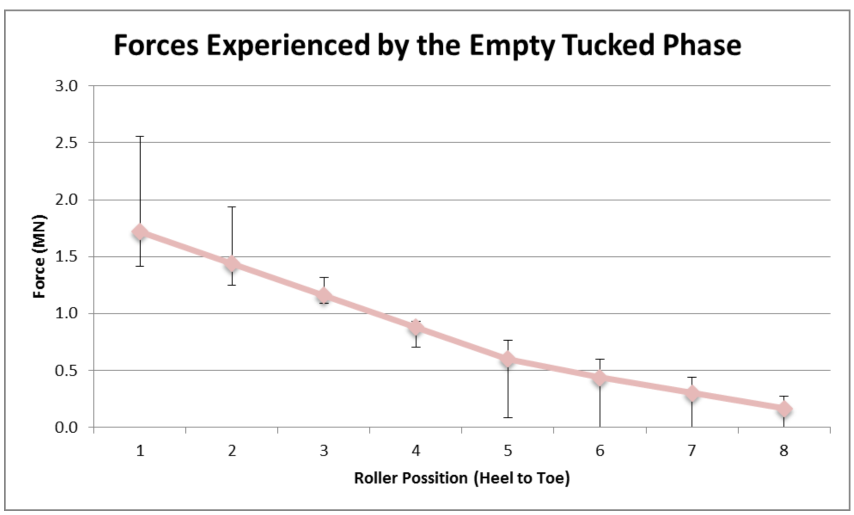
Forces Experienced by the Empty Tucked Phase
Force (MN)
3.0
2.5
2.0
1.5
1.0
0.5
0.0
1
2
3
4
5
6
7
8
Roller Possition (Heel to Toe)

C.2 Operation of MTS Frame

This section will be used as a safe work procedure for day to day operation of the MTS loading frame.

1. Turn on the pump bank and run on low pressure for warmup.
2. At the control computer select “New Specimen” and rename it appropriately (This step only required for day to day comparison or data collection).
3. Turn on the small pump for the horizontal ram, first making sure the solenoid valve is set to neutral (Digital Outputs in Figure 65 turned to the “Off” position). The pump is turned on with the light switch on the desk next to the monitor.
4. After 10 minutes turn the main pumps to high pressure
5. Engage the power then the pressure on the MTS frame indicated by the HPU and HSM 1 settings respectively. Set to low until stable and switch to high. See Figure 64.
    a. Off is stage 1 (one red line)
    b. Low is stage 2 (two orange lines)
    c. High is stage 3 (three green lines)
6. Using the “Manual Controls” panel in Figure 65, lift the main roller off the coupon by setting it to -17 (Negative direction is up, or retracted)
7. Spin the main roller a few rotations to spread around the lubrication. The operational rotation of the main roller is 15 degrees and risks pushing the grease out of position.
8. Position the roller at a random point with the hatched side downwards if using the 4340 coupon, or upwards if using the A128 E1 coupon.
9. Lift the shuttle and spin each lower shuttle roller a few complete rotations.
10. Using compressed air, blow off any brass or debris that have accumulated (may not be required with the use of rollers instead of brass guides).

11. Using the “Manual Controls” panel in Figure 65 lower the main roller to lower the main roller to the coupon.
12. Deselect the “Enable Manual Command” checkbox in the Manual Controls panel, and select the “Run” button on the Station Manager panel (Figure 64) in the MPT section (indicated as an arrow button).
13. Supervise the test. The most common indication of problems is the rapid oscillation of either the load or vertical displacement lines on monitor 2.
14. Upon detection of an issue, the MTS frame can be stopped by either the Emergency Stop button on the flex test control unit, or by clicking the Stop button in the MPT section. Should the ram be active it can be stopped by the light switch next to monitor 1.
15. At the end of the test period initiate shutdown by turning off the horizontal ram. It’s best to do this after full extension as mid push and full retraction can create problems for start-up of the next test period. Further details at the end of this section.

    Note: The MTS frame will ramp down to its lowest load (following the load pattern in this paper) and will remain there, waiting for the ram to retract.
16. Stop the MTS frame by selecting the “Stop” button in the MPT section of the Station Manager panel.
17. Select the “Unlock” option in the Station Manager
18. Select the “Enable Manual Command” checkbox in the Manual controls panel.
19. Unload the frame by moving the selector in the negative direction. Stopping as soon as the output reads 0 kN. Lifting the main roller off the coupon is not recommended, as it will settle down again after the frame is shut down.
20. Release the main pressure lines by selecting the “Low” setting for HSM 1 on the Station Manager panel.
21. After the system has stabilized, select the “Off” position for HSM 1.
22. Disable the main power by selecting “Low” then “Off” for the HPU setting.
23. Press and hold the “High Pressure” button on the main pump bank until it deselects. Wait for the psi to level out at approximately 190 psi.

24. Press the “Off” button on the main pump bank to turn it off.

Operational Notes:

- With further development of the program, the ram can also be stopped by the MTS controls. Allowing all processes to be stopped in this manner will increase safety of the system and allow for better remote monitoring or access.
- Stopping the horizontal ram mid push/pull for the shutdown will cause the solenoid valve to remain in the push/pull position. Upon start-up for the next test period the ram will begin moving the shuttle as soon as soon as the power is turned on. Unless caught, this movement will bend or damage the stop sensors in place and can push the limiters off the main platform. The unexpected shuttle movement can be fixed by turning all the digital outputs to the “Off” position (Figure 65), but this extra step and possible negligence can be avoided by waiting for the shuttle to reach the limiter before shutdown.
- Stopping the ram in the fully retracted position will cause the home sensor to be fully depressed and remain depressed until the next test period. Upon start-up, the beginning of the MTS program causes the horizontal ram to retract until reaching home. Because the shuttle is already in the home position it will immediately send the stop signal. There is a brief period where the shuttle retracts, causing the sensor to bend. Sensor damage can be avoided by using the digital outputs as seen in Figure 65 to manually move the shuttle off the limiter. Digital output 1 controls retraction, and digital output 2 controls extension of the ram. Alternatively stopping the ram in the fully extended position at the end of the test period will also prevent sensor damage.

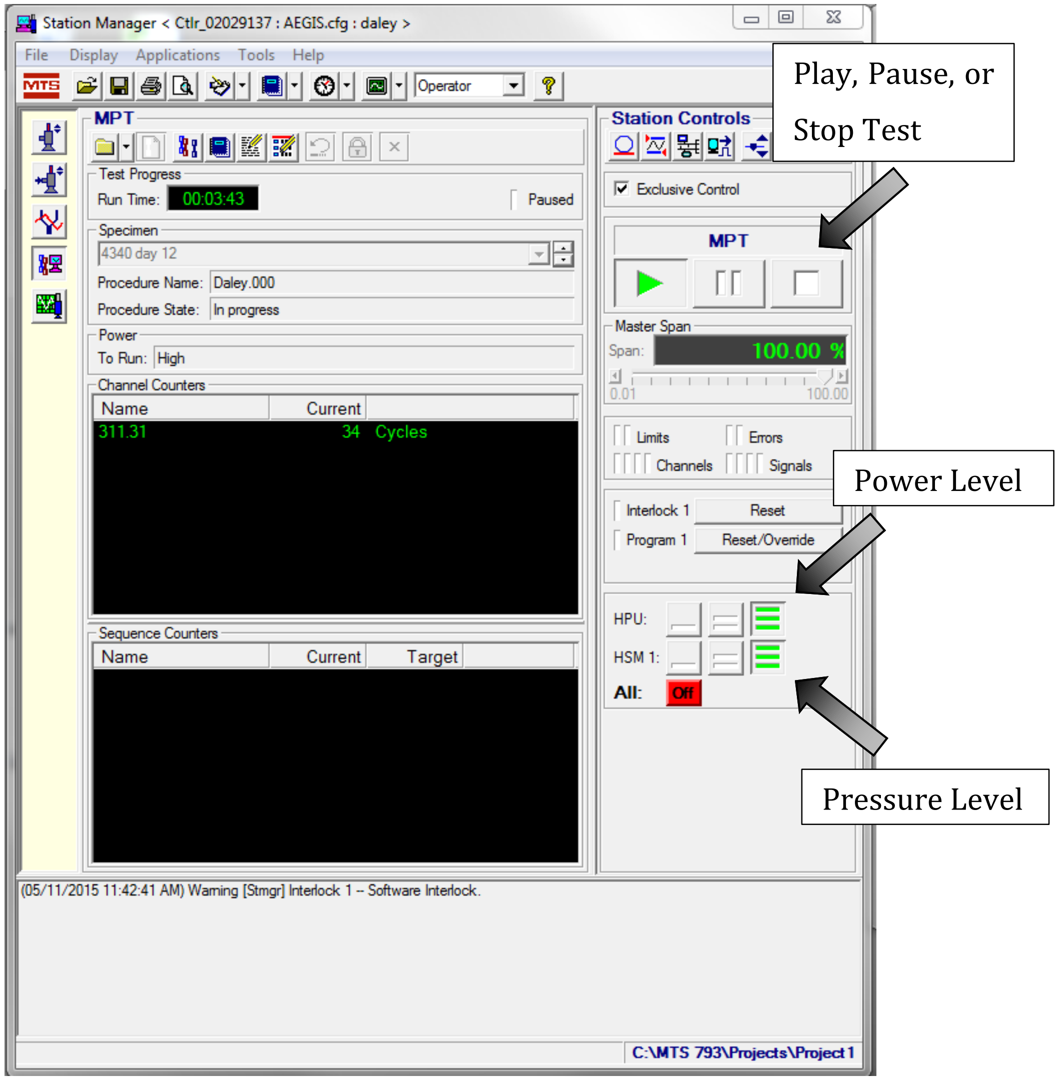

Figure 64: Main MTS control panel

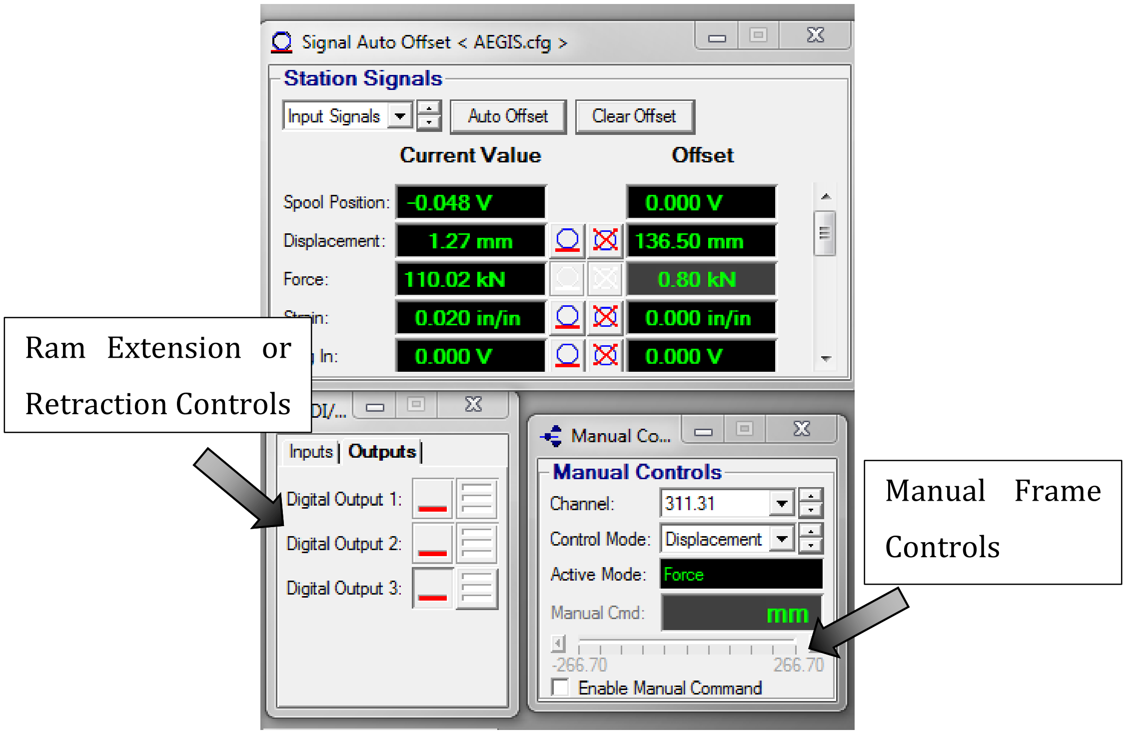

Figure 65: Manual Controls for Frame and Ram

Appendix D: Apparatus Construction Drawings

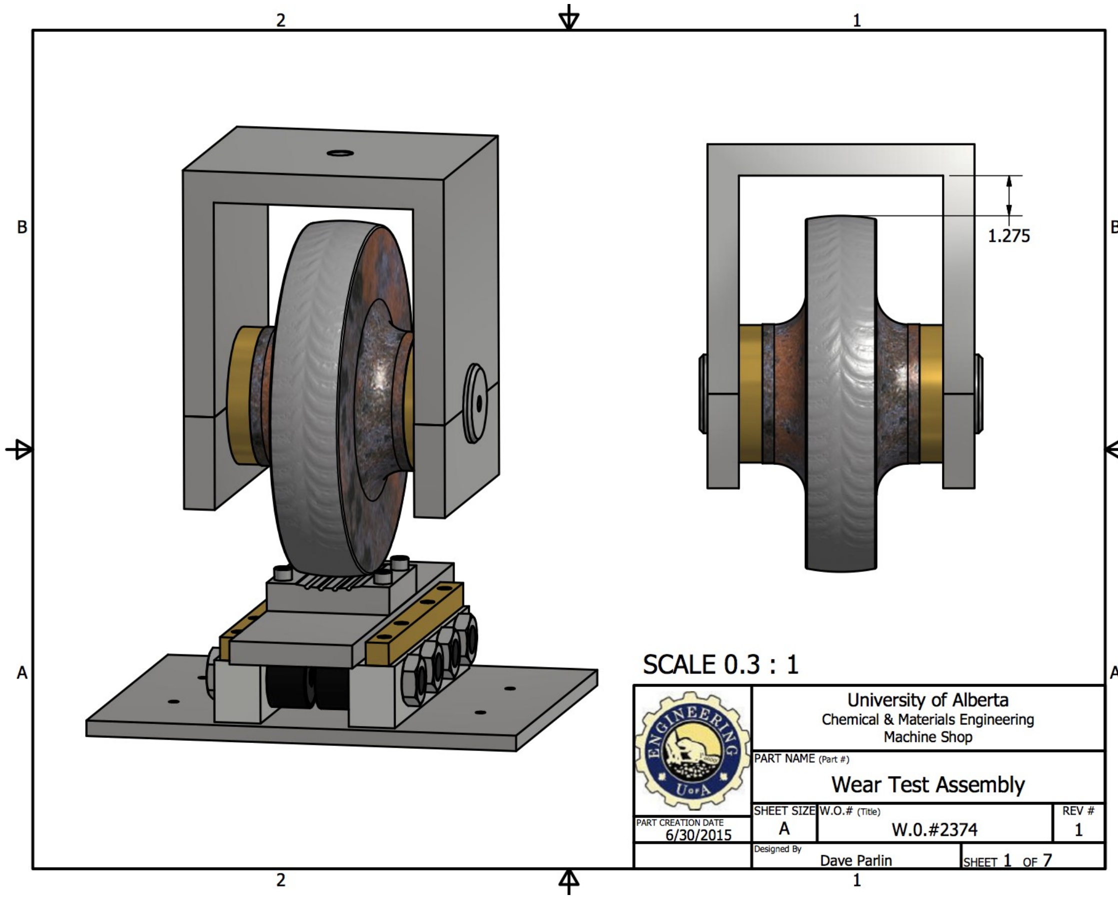

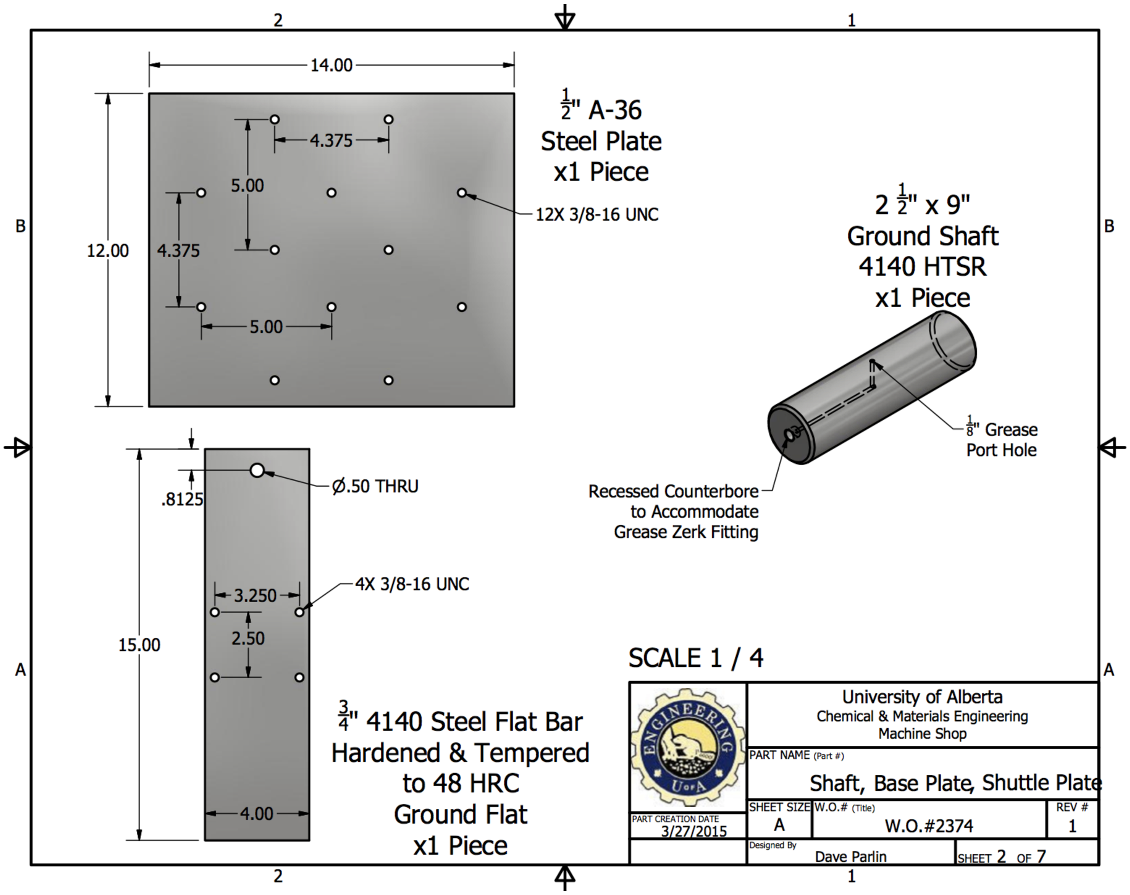

2
1
B
A
14.00
4.375
5.00
12.00
4.375
5.00
½" A-36
Steel Plate
x1 Piece
12X 3/8-16 UNC
2 ½" x 9"
Ground Shaft
4140 HTSR
x1 Piece
⅛" Grease
Port Hole
Recessed Counterbore
to Accommodate
Grease Zerk Fitting
.8125
Ø.50 THRU
15.00
3.250
4X 3/8-16 UNC
2.50
4.00
¾" 4140 Steel Flat Bar
Hardened & Tempered
to 48 HRC
Ground Flat
x1 Piece
SCALE 1 / 4
University of Alberta
Chemical & Materials Engineering
Machine Shop
PART NAME (Part #)
Shaft, Base Plate, Shuttle Plate
SHEET SIZE
A
W.O.# (Title)
W.O.#2374
REV #
1
PART CREATION DATE
3/27/2015
Designed By
Dave Parlin
SHEET 2 OF 7

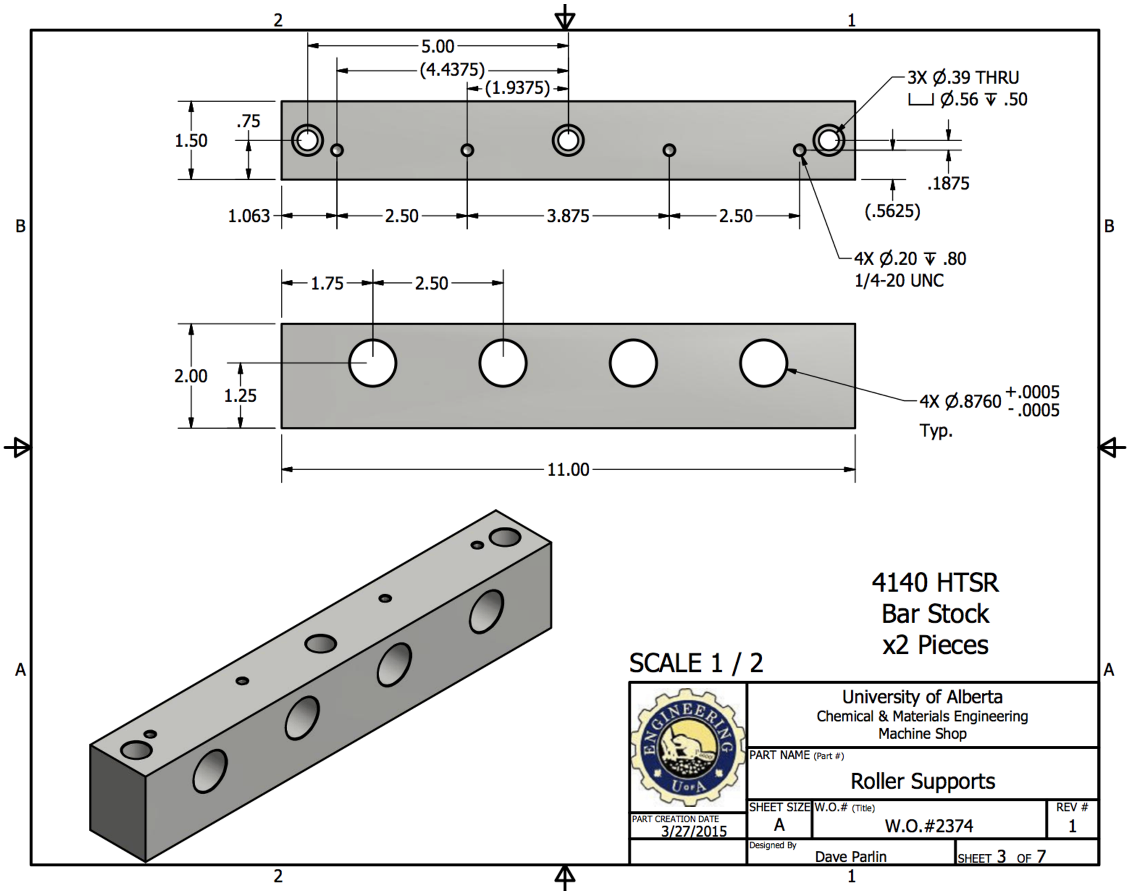
5.00
(4.4375)
(1.9375)
3X Ø.39 THRU
⌴ Ø.56 ↧ .50
1.50
.75
.1875
(.5625)
1.063
2.50
3.875
2.50
4X Ø.20 ↧ .80
1/4-20 UNC
1.75
2.50
2.00
1.25
4X Ø.8760 +.0005 -.0005
Typ.
11.00
4140 HTSR
Bar Stock
x2 Pieces
SCALE 1 / 2
University of Alberta
Chemical & Materials Engineering
Machine Shop
PART NAME (Part #)
Roller Supports
SHEET SIZE
A
W.O.# (Title)
W.O.#2374
REV #
1
PART CREATION DATE
3/27/2015
Designed By
Dave Parlin
SHEET 3 OF 7

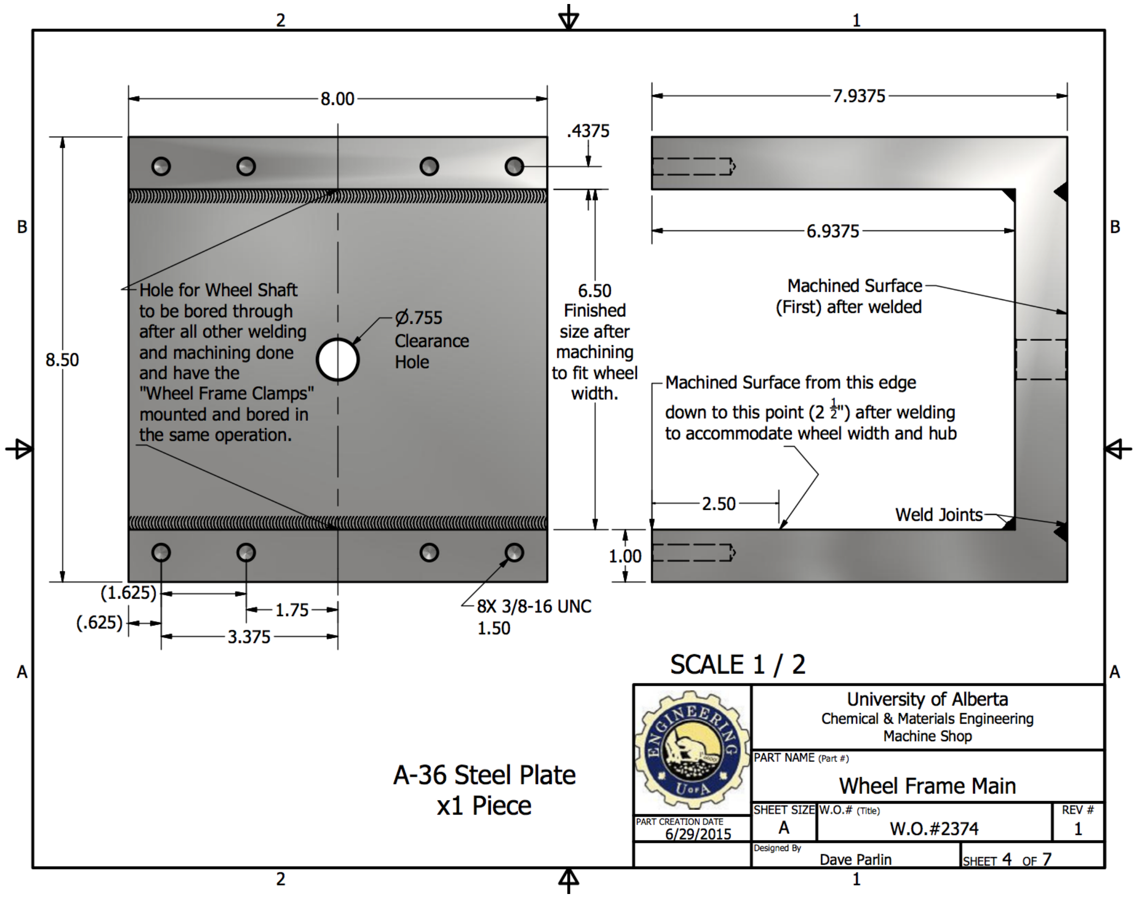

2
1
B
A
8.00
.4375
7.9375
6.9375
Hole for Wheel Shaft to be bored through after all other welding and machining done and have the "Wheel Frame Clamps" mounted and bored in the same operation.
Ø.755 Clearance Hole
6.50 Finished size after machining to fit wheel width.
Machined Surface (First) after welded
Machined Surface from this edge down to this point (2 ½") after welding to accommodate wheel width and hub
8.50
2.50
Weld Joints
1.00
(1.625)
1.75
(.625)
3.375
8X 3/8-16 UNC 1.50
SCALE 1 / 2
A-36 Steel Plate
x1 Piece
University of Alberta
Chemical & Materials Engineering
Machine Shop
PART NAME (Part #)
Wheel Frame Main
SHEET SIZE A
W.O.# (Title) W.O.#2374
REV # 1
PART CREATION DATE 6/29/2015
Designed By Dave Parlin
SHEET 4 OF 7

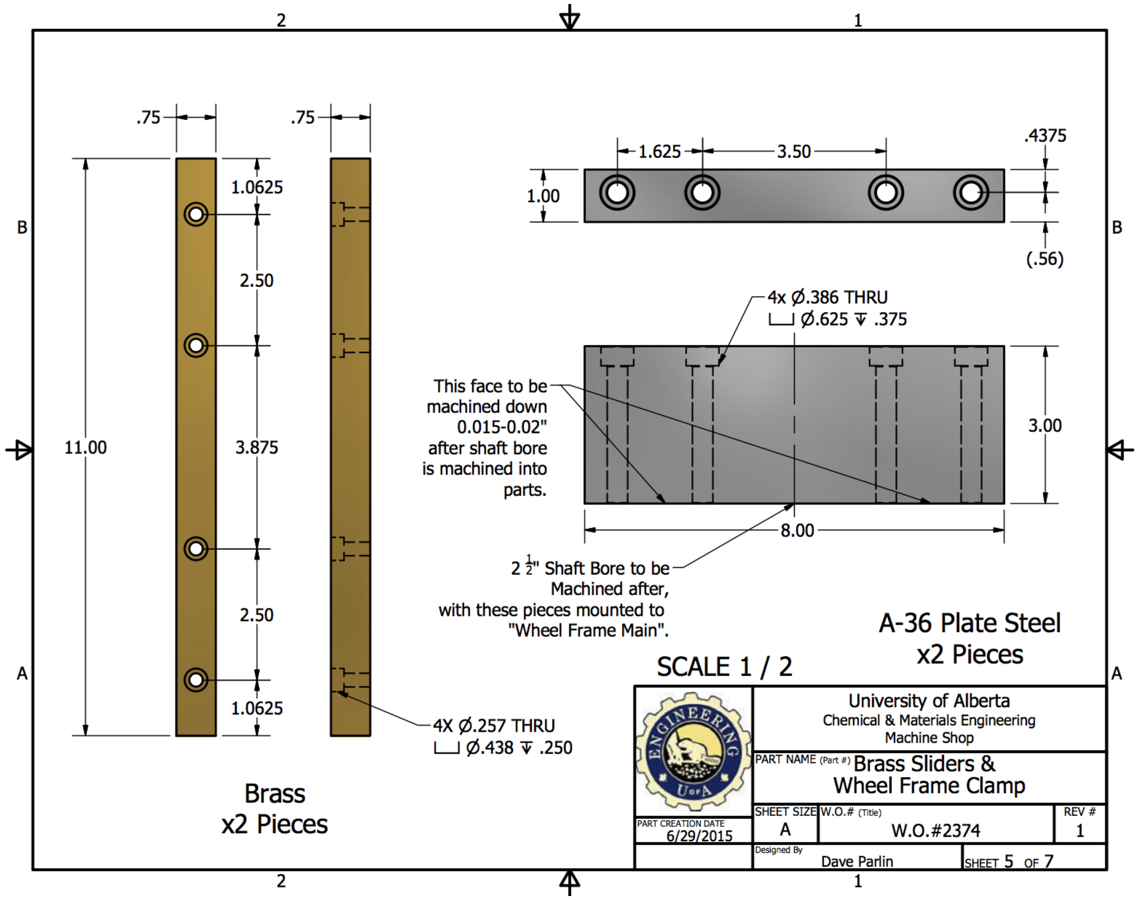

.75
1.0625
2.50
11.00
3.875
2.50
1.0625
4X Ø.257 THRU
⌴ Ø.438 ↧ .250
Brass
x2 Pieces
1.625
3.50
.4375
1.00
(.56)
4x Ø.386 THRU
⌴ Ø.625 ↧ .375
This face to be machined down 0.015-0.02" after shaft bore is machined into parts.
3.00
8.00
2 1/2" Shaft Bore to be Machined after, with these pieces mounted to "Wheel Frame Main".
A-36 Plate Steel
x2 Pieces
SCALE 1 / 2
ENGINEERING
U of A
University of Alberta
Chemical & Materials Engineering
Machine Shop
PART NAME (Part #) Brass Sliders & Wheel Frame Clamp
PART CREATION DATE 6/29/2015
SHEET SIZE A
W.O.# (Title) W.O.#2374
REV # 1
Designed By Dave Parlin
SHEET 5 OF 7

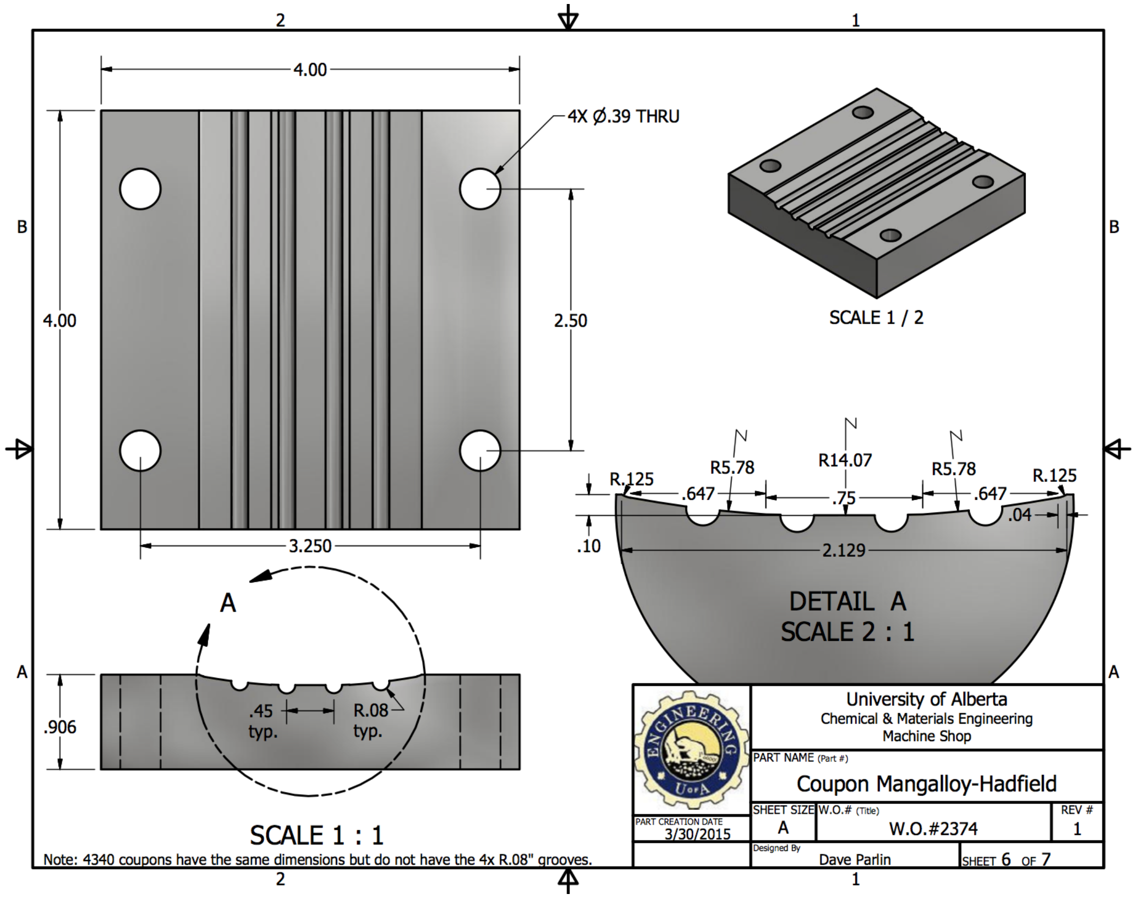

Note: the coupons for the 4340 or 4330 material are identical to this design but without the flutes (grooves in the roller path).

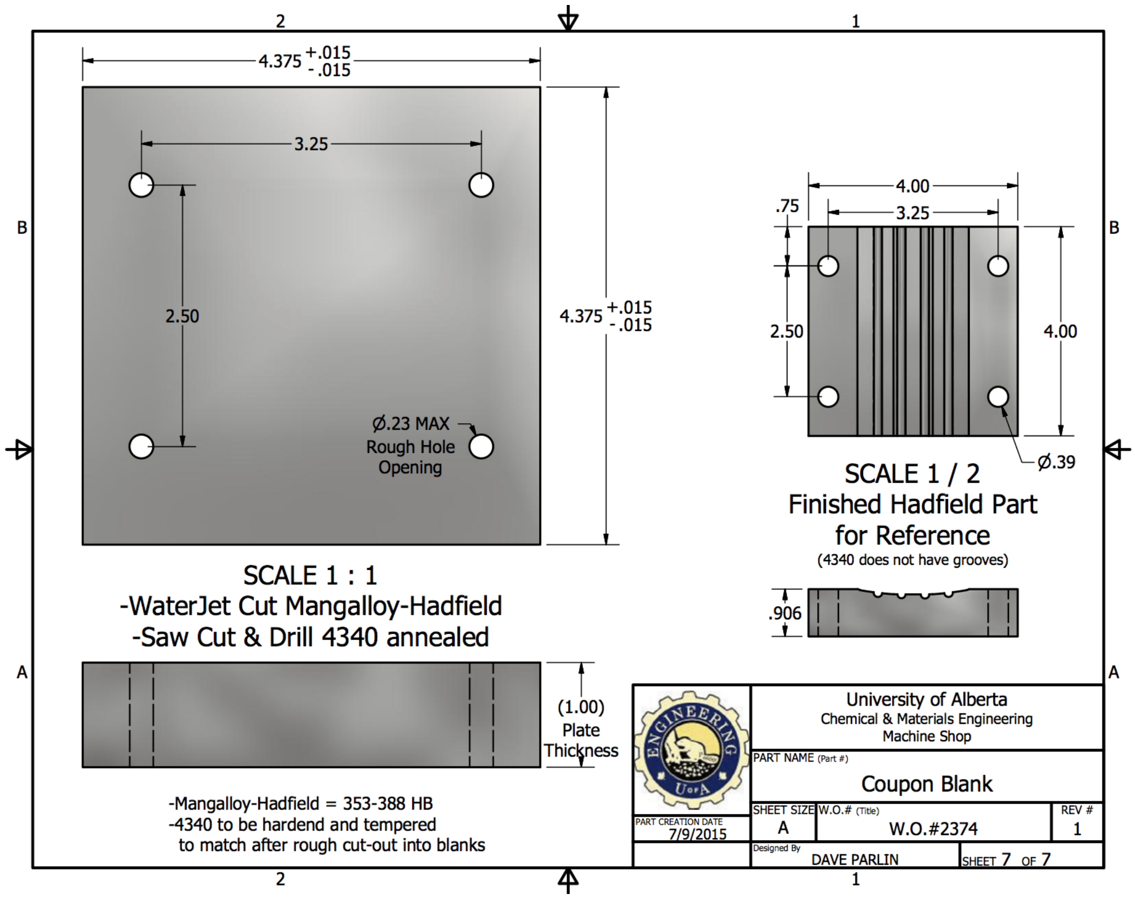
4.375 +.015 -.015
3.25
2.50
Ø.23 MAX Rough Hole Opening
SCALE 1 : 1
-WaterJet Cut Mangalloy-Hadfield
-Saw Cut & Drill 4340 annealed
(1.00) Plate Thickness
-Mangalloy-Hadfield = 353-388 HB
-4340 to be hardend and tempered
to match after rough cut-out into blanks
4.00
.75
4.00
Ø.39
.906
SCALE 1 / 2
Finished Hadfield Part
for Reference
(4340 does not have grooves)
University of Alberta
Chemical & Materials Engineering
Machine Shop
PART NAME (Part #)
Coupon Blank
SHEET SIZE A
W.O.# (Title) W.O.#2374
REV # 1
PART CREATION DATE 7/9/2015
Designed By DAVE PARLIN
SHEET 7 OF 7

Appendix E: Material and Hardening specifications

7/17/2015 https://mail-attachment.googleusercontent.com/attachment/u/0/?ui=2&ik=b948583fda&view=att&th=14e9cc039699d088&attid=0.1&disp=inline&safe=1&z...

EARLE M. JORGENSEN COMPANY

Order Confirmation

DATE: 7/17/2015
CUSTOMER NUMBER: 291580
QUOTE NUMBER: 258261
FOB: Delivered
CUSTOMER PO#: VERBAL - DAVE

6925 8TH STREET NW
ATTN:
EDMONTON AB T6P 1T9

CUSTOMER:
UNIVERSITY OF ALBERTA
CCIS - 181 UNIVERSITY OF ALBERTA
EDMONTON AB T6G 2G7
ATTENTION: DAVE
PHONE NO: 780-4923393

SHIP TO:
UNIVERSITY OF ALBERTA
C/O CHEMICAL & MATERIALS ENGIN
114 STREET - 89TH AVENUE - SOUTH ACADEMIC BUILDING
EDMONTON AB T6G 2G7

ITEM #	DESCRIPTION	ORDER QTY.	UOM	UNIT PRICE	EXT. PRICE	DATE/TYPE
507620	1 PC-82 LB 4340 HR ANN PLATE ASTM A829 1 F/C 12.000" X 24.000" RECTANGLE PO Line:0 CUTTING FLAME tolerance: +1/4 -0 THERMAL TREATING STRESS R **SHIP VIA:** OUR TRUCK	1	EA	C$561.00	C$561.00	7/28/2015
	LINE WEIGHT:	82	LB			

COPY

TOTAL WEIGHT:	82 LB
TOTAL:	C$561.00
Sales Tax:	C$28.04
Grand Total:	C$589.04

For further information about your order, please contact your material specialist: **CODY HINTON**
E-Mail: CHINTON@EMJMETALS.COM Phone: **(780)801-4015 (877)907-5055** Fax: **(780)463-1215**

******PLEASE, VERIFY ITEMS ON THIS CONFIRMATION.******
IF NO DISCREPANCIES ARE REPORTED, YOUR ORDER WILL SHIP AS SHOWN.

CONDITIONS: All items are subject to prior sale. All items are subject to price in effect at time of shipment unless we have specifically noted otherwise. Delivery date based upon lead time of quotation and is subject to change at time of order. All weights are theoretical and may be subject to adjustment. Any process not specifically quoted in the above price will be an additional charge. These commodities are controlled for export by the United States government under the Export Administration Regulations. Diversion contrary to U.S. law prohibited. Purchaser is responsible to comply with these regulations if the items are to be exported from the United States or re-exported from a foreign country. Please refer to our website for full terms & conditions at: http://www.emjmetals.com/SOTerms.pdf.
TERMS OF PAYMENT: Invoices are issued as of the date of delivery covering deliveries from our stocks and as of the date of the shipment covering direct mill shipments. The acceptance of any order or specification and terms of payment on all sales and orders is subject to approval of the Sellers Credit Department, and Seller may at any time decline to make any shipment or delivery or perform any work except upon receipt of payment or security or upon terms and conditions satisfactory to Sellers Credit Department.

https://mail-attachment.googleusercontent.com/attachment/u/0/?ui=2&ik=b948583fda&view=att&th=14e9cc039699d088&attid=0.1&disp=inline&safe=1&zw&sad... 1/1

JOYGLOBAL

JOY GLOBAL LONGVIEW OPERATIONS LLC
LONGVIEW, TEXAS, U.S.A.
ISO 9001:2008 Registered Quality System
Material Test Report

R 6118+9

REPORT OF CHEMICAL AND PHYSICAL TESTS OF STEEL PLATE — DATE: 03/26/15 — PAGE: 1 of 1

SOLD TO: Earle M. Jorgensen - Schaumburg
1900 Mitchell Blvd.
Schaumburg IL 60193

SALES ORDER NO.: 196142
PURCHASE ORDER NO.: P641823-423

GRADE: ASTM A829 Grade 4340, Annealed
HEAT NO.: E55924 ROLL NO.: 89994

SIZE: 1" x 96" x 294"
CUSTOMER PRODUCT: 507620

LADLE ANALYSIS

C	MN	S	P	SI	CR	NI	MO	AL	V	CU	NB
0.4100	0.7500	0.0050	0.0090	0.2900	0.8500	1.8800	0.2500	0.0250	0.0050	0.1900	0.0020

PHYSICAL ANALYSIS

HEAT TREAT	TEMP	TIME HRS/MINS	YIELD STRENGTH (psi)	TENSILE STRENGTH (psi)	2" GAGE %ELONG	%RA	HARDNESS LOW/HIGH	CHARPY TEST INFO TEMP	TYPE	FT/LBS	LAT EXP	% SHEAR
Annealed	1500F	36:30					223 - 223 BHN					

McQuaid-Ehn grain size per ASTM E112: 7

ELECTRIC FURNACE MELTED.
ASTM A829 GRADE 4340, 2014 EDITION. REDUCTION RATIO 16.0:1 CAST JOMINY TEST RESULTS ATTACHED.
MATERIAL TEST REPORT PREPARED IN ACCORDANCE WITH EN10204 3.1, REV 2004.

MATERIAL WAS MELTED AND MANUFACTURED IN THE U.S.A.
IN ACCORDANCE WITH THE RECORDS OF JOY GLOBAL LONGVIEW OPERATIONS LLC, I CERTIFY THE ABOVE INFORMATION IS CORRECT.

Anna Bowers
ANNA BOWERS
TECHNICAL SERVICES DEPARTMENT

Thermex METAL TREATING LTD.
7434 - 18 Street, Edmonton, AB T6P 1N8
Ph: (780) 440-4373 Fax: (780) 440-4376
Toll Free: 1-877-585-5055

Thermex Metal Treating Ltd.

Certification

Order No.: 161510
Date: 08/13/2015
Entry Date: 08/11/2015
Page: 1 of 1

To:
UNIVERSITY OF ALBERTA
TECHNICAL SERV. MACHINE SHOP
RM. 132 CHEMICAL MINERAL ENG.
EDMONTON AB T6G 2E1

141982

Purchase Order No.: DAVE PARLIN
Packing List No.:
Material: 4340

We are pleased to provide you with the following Certification

Quantity	Part Number / Part Name / Part Description	Pounds
8	TRACK SHOES, MATL 4340 QUENCH AND TEMPER TO 353-388 HB	42

Insp. Type	Scale	Minimum	Maximum	Number	Other
Customer Requirements:					
HB	HB	355.	388.	.	
Results:					
HB	HB	387.			

2 PCS TESTED BY M MORILLO ON AUG 12/15

Unless otherwise noted, hardness test results are based on random testing, using equipment calibrated in accordance with QSP 116, Thermex Quality System Procedure for Calibration. All process equipment is calibrated per QSP 116 and IP-038.

ROBERT DUCHARME
OPERATIONS MANAGER
THERMEX METAL TREATING LIMITED

All processing and testing personnel are trained and approved in accordance with QSP 124, Thermex Quality System Procedure for Training, Indoctrination and Qualification.

7434 - 18 Street Edmonton AB T6P 1N8 **Phone:** (780) 440 - 4373 **Fax:** (780) 440 - 4376

SOLUTIONS THROUGH METALLURGY **ISO 9001**

Thermex METAL TREATING LTD.
7434 - 18 Street, Edmonton, AB T6P 1N8
Ph: (780) 440-4373 Fax: (780) 440-4376
Toll Free: 1-877-585-5055

Thermex Metal Treating Ltd.

Certification

Order No.: 162582
Date: 10/02/2015
Entry Date: 09/30/2015
Page: 1 of 1

To:
UNIVERSITY OF ALBERTA
TECHNICAL SERV. MACHINE SHOP
RM. 132 CHEMICAL MINERAL ENG.
EDMONTON AB T6G 2E1

143124

Purchase Order No.: DAVE PARLIN
Packing List No.:
Material: 4140

We are pleased to provide you with the following Certification

Quantity	Part Number / Part Name / Part Description	Pounds
1	4" X 15" PLATE, MATL 4140 QUENCH AND TEMPER TO 45-50 HRC Shuttle Plate	13

Insp. Type	Scale	Minimum	Maximum	Number	Other
Customer Requirements:					
HRC	HRC	45.	50.	.	
Results:					
HRC	HRC	47.	49.		

1 PC TESTED BY C WALKER ON OCT 1/15

Unless otherwise noted, hardness test results are based on random testing, using equipment calibrated in accordance with QSP 116, Thermex Quality System Procedure for Calibration. All process equipment is calibrated per QSP 116 and IP-038.

ROBERT DUCHARME
OPERATIONS MANAGER
THERMEX METAL TREATING LIMITED

All processing and testing personnel are trained and approved in accordance with QSP 124, Thermex Quality System Procedure for Training, Indoctrination and Qualification.

7434 - 18 Street Edmonton AB T6P 1N8 **Phone:** (780) 440 - 4373 **Fax:** (780) 440 - 4376

SOLUTIONS THROUGH METALLURGY **ISO 9001**

Appendix F: Electronics Spec Sheets

F.1 Power Unit (Hydro-Tek 1hp AC)

8457970

SPECIFICATIONS

	Specifications		Hydraulic Diagram
Model	S20760TC12-XB1C/600-GH 07A-HPCX-PXS04		
Motor	1 HP, 115/230V AC, 9.08/4.54 Amps., 60 Hz		
Pump	.043 Cu. In./Rev.	0.63 Gallons/Minute	
Relief Pressure Range	1,000~3,000 PSI		
Relief Pressure Setting	3,000 PSI		
Operating Temperature Range	-30°C ~ 40°C (-22°F ~ 104°F)		
Storage Temperature Range	-30°C ~ 60°C (-22°F ~ 140°F)		
Reservoir Size	1 Gallon		
Duty Cycle	S1 Duty		
Port Sizes	P	6 ORB	
	T	6 ORB	

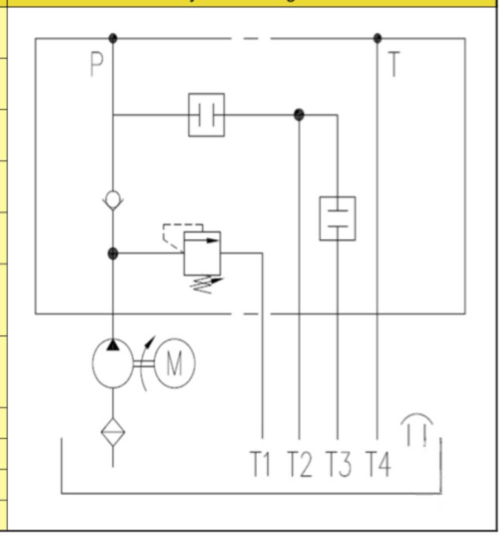

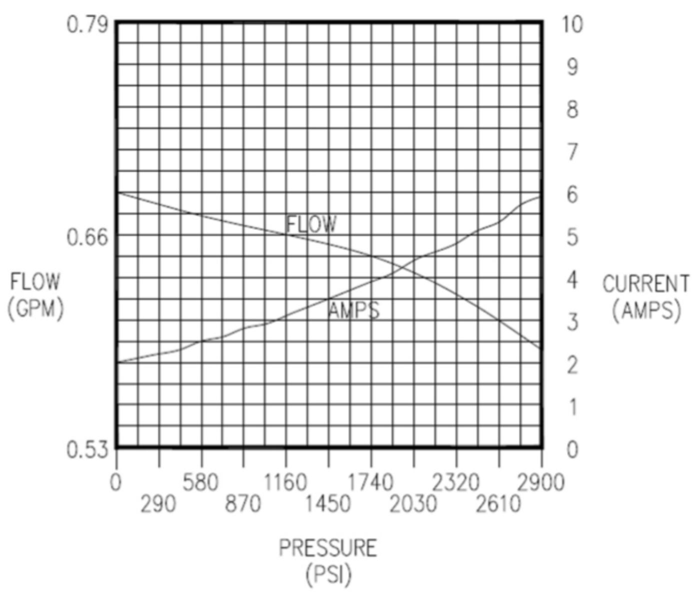

1

1 HP AC MULTIFUNCTION POWER UNIT

Hydro-Tek

INSTALLATION

Power Unit Dimensions (In.):

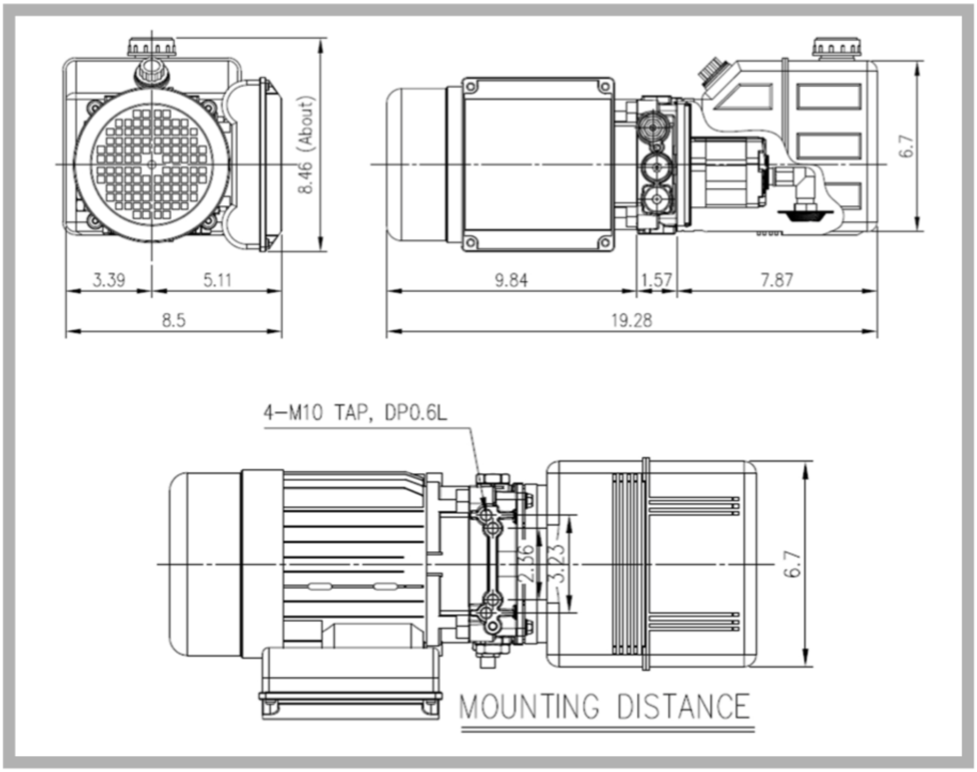

INSTALLATION INSTRUCTIONS:

1. Place the power unit into position and bolt onto the frame or appliance
2. Ensure the power unit reservoir is 80% full of oil prior to attaching the hoses
3. Connect up the power unit according to the Multifunction Instructions below.
4. Proceed to prepare the rest of the hydraulic circuit.
5. Check all hydraulic fittings and connections to ensure they are tight.
6. Wire up the power unit according to Diagram #2
7. When the power unit is used for the first time allow it to run at least 1 minute under no load to eliminate any entrained air then cycle the actuator two to three times and add oil if necessary.

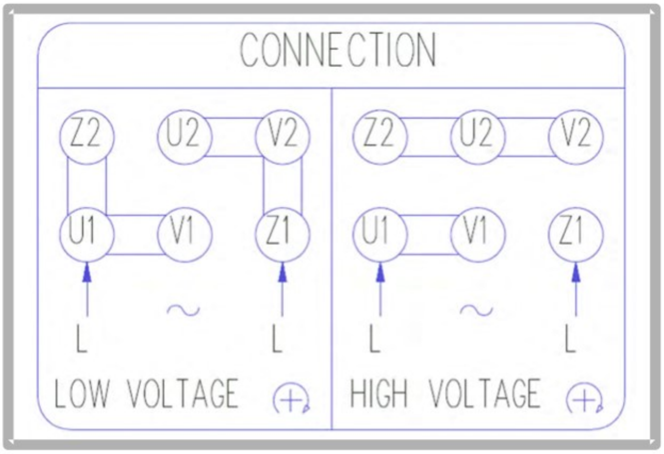

Diagram #2

WARNING! All wiring should be performed by a qualified electrician.

Multifunction Instructions:

This power unit is capable of controlling hydraulic cylinders and motors in 3 different ways.

#1 – Single Acting Power Unit

This power unit can easily be converted in to a single acting power unit. You will require the following components to make this conversion.

A single acting cartridge valve (Item# 8512691):

A cartridge valve coil:

115V AC (Item# 8512832)

24V DC (Item# 8512808)

or 12V DC (Item#8512774)

HYDAC Solenoid Valves

WK10G-01
Spool Type, Direct Acting
Up to 6 gpm (23 l/min) • 5000 psi (350 bar)

Hydraulic Symbol

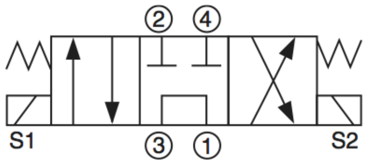

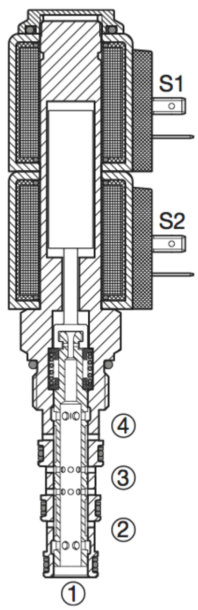

Description

A screw-in cartridge, solenoid operated, 4-way, 3 position, direct acting, spool type valve.

Operation

When de-energized the WK10G allows flow from port 3 to port 1, while blocking flow at ports 2 and 4. When coil S1 is energized the spool shifts and allows flow from port 3 to port 2 and from port 4 to port 1. When coil S2 is energized the spool shifts and allows flow from port 3 to port 4 and from port 2 to port 1.

Operation of Manual Override Option: To override, twist knurled screw and push or pull to shift spool.

Detented version - twist again after pushing/pulling to hold position.

Features

- Push/pull type manual override button, detented manual override option.

Specifications

Operating Pressure	5000 psi (350 bar)
Nominal Flow	6 gpm at 3000 psi (23 l/min at 210 bar) *Consult factory for flow rating above 3000 psi (210 bar)*
Internal Leakage	10 cu in/min. at 3000 psi and 158 SUS (160 cc/min at 210 bar and 34 cSt)
Fluid Operating Temp. Range	-4° to 248°F (-20° to 120°C) *(Consult factory for usage at temp. outside range.)*
Ambient Temperature Range	-4° to 140°F (-20° to 60°C)
Coil Duty Rating	Continuous from 85% to 115% of nominal voltage
Current Draw at 68°F (20°C)	1.5 A at 12VDC; 0.8 A at 24VDC
Minimum Pull-in Current	90% of nominal @ 5000 psi (350 bar)
Fluid Compatibility	Mineral-based or synthetics with lubricating properties
Viscosity	50 to 2000 SUS (7.4 to 420 cSt)
Filtration	21/19/16 or cleaner (per ISO 4406). Use with filter rated ß10 ≥ 200.
Installation	No orientation restrictions
Cavity	FC10-4 *(see Line Bodies & Cavities section)*
Cavity Tools	Rougher: 02580248 Finisher: 02580249
Cartridge Weight	0.64 lbs (0.29 kg)
Coil Weight	0.42 lbs (0.19 kg) - 2 coils required
Cartridge Material	Steel with hardened work surfaces. Zinc-plated exposed surfaces. Buna N or Viton® o-rings. PTFE back-up rings.
Coil Material	Class N high temperature magnet wire, steel shell, polyamid encapsulation.
Seal Kits Buna-N Viton®	FS104-N P/N: 03051912 FS104-V P/N: 03071275

Performance

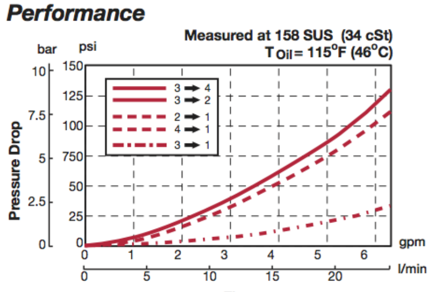

Dimensions

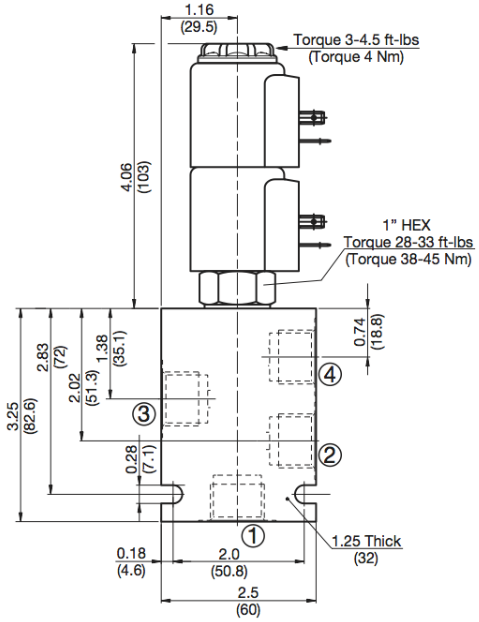

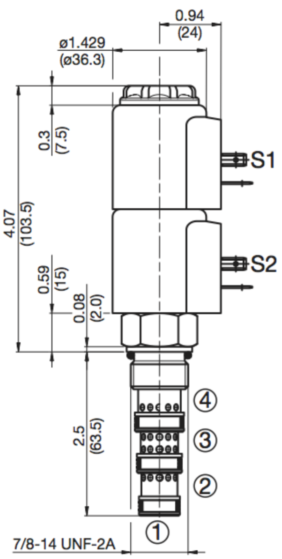

All measurements in inches (mm).
Subject to technical modifications

Model Code

WK10G-01-M-C-N-24 DN

Valve Model

Override Option
- *(omit)* = No manual override
- M = Push/pull type, not detented
- A = Push/pull type, detented

Body & Ports
- C = Cartridge only
- AS8 = SAE-8 ports, aluminum body
- SS8 = SAE-8 ports, steel body

Seals
- N = Buna-N
- V = Viton®

Coil Voltage
- 0 = No coil, cartridge only
- DC 12 = 12 VDC
- 24 = 24 VDC
- 36 = 36 VDC
- 110 = 110 VDC *(only available with connector DG)*
- AC 24 = 24 VAC
- 115 = 115 VAC
- 230 = 230 VAC

Coil Connector
- DC DG = EN 175301-803-A
- DS = Dual spade (SAEJ858a)*
- DL = Leadwires (2) - 18" long (46 cm)*
- DW = WeatherPak™ on leadwires - 9.5" long (24 cm)*
- DN = Deutsch™ DT04-2P, molded, axial (IP69K Rated)*
- DT = Amp Junior Timer™, molded, radial mount*
- AC AG = EN 175301-803-A

Coil Model 40-1836, 2 per assembly
For other coil connector types consult factory

*Coils with internal diode are available, consult factory.

Manual Override Options

Option M - Non Detented

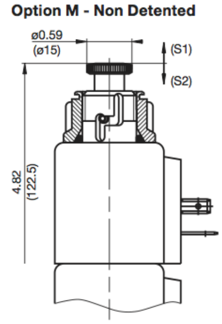

Option A - Detented

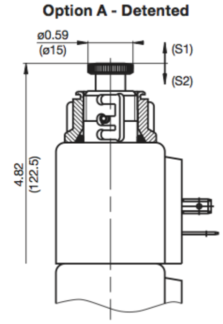

*Standard Line Bodies**

Code	Part No	Material	Pressure Rating	Weight
FH104-AS8	03038110	Aluminum, anodized	3500 psi (245 bar)	0.72 lb (0.33 kg)
FH104-SS8	03037868	Steel, zinc plated	6000 psi (420 bar)	2.12 lb (0.96 kg)

**Please refer to Line Bodies & Cavities section for details*

J54 Digital Inputs

Connector **J54 Dig In** accommodates up to three digital signals from external devices. You can use digital input signals to trigger test events with your controller applications.

- All of the inputs are optically isolated.
- Channel inputs can be 3 volts (minimum) and 26 volts (maximum) from an external voltage source.

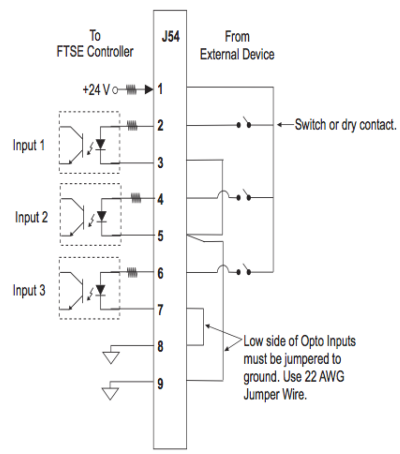

Cable specification

The cabling information shown assumes a single cable destination (with an overall shield). In other applications, the cable may have more than one destination. For these applications an overall shield is not practical and non-EMI connectors and back shells are permissible.

- 9 pin contact type D male EMI connector
- Back shell–EMI metallized plastic
- Cable–shielded twisted pairs as required (24 AWG minimum) with drain wire(s) connected to the metallized backshell at the chassis.

J55 Digital Outputs

Connector **J55 Dig Out** provides three general purpose digital outputs that can send digital logic signals to external switches or logic devices.

- The digital output relays are rated for a maximum of 1 Amp max, 30 V DC/AC max.
- The outputs are optically isolated.

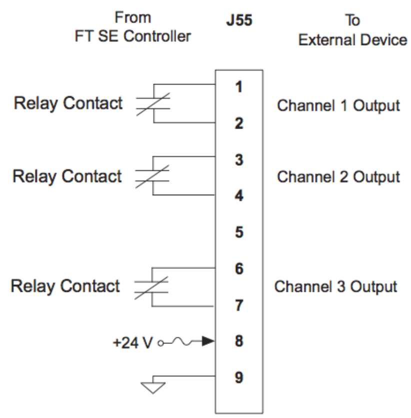

Cable specification

The cabling information shown assumes a single cable destination (with an overall shield). In other applications, the cable may have more than one destination. For these applications an overall shield is not practical and non-EMI connectors and back shells are permissible.

- 9 pin contact type D male EMI connector
- Back shell–EMI metallized plastic
- Cable–shielded twisted pairs as required (24 AWG minimum) with drain wire(s) connected to the metallized backshell at the chassis.

Run/Stop setup

If required, digital output 1 (pins 1 and 2) can be set up as a Run/Stop connector. Use the following procedures to set up this Run/Stop connector:

F.4 Limit Switch (LS-085-15-06-F045-C1-A)

SERIES LS SWITCHES

SNAP ACTION SWITCHES

E•SWITCH®

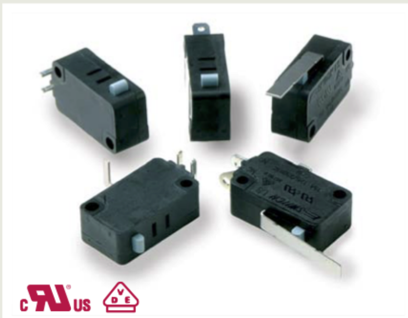

SPECIFICATIONS

Contact Rating:	Gold .4VA max. @ 20 VDC or VAC Max. 15 Amps @ 125/250 VAC-UL, CUL, VDE
Life Expectancy:	50,000 cycles minimum
Mechanical Life:	1,000,000 cycles typical
Insulation Resistance:	100 MΩ min.
Dielectric Strength:	1,500 VAC for 60 seconds
Operating Temperature:	-25° C to 85° C (std)
Operating Force:	See Chart

MATERIALS

Switch Housing:	High Temperature PBT (UL94 V0)
Actuator Button:	High Temperature PBT (UL94 V0)
Contacts:	Silver (std) or Gold
Terminals:	Copper Alloy

FEATURES & BENEFITS

- Available in gold & 15amp versions
- Wide variety of actuator, operating force & termination options

APPLICATIONS/MARKETS

- Appliance
- Timing controls
- Vending machines
- Gaming
- Industrial controls
- Power tools

HOW TO ORDER

SERIES	OPERATING TEMP.	CURRENT RATING	ACTUATOR	OPERATING FORCE	TERMINATION	CIRCUIT
LS	▯▯▯	▯▯	▯▯	F ▯▯▯	▯▯	▯
	085 = 85C	R1 = Gold 15 = 15A	See Chart	See Chart	S1 = Solder Lug C1 = 0.187" Quick Connect C2 = 0.250" Quick Connect V1 = Right Angle PCB Pin V2 = Left Angle PCB Pin	A = SPDT B = SPST NC C = SPST NO

Example Ordering Number

LS–085–15–03–F040–C2–A

Specifications subject to change without notice.

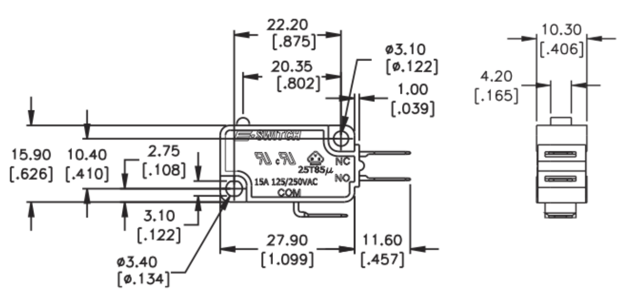

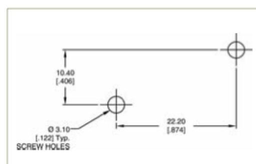

MOUNTING

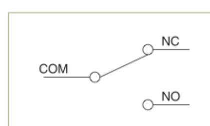

SCHEMATIC

SERIES LS SWITCHES

SNAP ACTION SWITCHES

ACTUATOR OPTIONS

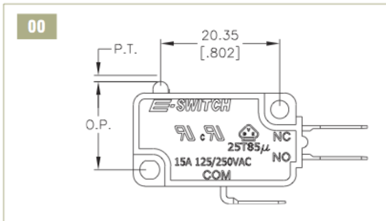

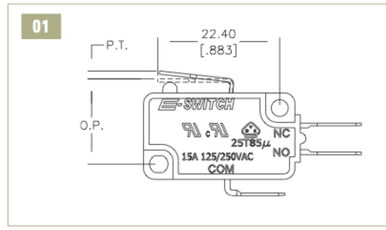

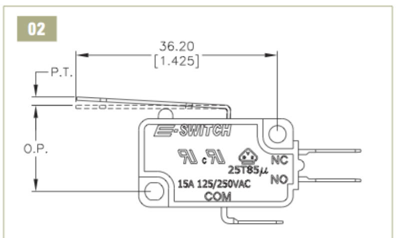

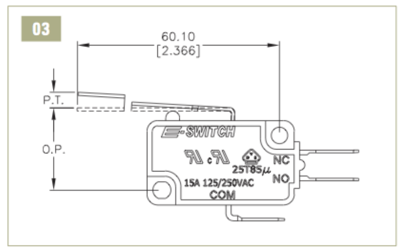

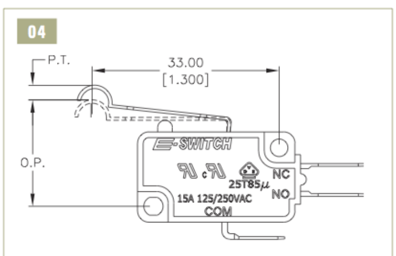

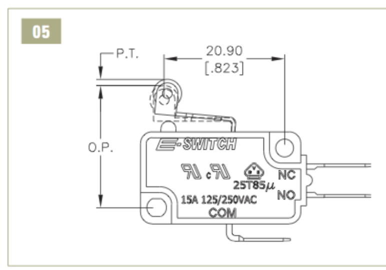

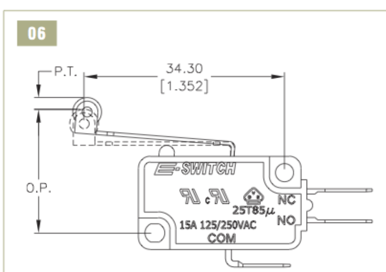

PT= Pretravel   OP= Operating Point   OT= Over Travel

ACTUATOR AND OPERATING FORCE CHART

Actuator	Actuation/Return Force			Pre-Travel	Operating Position
00	100+/-30	160+/-40	250+/-50	2.0 max	14.7+/-0.5
01	100+/-30	160+/-40	250+/-50	2.0 max	15.3+/-0.5
02	45+/-20	75+/-25	120+/-40	4.1 max	15.5+/-0.8
03	25+/-10	40+/-15	60+/-25	8.5 max	15.3+/-2.0
04	50+/-20	85+/-30	140+/-40	5.2 max	19.0+/-1.5
05	100+/-30	160+/-40	250+/-50	2.7 max	20.7+/-0.8
06	45+/-15	75+/-25	120+/-40	5.5 max	20.7+/-1.5

TERMINATION OPTIONS

S1 SOLDER LUG

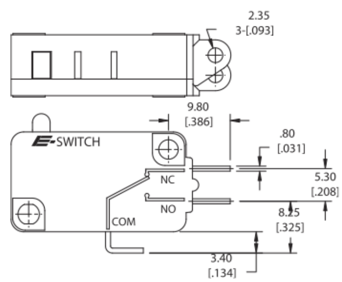

C1 0.187" QUICK CONNECT

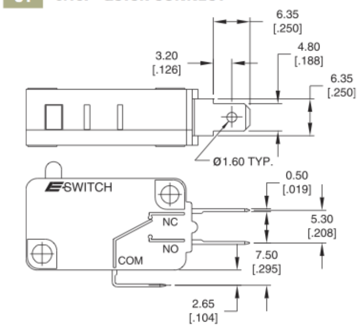

V1 RIGHT ANGLE PCB PIN

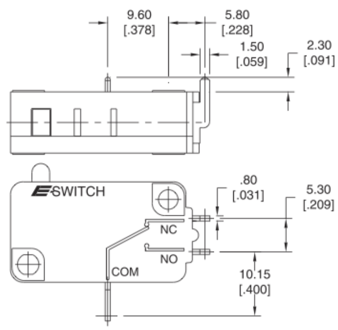

C2 0.250" QUICK CONNECT

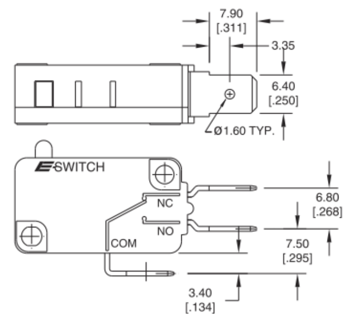

F.5 Relays (G2R-1--SD12S)

General-purpose Relay
G2R-□-S (S)

CSM_G2R-_-S_(S)_DS_E_1_1

Slim and Space-saving Power Plug-in Relay

- Lockable test button models now available.
- Built-in mechanical operation indicator.
- Provided with nameplate.
- AC type is equipped with a coil-disconnection self-diagnostic function (LED type).
- High switching power (1-pole: 10 A).
- Environment-friendly (Cd, Pb free).
- Wide range of Sockets also available.

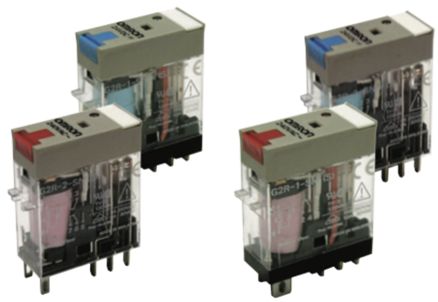

For the most recent information on models that have been certified for safety standards, refer to your OMRON website.

Model Number Structure

Model Number Legend

G2R □ □ □ □ S □ □ (S)
1 2 3 4 5 6 7 8

1. Relay Function
Blank: General-purpose

2. Number of Poles
1: 1 pole
2: 2 poles

3. Contact Form
Blank: SPDT

4. Contact Type
Blank: Single

5. Terminals
S: Plug-in

6. Classification
Blank: General-purpose
N: LED indicator
D: Diode
ND: LED indicator and diode
NI: LED indicator with test button
NDI: LED indicator and diode with test button

7. Rated Coil Voltage

8. Mechanical operation indicator and Nameplate
(S): Models with mechanical operation indicator and Nameplate

Ordering Information

When your order, specify the rated voltage.

List of Models

Classification		Enclosure rating	Coil ratings	Contact form	
				SPDT	DPDT
Plug-in terminal	General-purpose	Unsealed	AC/DC	G2R-1-S (S)	G2R-2-S (S)
	LED indicator			G2R-1-SN (S)	G2R-2-SN (S)
	LED indicator with test button			G2R-1-SNI (S)	G2R-2-SNI (S)
	Diode		DC	G2R-1-SD (S)	G2R-2-SD (S)
	LED indicator and diode			G2R-1-SND (S)	G2R-2-SND (S)
	LED indicator and diode with test button			G2R-1-SNDI (S)	G2R-2-SNDI (S)

Note: 1. The standard models are compliant with UL/CSA and VDE standards. Also, an EC compliance declaration has been made for combinations with the P2RF-E and P2RF-S. The Relays bear the CE Marking.
2. Refer to *Connecting Sockets*, below, for applicable Socket models.
3. When ordering, add the rated coil voltage and "(S)" to the model number. Rated coil voltages are given in the coil ratings table.
Example: G2R-1-S 12 VDC (S)
Rated coil voltage

Accessories (Order Separately)

Connecting Sockets

Applicable Relay model	Track/surface-mounting Socket		Back-mounting Socket	
	Screwless clamp terminal	Screw terminal	Terminals	Model
1 pole G2R-1-S (S)	• P2RF-05-S (See note.) + (P2CM-S (option))	• P2RF-05-E • P2RF-05	PCB terminals	P2R-05P, P2R-057P
			Solder terminals	P2R-05A
2 poles G2R-2-S (S)	• P2RF-08-S (See note.) + (P2CM-S (option))	• P2RF-08-E • P2RF-08	PCB terminals	P2R-08P, P2R-087P
			Solder terminals	P2R-08A

Note: Use of the P2CM Clip & Release Lever is recommended to ensure stable mounting.

Accessories for Screwless Clamp Terminal Socket (Option)

Name	Model
Clip & Release Lever	P2CM-S
Nameplate	R99-11 Nameplate for MY
Socket Bridge	P2RM-SR (for AC), P2RM-SB (for DC)

Mounting Tracks

Applicable Socket	Description	Model
Track-connecting Socket	Mounting track	50 cm (ℓ) x 7.3 mm (t): PFP-50N 1 m (ℓ) x 7.3 mm (t): PFP-100N 1 m (ℓ) x 16 mm (t): PFP-100N2
	End plate	PFP-M
	Spacer	PFP-S
Back-connecting Socket	Mounting plate	P2R-P*

*Used to mount several P2R-05A and P2R-08A Connecting Sockets side by side.

Specifications

Coil Ratings

Rated voltage		Rated current*		Coil resistance*	Coil inductance (H) (ref. value)		Must operate voltage	Must release voltage	Max. voltage	Power consumption (approx.)
		50 Hz	60 Hz		Armature OFF	Armature ON	% of rated voltage			
AC	24 V	43.5 mA	37.4 mA	253 Ω	0.81	1.55	80% max.	30% max.	110%	0.9 VA at 60 Hz
	110 V	9.5 mA	8.2 mA	5,566 Ω	13.33	26.83				
	120 V	8.6 mA	7.5 mA	7,286 Ω	16.13	32.46				
	230 V	4.4 mA	3.8 mA	27,172 Ω	72.68	143.90				
	240 V	3.7 mA	3.2 mA	30,360 Ω	90.58	182.34				

Rated voltage		Rated current*	Coil resistance*	Coil inductance (H) (ref. value)		Must operate voltage	Must release voltage	Max. voltage	Power consumption (approx.)
				Armature OFF	Armature ON	% of rated voltage			
DC	6 V	87.0 mA	69 Ω	0.25	0.48	70% max.	15% min.	110%	0.53 W
	12 V	43.2 mA	278 Ω	0.98	2.35				
	24 V	21.6 mA	1,113 Ω	3.60	8.25				
	48 V	11.4 mA	4,220 Ω	15.2	29.82				

*The rated current and coil resistance are measured at a coil temperature of 23°C with tolerances of ±10%.

Contact Ratings

Number of poles	1 pole		2 poles	
Load	Resistive load ($\cos\phi = 1$)	Inductive load ($\cos\phi = 0.4$; L/R = 7 ms)	Resistive load ($\cos\phi = 1$)	Inductive load ($\cos\phi = 0.4$; L/R = 7 ms)
Rated load	10 A at 250 VAC; 10 A at 30 VDC	7.5 A at 250 VAC; 5 A at 30 VDC	5 A at 250 VAC; 5 A at 30 VDC	2 A at 250 VAC; 3 A at 30 VDC
Rated carry current	10 A		5 A	
Max. switching voltage	440 VAC, 125 VDC		380 VAC, 125 VDC	
Max. switching current	10 A		5 A	
Max. switching power	2,500 VA, 300 W	1,875 VA, 150 W	1,250 VA, 150 W	500 VA, 90 W
Failure rate (reference value)	100 mA at 5 VDC		10 mA at 5 VDC	

Note: P level: $\lambda_{60} = 0.1 \times 10^{-6}$/operation

Characteristics

Item	1 pole	2 poles
Contact resistance	100 mΩ max.	
Operate (set) time	15 ms max.	
Release (reset) time	AC: 10 ms max.; DC: 5 ms max. (w/built-in diode: 20 ms max.)	AC: 15 ms max.; DC: 10 ms max. (w/built-in diode: 20 ms max.)
Max. operating frequency	Mechanical: 18,000 operations/hr Electrical: 1,800 operations/hr (under rated load)	
Insulation resistance	1,000 MΩ min. (at 500 VDC)	
Dielectric strength	5,000 VAC, 50/60 Hz for 1 min between coil and contacts*; 1,000 VAC, 50/60 Hz for 1 min between contacts of same polarity	5,000 VAC, 50/60 Hz for 1 min between coil and contacts*; 3,000 VAC, 50/60 Hz for 1 min between contacts of different polarity 1,000 VAC, 50/60 Hz for 1 min between contacts of same polarity
Vibration resistance	Destruction: 10 to 55 to 10 Hz, 0.75 mm single amplitude (1.5 mm double amplitude) Malfunction: 10 to 55 to 10 Hz, 0.75 mm single amplitude (1.5 mm double amplitude)	
Shock resistance	Destruction: 1,000 m/s^2 Malfunction: 200 m/s^2 when energized; 100 m/s^2 when not energized	
Endurance	Mechanical: AC coil: 10,000,000 operations min.; DC coil: 20,000,000 operations min. (at 18,000 operations/hr) Electrical: 100,000 operations min. (at 1,800 operations/hr under rated load) (DC coil type)	
Ambient temperature	Operating: –40°C to 70°C (with no icing or condensation)	
Ambient humidity	Operating: 5% to 85%	
Weight	Approx. 21 g	

Note: Values in the above table are the initial values.
*4,000 VAC, 50/60 Hz for 1 minute when the P2R-05A or P2R-08A Socket is mounted.

Approved Standards

UL 508 (File No. E41643)

Model	Contact form	Coil ratings	Contact ratings	Oper-ations
G2R-1-S (S)	SPDT	5 to 110 VDC 6 to 240 VAC	10 A, 30 VDC (resistive) 10 A, 250 VAC (general use) TV-3 (NO contact only)	6 x 10^3
G2R-2-S (S)	DPDT		5 A, 30 VDC (resistive) 5 A, 250 VAC (general use) TV-3 (NO contact only)	6 x 10^3

CSA 22.2 No.0, No.14 (File No. LR31928)

Model	Contact form	Coil ratings	Contact ratings	Oper-ations
G2R-1-S (S)	SPDT	5 to 110 VDC 6 to 240 VAC	10 A, 30 VDC (resistive) 10 A, 250 VAC (general use) TV-3 (NO contact only)	6 x 10^3
G2R-2-S (S)	DPDT		5 A, 30 VDC (resistive) 5 A, 250 VAC (general use) TV-3 (NO contact only)	6 x 10^3

IEC/VDE (Certificate No. 40015012 EN 61810-1)

Contact form	Coil ratings	Contact ratings	Operations
1 pole	6, 12, 24, 48 VDC 24, 110, 120, 230, 240 VAC	5 A, 440 VAC ($\cos\phi = 1.0$) 10 A, 250 VAC ($\cos\phi = 1.0$) 10 A, 30 VDC (0 ms)	100 x 10^3
2 poles	6, 12, 24, 48 VDC 24, 110, 120, 230, 240 VAC	5 A, 250 VAC ($\cos\phi$ =1.0) 5 A, 30 VDC (0 ms)	100 x 10^3

LR

Number of poles	Coil ratings	Contact ratings	Operations
1 pole	5 to 110 VDC 6 to 240 VDC	10 A, 250 VAC (general use) 7.5 A, 250 VAC (PF0.4) 10 A, 30 VDC (resistive) 5A, 30VDC (L/R=7ms)	100 x 10^3
2 poles	5 to 110 VDC 6 to 240 VDC	5 A, 250 VAC (general use) 2 A, 250 VAC (PF0.4) 5 A, 30 VDC (resistive) 3A, 30VDC (L/R=7ms)	100 x 10^3

Engineering Data

Maximum Switching Power

Plug-in Relays

G2R-1-S (S)

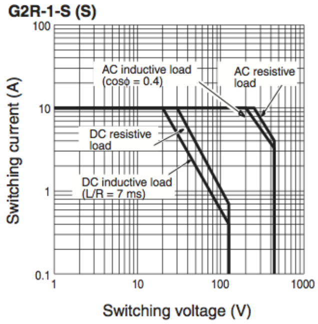

G2R-2-S (S)

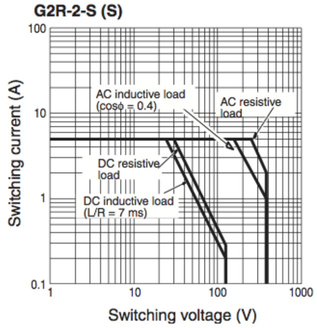

Endurance

Plug-in Relays

G2R-1-S (S)

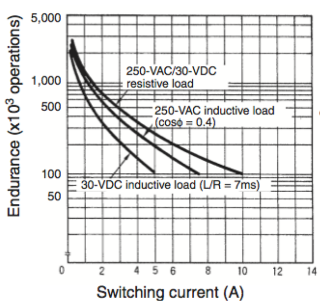

G2R-2-S (S)

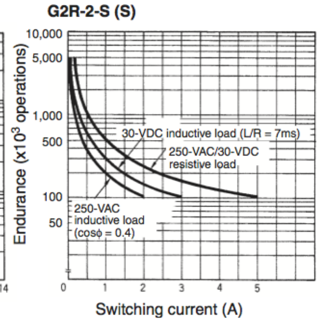

Ambient Temperature vs Maximum Coil Voltage

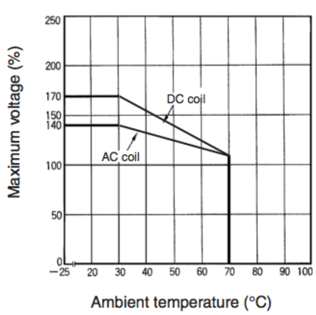

Note: The maximum voltage refers to the maximum value in a varying range of operating power voltage, not a continuous voltage.

F.6 Digital Input

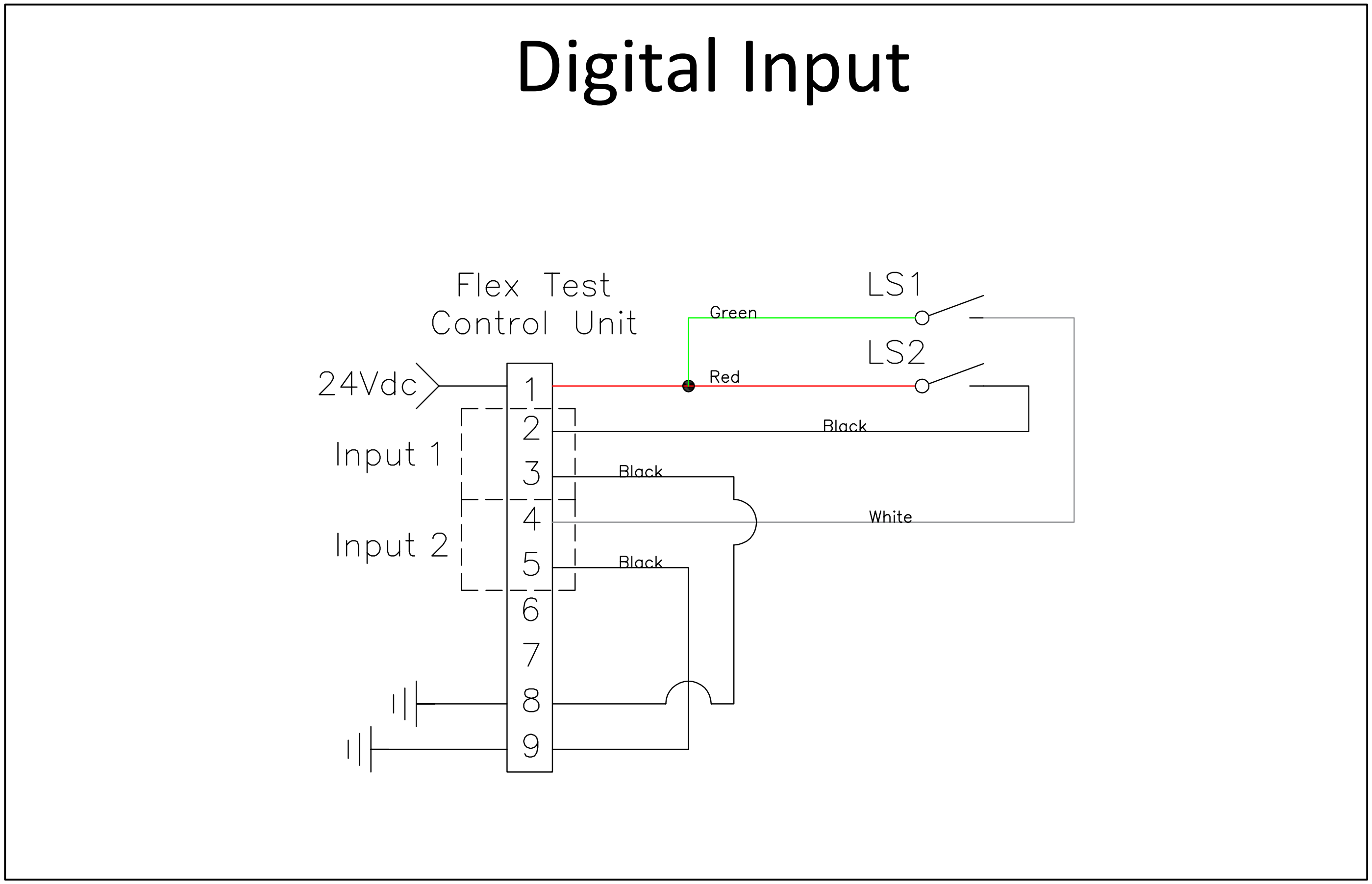

F.7 Digital Output

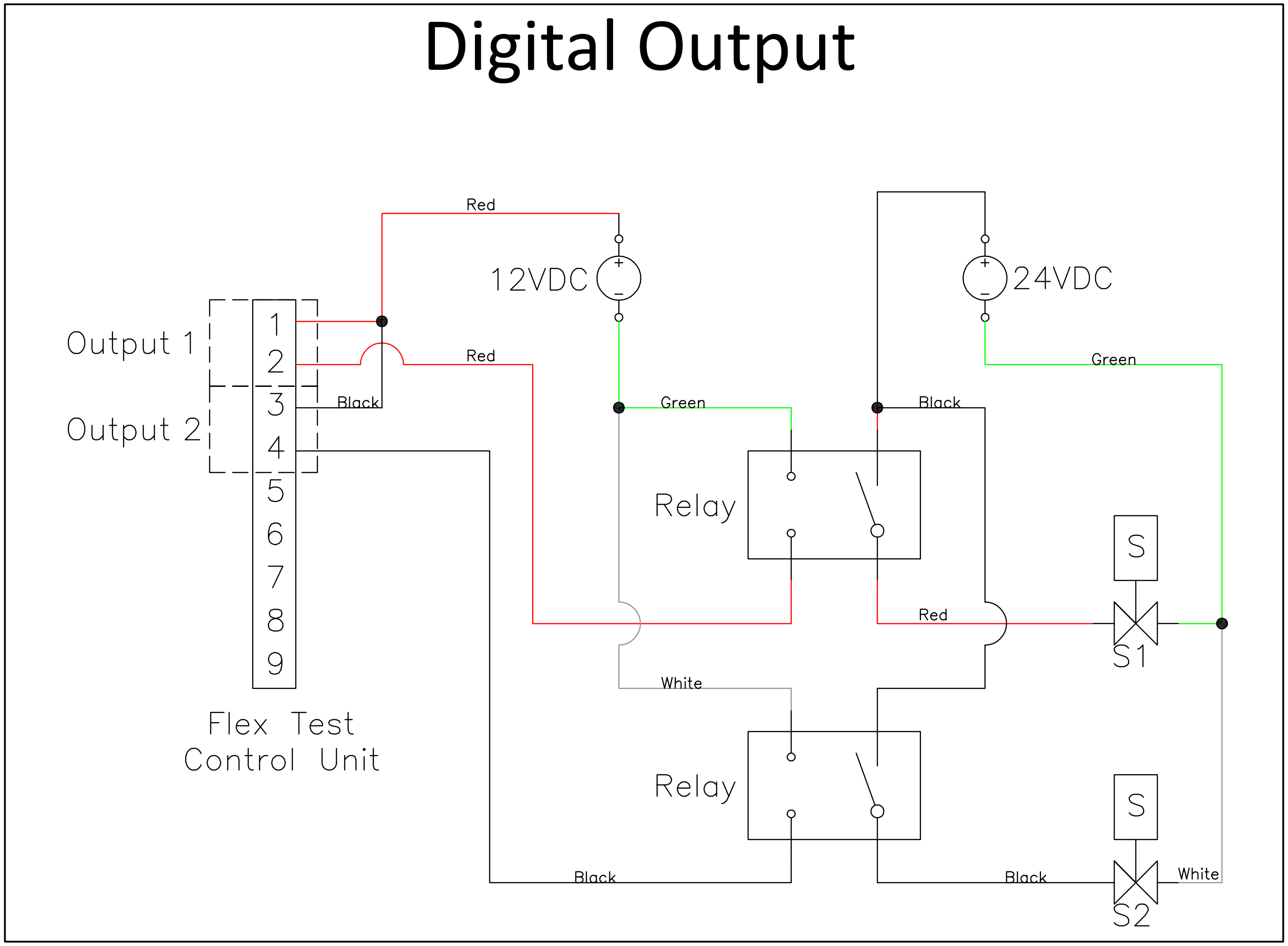

F.8 FMEA for Test Apparatus

Item	Potential failure mode	Potential cause(s) / mechanism	Cycle Phase	Local effects of failure	Next higher level effect	System Level End Effect	(P) Probability (estimate)	(S) Severity	Detection (Indications to Operator, Maintainer)	(D) Detection Dormancy Period	Risk Level P*S (+D)	Mitigation / Requirements
Main Roller Frame	Bend down in middle	Lower legs extend outwards	Loading	Separation of wheel frame clamps	Disconection with main roller	Main roller drops off, test becomes ineffective	L	M	Gap between roller frame and bushing	.5 Days	L	Reinforce if needed
Roller Bushings	Fatigue wear of bushing	Thinning of bushing, increased friction	Rolling	Lubrication contamination	Increased stress on hydraulic ram	Bushing replacement	L	L	Roller stability	1 Days	L	Check roller for snugg fit to roller pin
Load Cylinder	Rotation in the load cell	Higher rolling resistance on one side of roller	Rolling	Twisting of roller	Damage to roller path, roller, and coupon bolts	unreparable damage to roller and coupon	L	M	Misalignment with coupon	.25 Days	M	Set horizontal brace across roller frame
Load Cylinder	Misalignment in load cell	Horizontal pressure from apparatus	Rolling	Damage to load cylinder seals	Damage to load cylinder	Oil spillage, load cell repairs required	L	H	Periodic inspection	.5 Days	M	Set horizontal brace across roller frame
Coupon Bolts	Shearing	Horizontal forces from ram	Rolling	Coupon detatches from shuttle	Damage to coupon roller path	Test stops / coupon damage	L	L	Visual Inspection	1 Days	L	Replace bolts as needed (Bigger?)
Shuttle Plate	Excessive wear to underside	Contact stress exceeding strength	Loading/Rolling	Damage to shuttle	Damage to shuttle rollers if unaddressed	Shuttle replacement (stronger)	M	L	Visual Inspection / Math Calc	1 Days / prior to test	L	Repeating Visual inspection
Shuttle Rollers	Excessive wear	Contact stress exceeding strength	Loading/Rolling	Damage to roller surface or internal bearings	Damage to shuttle if unadressed	Roller replacement (Stronger)	M	L	Visual Inspection / Math Calc	1 Days / prior to test	L	Repeating Visual inspection
Brass guides	Excessive wear	Wear from shuttle contact	Rolling	Increased shuttle path area, roller contamination	Stress on shuttle underside, coupon instability	Cleaning and supervision required	H	M	Visual Inspection	.5 Days	M	Replace with roller pins
Hydraulic Ram	Oil leakage	pressure exceeding strength	Rolling	Leaking oil	Reduced capability	Horizontal movement stops / test stops	L	M	Visual Inspection	1 Days	L	Repeating Visual inspection
Ram support	Break off end of U-Bar supports	Ram pressure exeeding support strength	Rolling	Support breaks, ram fully extends	Ram rests under high pressure	Test stops, potential damage to hydraulic power unit	L	H	Visual Inspection	1 Days	M	Repeating Visual inspection
Power unit	Breaks down	Wears out from continued use	Loading/Rolling	Test Stops	Potential oil leakage	power unit replacement required	L	M	Visual and Audible inspection	1 Days	L	Repeating Inspection
Hydraulic Lines	Leakage	Wears out from continued use	Loading/Rolling	Oil Leakage	Test stops	Pressure line replacement	L	M	Visual Inspection	1 Days	L	Repeating Visual inspection
Solenoid Valve	Inner Coil Failure	Wears out from continued use	Loading/Rolling	Test Stops	Potential high pressure on power unit	Solenoid valve replacement	L	M	Visual Inspection	1 Days	L	Repeating Visual inspection
Shuttle limit stops	Arm damage / breakage	Ram doesn't stop, forces sensor arm into stop	Rolling	Test Stops	Ram and power unit remain on high pressure	Replacement of limit stops, potential damage to hydraulics	M	M	Visual Inspection	1 Days	M	When shutting test down, ensure ram is extended
Shuttle limit stops	Sensor failure	Wears out from continued use	Loading/Rolling	Test Stops	Ram and power unit remain on high pressure	Replacement of limit stops, potential damage to hydraulics	M	M	Visual Inspection	1 Days	M	Repeating Visual inspection

Appendix G: Raw Data

G.1 Sample Shovel Data (initial 36 of 3,600 data points)

Header:	Date	Time	HOIST_REI	HOIST_REI	H_VOLTS_	H2_VOLTS	H_FLD_AM	H_AMPS_S	Program:A	H_RAW_C
Data	3/17/2015	12:45:44;6	23.32034	18.68911	168.2076	157.7992	100.1471	1035.092	15.16592	4436
Data	3/17/2015	12:45:44;7	23.32659	18.5211	135.1418	136.8158	99.67194	745.2373	15.08141	4441
Data	3/17/2015	12:45:44;8	19.62287	16.73665	120.7733	116.7328	104.3051	999.0208	15.01099	4446
Data	3/17/2015	12:45:44;9	19.61974	15.25366	115.9838	118.5682	99.19675	1112.729	14.94056	4451
Data	3/17/2015	12:45:45;0	18.65314	14.3708	110.2503	109.8841	99.55315	939.3286	14.87014	4455
Data	3/17/2015	12:45:45;1	5.799585	4.435457	95.46732	102.6183	105.7307	1028.318	14.8138	4460
Data	3/17/2015	12:45:45;2	3.328349	2.571853	80.03966	93.68694	99.79074	1084.897	14.77155	4463
Data	3/17/2015	12:45:45;3	1.95822	2.432183	43.86523	62.4131	99.55315	531.3707	14.7293	4464
Data	3/17/2015	12:45:45;4	0.453581	0	15.12833	27.70113	102.0479	882.566	14.7293	4465
Data	3/17/2015	12:45:45;5	0.009384	0	18.9507	22.18858	99.31555	1140.012	14.71521	4465
Data	3/17/2015	12:45:45;6	0	0	14.25332	13.87221	98.00877	955.0756	14.71521	4465
Data	3/17/2015	12:45:45;7	0	0	0.736844	3.741957	104.5427	944.4554	14.71521	4465
Data	3/17/2015	12:45:45;8	0	0	-2.11843	-0.35257	100.0283	1269.284	14.71521	4465
Data	3/17/2015	12:45:45;9	0	0	-3.06251	-7.45718	99.43435	1195.126	14.7293	4464
Data	3/17/2015	12:45:46;0	0.006256	0	0.460527	-2.0162	105.7307	1087.644	14.7293	4464
Data	3/17/2015	12:45:46;1	0.006256	0	13.40135	7.164614	100.9787	1200.986	14.74338	4463
Data	3/17/2015	12:45:46;2	0	0	16.30267	14.49291	102.7607	1222.043	14.74338	4463
Data	3/17/2015	12:45:46;3	0.006256	0	7.898044	13.3319	97.65237	1238.705	14.74338	4463
Data	3/17/2015	12:45:46;4	0	0	12.6645	9.010131	98.60277	1090.207	14.74338	4463
Data	3/17/2015	12:45:46;5	0	0	14.71385	9.238928	99.31555	1123.349	14.74338	4463
Data	3/17/2015	12:45:46;6	0.006256	0	11.37503	13.27708	104.4239	1153.561	14.74338	4463
Data	3/17/2015	12:45:46;7	0.003128	0	14.25332	10.98435	106.5623	958.0052	14.74338	4463
Data	3/17/2015	12:45:46;8	0.006256	0	12.82569	9.538077	105.3743	1061.643	14.74338	4463
Data	3/17/2015	12:45:46;9	0.006256	0	9.717127	8.460732	104.0675	1013.852	14.74338	4463
Data	3/17/2015	12:45:47;0	0	0	7.875018	7.592878	98.72157	1227.17	14.74338	4463
Data	3/17/2015	12:45:47;1	0	0	10.33884	3.033565	101.3351	982.1751	14.74338	4463
Data	3/17/2015	12:45:47;2	0	0	6.286199	5.267163	104.6615	1028.867	14.75746	4462
Data	3/17/2015	12:45:47;3	0	0	11.55924	10.97323	101.2163	1242.917	14.75746	4462
Data	3/17/2015	12:45:47;4	0.006256	0	12.94082	13.3945	99.43435	1294.735	14.75746	4462
Data	3/17/2015	12:45:47;5	0.006256	0	9.325679	11.58522	102.8795	1250.241	14.75746	4462
Data	3/17/2015	12:45:47;6	-39.9277	-16.6105	9.210547	8.479832	99.07797	1062.192	14.77155	4461
Data	3/17/2015	12:45:47;7	-62.0531	-62.0531	10.73029	10.09465	99.55315	1226.254	14.77155	4461
Data	3/17/2015	12:45:47;8	-90.0844	-90.0844	-7.36844	-6.92626	103.9487	798.704	14.77155	4460
Data	3/17/2015	12:45:47;9	-96.2812	-96.2812	-47.5264	-42.8644	98.84036	173.5835	14.78563	4458
Data	3/17/2015	12:45:48;0	-99.8943	-99.8849	-126.806	-103.917	99.55315	-439.635	14.84197	4453
Data	3/17/2015	12:45:48;1	-99.8974	-99.8943	-213.938	-176.706	103.7111	-817.564	14.94056	4445
Data	3/17/2015	12:45:48;2	-99.8943	-99.8943	-277.353	-255.586	104.4239	-530.821	15.09549	4432
Data	3/17/2015	12:45:48;3	-99.8974	-99.8974	-357.277	-351.48	99.31555	-455.931	15.30676	4416
Data	3/17/2015	12:45:48;4	-99.8974	-99.8974	-456.106	-442.9	103.4735	-548.033	15.57437	4396

G.2 Coupon Cycle and Mass Readings

Mat Type	A322 4340	
Day	Mass (g)	Cycles
0	1,720.38	0
1	1,720.32	2,595
2	...	...
3	...	2,271
4	...	...
5	...	...
6	1,720.21	2,309
7	...	2,323
8	...	909
9	...	2,814
10	1,720.08	2,605
11		1,924
12		2,759
13		2,603
14	1,719.83	2,880
15		1,950
16		1,540
17		2,029
18		2,787
19		2,337
20	1,719.54	1,852
21		2,540
22		1,357
23		2,593
24		2,553
25		1,894

26	1,719.23	2,686
27		1,413
28		2,388
29		2,773
30	1,719.03	2,681
31		3,333
32		2,777
33	1,718.92	1,595
34		1,628
35		1,824
36	1,718.71	3,600

Appendix H: Hoist Force to Roller Force Code

```
Dim RollerCountMaster As Integer
Dim SpaceBetween As Double
Dim PivotOn As Double
Dim PivotToRope As Double
Dim RopeForce As Double
Dim NormalForce As Double
Dim CounterWeight As Double
Dim CounterWeightDist As Double
Dim PctDone As Single
Dim LoadedForce As Variant
Dim TotalForce As Double
Dim SupportLength As Double
Dim ToeWeight As Double
Dim HealWeight As Double
Dim MomentX As Double
Dim ForceDist As Double

Sub MainCode()
Application.ScreenUpdating = False
Sheets("Roller Loading").Select

RollerCountMaster = Cells(24, 8)
RollerCount = RollerCountMaster
SpaceBetween = Cells(25, 8)
PivotOn = Cells(26, 8)
PivotToRope = Cells(27, 8)
RopeForce = Cells(34, 8)
NormalForce = Cells(32, 8)
CounterWeight = Cells(31, 8)
```

```
CounterWeightDist = Cells(30, 8)
ReDim LoadedForce(1 To RollerCount, 1 To 1) As Double

Sheets("combined digs").Select
Call SmoothCurve
For E = 2 To 3626
SupportLength = (RollerCount) * SpaceBetween
   RopeForce = Cells(E, 69)
   TotalForce = NormalForce + CounterWeight + RopeForce
   MomentX = (CounterWeight * CounterWeightDist + RopeForce * PivotToRope) /
TotalForce
   ToeWeight = 4 * TotalForce / SupportLength - 6 * (SpaceBetween * 4 - MomentX)
* TotalForce / (SupportLength * SupportLength)
   HealWeight = -2 * TotalForce / SupportLength + 6 * (SpaceBetween * 4 -
MomentX) * TotalForce / (SupportLength * SupportLength)
Line1:
   If HealWeight < 0 Then
      SupportLength = SupportLength - 0.01
      ToeWeight = 4 * TotalForce / SupportLength - 6 * (SpaceBetween * 4 -
MomentX) * TotalForce / (SupportLength * SupportLength)
      HealWeight = -2 * TotalForce / SupportLength + 6 * (SpaceBetween * 4 -
MomentX) * TotalForce / (SupportLength * SupportLength)
      GoTo Line1
   End If
Line2:
   If ToeWeight < 0 Then
      SupportLength = SupportLength - 0.01
      HealWeight = 4 * TotalForce / SupportLength - 6 * (SpaceBetween * 3 +
MomentX) * TotalForce / (SupportLength * SupportLength)
```

```
    ToeWeight = -2 * TotalForce / SupportLength + 6 * (SpaceBetween * 3 +
MomentX) * TotalForce / (SupportLength * SupportLength)
    GoTo Line2
  End If

  If HealWeight > ToeWeight Then
    ForceDist = (HealWeight - ToeWeight) / SupportLength
    LoadedForce(1, 1) = ((HealWeight + (HealWeight - ForceDist * SpaceBetween))
/ 2) * SpaceBetween
    For i = 2 To RollerCount
      If (HealWeight - (i - 0.5) * SpaceBetween * ForceDist) > ToeWeight Then
        LoadedForce(i, 1) = (HealWeight - ForceDist * (i - 0.5) * SpaceBetween) *
SpaceBetween
      Else
        If (HealWeight - (i - 0.5) * SpaceBetween * ForceDist) > 0 Then
          LoadedForce(i, 1) = ((HealWeight - (i - 0.5) * SpaceBetween * ForceDist) *
(SupportLength - (i - 0.5) * SpaceBetween) / 2) * SpaceBetween
        Else
          LoadedForce(i, 1) = 0
        End If
      End If
    Next i
  Else
    ForceDist = (ToeWeight - HealWeight) / SupportLength
    LoadedForce(RollerCount, 1) = (ToeWeight - ForceDist * SpaceBetween / 2) *
SpaceBetween
    For i = 1 To RollerCount - 1
      If (ToeWeight - (i + 0.5) * SpaceBetween * ForceDist) > HealWeight Then
        LoadedForce(RollerCount - i, 1) = (ToeWeight - ForceDist * (i + 0.5) *
SpaceBetween) * SpaceBetween
```

```
        Else
          If (ToeWeight - (i + 0.5) * SpaceBetween * ForceDist) > 0 Then
            LoadedForce(RollerCount - i, 1) = ((ToeWeight - (i + 0.5) * SpaceBetween
* ForceDist) * (SupportLength - (i + 0.5) * SpaceBetween) / 2) * SpaceBetween
          Else
            LoadedForce(RollerCount - i, 1) = 0
          End If
        End If
      Next i
    End If
    For j = 1 To RollerCount
      Cells(E, 29 + j) = LoadedForce(j, 1)
    Next j
    PctDone = E / 3626
    UpdateProgressBar PctDone
Next E
Sheets("Roller Loading").Select
End Sub
```